DISSERTATION

Experimental Investigations and Application Analysis of a Particle-based High Temperature Thermal Energy Storage

ausgeführt zum Zwecke der Erlangung des akademischen Grades eines
Doktors der technischen Wissenschaften
(Dr. techn.)
eingereicht an der Technischen Universität Wien,
Fakultät für Maschinenwesen und Betriebswissenschaften
von

Dipl.-Ing. Peter Philipp STEINER

Mat.Nr.: 00728116
Buchenstraße 1
8243 Pinggau

unter der Leitung von
Univ. Prof. Dipl.-Ing. Dr. techn. Markus Haider
Institut für Energietechnik und Thermodynamik, E302

begutachtet von

Ao.Univ.Prof. Dipl.-Ing. Dr.techn.
Heimo Walter
Institut für Energietechnik und Thermodynamik
Getreidemarkt 9, E302
1060 Wien

Ao.Univ.Prof. Dipl.-Ing. Dr.techn.
Franz Winter
Institut für Verfahrenstechnik, Umwelttechnik und Techn. Biowissenschaften
Getreidemarkt 9, E166
1060 Wien

Diese Arbeit wurde vom FFG im Rahmen des K-Projekts GSG-GreenStorageGrid (Projekt Nr. 836636) unterstützt.

Ich nehme zur Kenntnis, dass ich zur Drucklegung meiner Arbeit unter der Bezeichnung

Dissertation

nur mit Bewilligung der Prüfungskommission berechtigt bin.

Eidesstattliche Erklärung
Ich erkläre an Eides statt, dass die vorliegende Arbeit nach den anerkannten Grundsätzen für wissenschaftliche Abhandlungen von mir selbstständig erstellt wurde. Alle verwendeten Hilfsmittel, insbesondere die zugrunde gelegte Literatur, sind in dieser Arbeit genannt und aufgelistet. Die aus den Quellen wörtlich entnommenen Stellen, sind als solche kenntlich gemacht.

Das Thema dieser Arbeit wurde von mir bisher weder im In-noch Ausland einer Beurteilerin/einem Beurteiler zur Begutachtung in irgendeiner Form als Prüfungsarbeit vorgelegt. Diese Arbeit stimmt mit der von den Begutachtern beurteilten Arbeit überein.

Wien, Juli, 2017

_____

Unterschrift

Kurzfassung

In den vergangenen Jahren haben sich weltweit viele Forschungseinrichtungen auf Energiespeicher fokussiert. Wegen dem stark wachsenden Segment an erneuerbaren Energien im Stromnetz und den damit einhergehenden Auswirkungen auf die Netzstabilität, steigt der Bedarf zur Speicherung großer elektrischer Energiemengen. Da durch kalorische Kraftwerke der Großteil des weltweiten Strombedarfs gedeckt wird, kommt im Sinne der Netzregelung insbesondere der Integration thermischer Energiespeicher (TES) in Kraftwerksprozesse eine besondere Bedeutung zu.

Stand der Technik TES leiden unter hohen Kosten und einem begrenzten Temperaturbereich der Speichermedien. Flüssigsalz, als das verbreitetste Wärmespeichermedium, erstarrt unter etwa 250 °C und zersetzt sich über ca. 560 °C. Sowohl die Problematik der erhöhten Kosten, als auch die Beschränkung des Temperaturbereichs, können mit neuen TES-Technologien, die auf Feststoffe als Wärmespeichermedium setzen, überwunden werden.

Viele Feststoff-basierende Technologien, wie beispielsweise Betonspeicher oder Festbettregeneratoren, kommen zur Zeit auf den Markt. An der TU Wien wurde eine weitere Technologie, welche als SandTES bezeichnet wird, entwickelt. Diese Technologie nutzt Feststoff-Partikel wie Quarzsand als Wärmespeichermedium, mit den Vorteilen niedriger Kosten und herausragender Temperaturbeständigkeit. Das Herzstück dieses TES Systems bildet ein Wirbelschicht-Wärmeübertrager. Dieser ermöglicht eine gegenläufige horizontale Strömung der Partikel-Luft-Suspension und eines Arbeitsmediums, wodurch ein exergetisch effizienter Wärmeübertrager entsteht. Das Konzept des SandTES-Systems und zwei wesentliche zum Wärmeübertrager gehörende Kerntechnologien werden in dieser Arbeit vorgestellt.

Um die vorangegangenen Simulations- und Versuchsergebnisse zu validieren und gleichzeitig die Machbarkeit nachzuweisen, wurde eine 280 kW_{th} Pilotanlage gebaut. Die Versuchsanordnung ebenso wie die ersten grundlegenden Versuchsergebnisse werden präsentiert und im Detail diskutiert. Neben dem dynamischen Verhalten liefert speziell der Höhenunterschied der Bettoberfläche entlang der Wärmeübertragerachse, als die Antriebsfeder der Strömung des Wirbelschicht-Bettes, wichtige Daten für eine weitere optimierte Skalierung.

Um die Vorteile einer derartigen TES-Technologie aufzuzeigen, wurden einige potentielle Anwendungsfelder in der Elektrizitätserzeugung analysiert. Besonders die herausragende Temperaturbeständigkeit des Wärmespeichermediums, aber auch die vergleichsweise niedrigen Kosten, scheinen erfolgsversprechend.

Unter den kalorischen Kraftwerken kommen Kohle-gefeuerte Kraftwerke am häufigsten vor. Solange alternative Technologien wie Batteriespeicher in dieser Größenordnung unwirtschaftlich sind, müssen die bestehenden Kraftwerke selbst durch erhöhte Flexibilität die Stromschwankungen im Netz ausgleichen. Da diese Kraftwerke für Grundlast ausgelegt waren, leidet die Lebensdauer stark unter der gestiegenen Anzahl an Lastwechseln und der gesenkten Minimallast. Die Einbindung eines TES kann gleichzeitig die Minimallast des Kraftwerks senken, die Lastgradienten steigern und trotzdem die Lebensdauer erhalten.

Kalorische Kraftwerke können auch mit Solarenergie angetrieben werden. Verglichen mit Fotovoltaikanlagen können die sogenannten konzentrierenden Solarkraftwerke sehr einfach einen TES einbinden, was Stromerzeugung nach Bedarf, selbst nach dem Sonnenuntergang, ermöglicht. Verschiedene Konzepte die den Speicherkreislauf, aber auch den Kraftprozess, beleuchten wurden hinsichtlich einer potentiellen Anwendung eines Hochtemperatur-TES analysiert.

Abstract

Much research in recent years has focused on energy storage. Due to the rising number of renewables with their impact on the stability of the electric grid, electricity has to be stored in huge amounts. Since most of the electricity worldwide is generated by thermal power plants, the integration of thermal energy storage (TES) into these power plant processes seems promising.

State of the art TES suffer from high costs and a limited temperature range. Molten salt as the most common heat storage medium (HSM) freezes below approximately 250 °C and decomposes beyond about 560 °C. Both issues can be overcome with solids as HSM.

Several technologies based on solids, like fixed-bed regenerators or concrete TES, are entering the market. At TU Wien another technology, called sandTES, was developed. This technology is based on particles like quartz sand, which is a low cost product able to persist highest temperatures. The heart piece of the TES system is a fluidized bed heat exchanger (HEX), allowing an exergetically efficient counter current heat exchange in the horizontal flow direction. The basic ideas behind the TES system as well as the two key technologies of the HEX are introduced in this work.

For validating simulations and results of preliminary small-scale test rigs and also getting a full proof of concept, a 280 kW_{th} pilot plant was erected. The experimental set-up and the first fundamental measurement results are presented and discussed in detail. Especially the slope of the fluidized bed level along the HEX axis, which is the driving force of the particle flow, and the overall dynamic behaviour are essential data for a further reliable and optimized scale-up.

Finally, for outlining the benefits of the sandTES technology, several application scenarios have been analyzed in detail. Especially the high temperature capability and the low cost HSM are outstanding, compared to state of the art TES technologies.

Many thermal power plants are based on coal as primary energy source. To compensate for the volatile electricity generation of renewables, a much more flexible power plant is needed, since battery storage is not available in this order of magnitude. These power plants suffer in terms of longevity from an increasing number of load changes and the need to run in deep load more often. The integration of a TES can lead to a lower minimum load of the plant, enhancing the load change gradients by still enabling the durability of the plant.

Another thermal power plant technology uses solar radiation as energy source. Compared to photovoltaics these so called concentrated solar power (CSP) plants can easily implement a TES, allowing electricity generation on demand, even if the sun set down. Various concepts regarding the storage cycle as well as the power cycle have been analyzed, for showing the potential of implementing a high temperature particle TES.

Preface

The aim of my work at the Institute for Energysystems and Thermodynamics of TU Wien, which lead to this thesis, was to validate all the preceding theoretical and experimental activities related to the so called sandTES-technology.

My entry point in the sandTES-project was a hazardous fire at the institute's laboratory. Prof. Markus Haider, as the head of the institute, hired me for managing the interfaces with the stakeholders of the new laboratory build-up. Simultaneously, the promotion of the already basic-engineered sandTES pilot plant, which has been planned to be located in the new laboratory in the first place, was on my agenda.

Right ahead I want to thank Markus Haider for trusting in me and giving me the opportunity to manage the pilot plant build-up. Through the years it has been a challenging and time-consuming task, but with the ability to learn a lot, both in technical and interpersonal skills. Due to a close collaboration during the project, I had the chance to profit from Markus' comprehensive technical knowledge and his visionary spirit.

Prof. Heimo Walter as head of the SeLaTES project, which was partly funding the sandTES project, always took time for discussing issues regarding the pilot plant design or the laboratory infrastructure. I also enjoyed the numerous conversations about general topics apart from work in an amicable atmosphere.

The first phase of my work was coined of organizational tasks and learning about the basic concepts of the sandTES technology. I am very grateful for the introduction and continuing advice of Karl Schwaiger and Martin Hämmerle from the beginning during the whole pilot plant planning process.

The design process of the pilot plant could not have been done all alone, wherefore several colleagues attended this phase of the project. Michael-Dario (Dido) Obermaier created the current design of the pilot plant's heat exchanger and gave us a more applicatory view of things. His hands-on mentality and the combination of experience and theoretical background have been useful all over the project. Next Johannes Höflinger joined the team, since the erection deadline came closer. Besides several constructive services his main achievement was the design of the pilot plant's silos. Martin Koller as the most recent member directly supported me by rearranging the pilot plant set up or organizational work like purchasing. One of his main tasks has been the design of the piping of all the SeLaTES-plants. Besides the regular team members, Thomas Fellner, Michael Hameter as project member of SeLaTES and Michael Ludwig as the electrical technician gave useful advice at planning the electric parts of the plant.

I also want to thank Karin Stranimaier and Martina Hantschl, the institute's secretaries, for their organizational skills and support at accounting. Franz Trummer, mostly working in the background, cared about IT-issues and helped saving time by providing perfectly working computer systems.

Due to delays of several stakeholders of the new laboratory build-up, the erection of the sandTES pilot plant started after about one year of detail engineering. The new site in front of the laboratory on a former parking lot made many things more complicated. However, Andreas Hofer and Dido together with Wolfgang Faulend, Roswitha Steininger and Michael Ludwig managed to build up the pilot plant as envisaged, despite a cold winter was interfering the work.

Finally, I appreciate the effort of Martin Hämmerle and Georg Urschitz, who together with several bachelor and master students accompanied the start-up process of the pilot plant.

At this point, all the institute members, including the other research areas and projects are thanked, due to their patience at refraining from the laboratory workers. Prof. Andreas Werner together with Prof. Markus Haider managed to guarantee sufficient resources also during the start-up process.

After about two years of managing the pilot plant project, the second phase of my work started. In this phase I started with application analysis for the sandTES concept, resulting in several publications and this thesis. Especially Karl Schwaiger and Heimo Walter encouraged me to do so, wherefore I am very thankful. Thanks to Markus Haider and his support I was able to join several conferences all over the world.

Furthermore, after starting up the pilot plant, the experimental work began, providing the main results of this thesis. Also in this more scientific field I have learned a lot and fairly widened my horizon.

At the same time I started teaching the basic thermodynamics exercise and later on the thermal plant exercise. Prof. Karl Ponweiser and Prof. Heimo Walter gave me the chance to improve my teaching skills, which I really appreciate.

In the last months of my work three new colleagues entered the office. David Wünsch and Verena Sulzgruber, both at some point working on the Advanced Regenerator - a sandTES-spin off - and Daniel Lange accompanied me at writing my thesis. Together with Michael Hameter and Martin Koller, they completed our group. Several discussions at lunch and during the day lead to interesting ideas or solutions for problems.

Last but not least, I am grateful for all my friends and relatives, who inspired me, who cheered me up and supported me in any way. Especially my parents Peter and Ida Steiner are thanked for encouraging me to find my way and supporting me not only financially during my live. This work is devoted to them!

List of Publications

Patents

1. P. Steiner, M. Haider, K. Schwaiger, H. Walter, M. Hämmerle: *Wärmekraftwerk*; Patent granted, 2017

Journal Paper

1. P. Steiner, K. Schwaiger, M. Haider, H. Walter: *Flow Characteristics of a Fluidized Bed Heat Exchanger used for High Temperature Thermal Energy Storage*; Submitted to Applied Energy, 2017

Conference Presentation and Proceedings

1. P. Steiner, K. Schwaiger, H. Walter, M. Haider: *Active Fluidized Bed Technology used for Thermal Energy Storage*; Proceedings of the ASME 2016 Power and Energy Conference, PowerEnergy2016, Charlotte, North Carolina, USA, 2016

2. P. Steiner, K. Schwaiger, M. Haider, H. Walter, M. Hämmerle: *Increasing Load Flexibility and Plant Dynamics of Thermal Power Plants via the Implementation of Thermal Energy Storages*; Proceedings of the ASME 2016 Power and Energy Conference, PowerEnergy2016, Charlotte, North Carolina, USA, 2016

3. P. Steiner, K. Schwaiger, M. Haider, H. Walter: *System Analysis of Central Receiver Concepts with High Temperature Thermal Energy Storages: Receiver Technologies and Storage Cycles*; AIP conference proceedings: SolarPaces2016, Abu Dhabi (UAE), 2016

4. P. Steiner, M. Haider, K. Schwaiger: *Flexibilisierung und Mindestlastabsenkung kalorischer Kraftwerke mittels Einbindung thermischer Hochtemperatur-Energiespeicher*; Tagungsband Kraftwerkstechnisches Kolloquium, Dresden, Germany, 2016

5. P. Steiner, K. Schwaiger, H. Walter, M. Haider, M. Hämmerle: *Fluidized Bed Particle Heat Exchanger for Supercritical Carbon Dioxide Power Cycles*; Proceedings of the ASME 2016 International Mechanical Engineering Congress and Exposition, IMECE2016, Phoenix, Arizona, USA, 2016

Conference Presentation

1. P. Steiner, K. Schwaiger, M. Haider: *CSP-Systems based on sCO2-Power Cycles and Particle based Heat Storage*; Presentation at 1st European Seminar on Supercritical CO2 (sCO2) Power Systems, Vienna (Austria), 2016

Contents

List of Figures

List of Tables

Nomenclature

Abbreviations

Symbol	Description
ACAES	Adiabatic Compressed Air Energy Storage
Al_2O_3	Corundum
CAES	Compressed Air Energy Storage
CCS	Carbon Capture and Storage
CD	Crescent Dunes
CFPP	Coal-fired Power Plant
CO_2	Carbon Dioxide
CSP	Concentrated Solar Power
HEX	Heat Exchanger
HSM	Heat Storage Medium
HTM	Heat Transfer Medium
LCOE	Levelized Cost of Electricity
Na	Sodium
PCS	Process Control System
PHS	Pumped Hydro Energy Storage
PV	Photovoltaics
RPP	Reference Power Plant North Rhine-Westphalia
NRW	
sCO2	Supercritical Carbon Dioxide
SiC	Silicon Carbide
SiO_2	Quartz
SME	Super Magnetic Energy Storage
SS	Solar Salt
TES	Thermal Energy Storage
VP1	Therminol VP-1

Latin Symbols

Symbol	Unit	Description
Ar	-	Archimedes number
C	-	Constant
c_P	$\frac{\mathrm{J}}{\mathrm{kgK}}$	Isobaric heat capacity
d	mm	Diameter
E	$\frac{\mathrm{MJ}}{\mathrm{m}^3}$	Energy density
G	$\frac{\mathrm{kg}}{\mathrm{m}^2 \cdot \mathrm{s}}$	Mass flux
g	$\frac{\mathrm{m}}{\mathrm{s}^2}$	Gravitational constant
H	m	Height
m	kg	Mass

(continued)

Symbol	Unit	Description
p	bar	Pressure
Re	-	Reynolds number
T	°C	Temperature
u	$\frac{\mathrm{m}}{\mathrm{s}}$	Velocity
V	m^3	Volume

Greek Symbols

Symbol	Unit	Description
Δ	-	Difference
μ	-	Fluidization grade
ν	$\frac{\mathrm{m}^2}{\mathrm{s}}$	Kinematic viscosity
Ψ	-	Porosity
ρ	$\frac{\mathrm{kg}}{\mathrm{m}^3}$	Density
ζ	-	Pressure drop coefficient

Subscripts

Symbol	Description
act	Actual superficial
b	Fixed bed
f	Fluid
fb	Fluidized Bed
HEX	Heat Exchanger
io	Inlet to Outlet
max	Maximum
mf	Minimum fluidization
min	Minimum
$Nozzle$	Nozzle
p	Particle
V	Volumetric
$Valve$	Valve

1 Introduction

1.1 Motivation

Much research in recent years has focused on changes in energy supply. Since the global population as well as the energy demand per head are still rapidly rising, the replacement of conventional primary energy sources like fossil fuels by renewables gets more and more important. Not only the idea of sustainability, but also the control of the climate change is a major concern. To hold the increase of the global average temperature below 2 °C above pre-industrial levels, the Paris climate agreement claims a reduction of the carbon dioxide (CO_2) emissions to zero until about 2060 [9, 31]. Besides the global warming, environmental pollution, especially air pollution leads to severe risks for health, which can be observed in smog stricken cities like Beijing. Thus, huge changes regarding the energy industries and markets are needed, which can be expected in the next decades. This so called Energiewende will be one of the main challenges for present and future generations.

Today, by far the biggest stake of the global primary energy demand consists of fossil fuels like coal, oil and natural gas. Also for the electricity generation the tendencies remain the same, although this sector benefits from the integration of greenhouse neutral nuclear power or renewables like hydro power, photovoltaics or wind power. The number of installed and planned nuclear power plants, still remaining a hazardous technology, is rising in recent years [12]. Renewables can be applied in various cases, strongly depending on regional boundaries. Countries like Austria or Norway with their mountainous landscape and their numerous streams are predestined for conventional hydro power. For example, in Austria about 70 % of the electric power is generated by hydro power plants [6]. Other countries with a high solar irradiance like Chile are favoured for concentrated solar power (CSP) plants or photovoltaics (PV). Geothermal Power is only rarely available, for example in Iceland. Just wind power and biomass are technologies, which are largely independent of the region. However, wind power is criticized in relation to noise exposure and animal protection. Biomass on the other hand is greenhouse gas neutral, but suffers from air pollution all the same as fossil fired power plants.

Apart from these renewables, the so called carbon capture and storage (CCS) technology could be an approach for reducing greenhouse gases. The produced CO_2 of the conventional fossil fired power plants could be separated and stored e.g. in caverns. Of course, this affects the efficiencies of these power plants and doesn't fit for the idea of sustainability.

Especially the electricity generation of the widespread renewables photovoltaics and wind power is highly fluctuating. To ensure a stable grid, the electricity generation has to be decoupled from the electricity consumption. Either the remaining conventional power plants are able to change their loads sufficiently fast, or storage capacities have to be installed. At the moment, while changing to a solely renewable electricity generation, many thermal power plants, which have been designed for base load, have to change their load much more often than envisaged, which reduces the durability of the power plant. Furthermore the decreased number of consecutive full load operation hours leads to economical issues. However, at least after shutting down the last conventional thermal power plant, sufficient storage capacities are demanded.

As electricity cannot be stored directly in these amounts, storage technologies based on other physical principles have to be considered. The most suitable storage type for a certain application has to be chosen by criteria as efficiency, cost, order of magnitude, dynamic behaviour or environmental impacts. Figure 1 shows an overview of the most common storage types, grouped by their physical principle, followed up by a brief introduction of some chosen technologies.

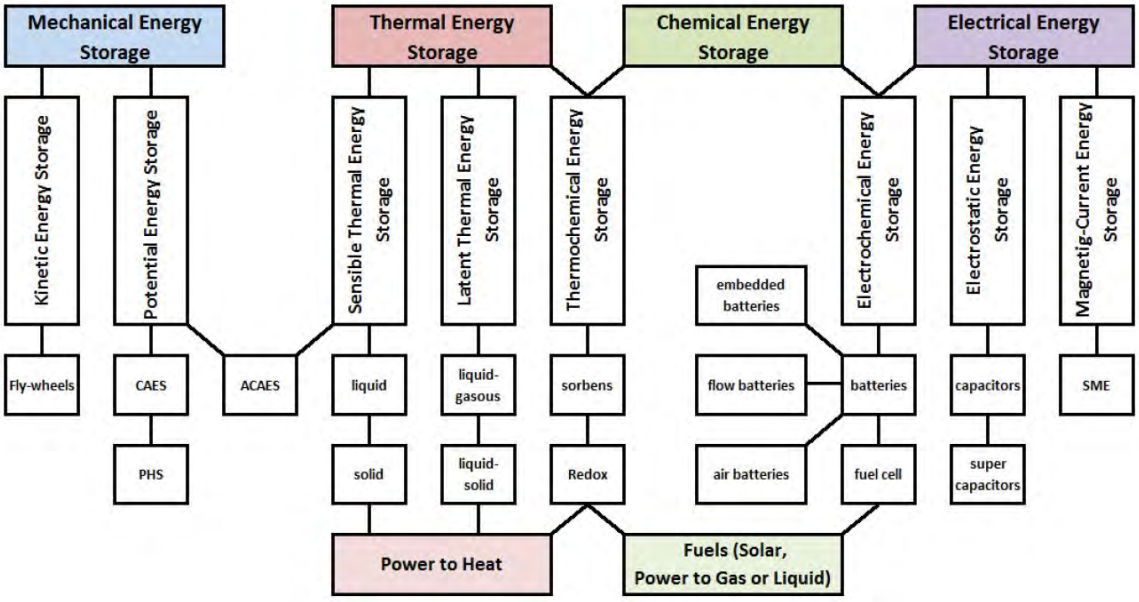

Figure 1: Overview of storage technologies [26]

Mechanical energy storage can be divided in potential and kinetic energy storage. Pumped hydro plants, as potential energy storage, are the most relevant for electricity storage, regarding the installed capacities. The round-trip efficiencies are rather high, reaching values in the range of 85 % [18]. However, for those, a special topography is required. Also the environmental impacts e.g. by building the reservoirs have to be minded. In Europe, the potential of economic feasible pumped hydro plants is already nearly exhausted.

Another potential energy storage, which is widely independent of the geographic location, is the compressed air energy storage (CAES). Both of the two plants built until now are diabatic CAES. After compression, heat gets lost to the ambient and has to be reinserted before the expansion by any heater. The CAES plant Huntorf in Germany shows rather low storage efficiency below 50 %. By using additional thermal energy storage (TES) the heat after compression can be stored and reinserted before expansion. This leads to efficiencies in the range of 70 % for these so called adiabatic compressed air energy storage (ACAES) [11].

For short duration kinetic energy storage like fly wheels are considered. The development tends to apply magnetic bearings for increasing the storage efficiency of this technology.

Electromagnetic storage with superconducting magnetic energy storage and super capacitors is envisaged for ultra short time storage. The capacities mostly remain in the range of a few kilowatts, but with very high efficiencies [17].

Electrochemical storage, mostly referring to batteries and accumulators, is a widespread technology, especially at small-scale applications. For huge energy amounts the cost of rare materials and the impacts on the environment seem to be problematic.

Thermochemical storage is in an early stage of development and furthermore envisaged for long term storage. Heat can be stored e.g. by dehydrating the used storage material. The thermal energy transformed to chemical bond energy can be stored for long periods with neglect able losses. To release the heat, the material has to be hydrated again, which can be a challenging task.

Besides thermochemical storage and various well known TES like hot water storage tanks, latent TES are considered due to their comparatively high energy densities. However, these suffer from poor heat conduction of the storage material, which results in large heat exchanger (HEX) surfaces with e.g. complex finned tube geometries [1].

Generally it can be stated, that there is not the one right type of storage. Much more the right storage depends on the application case. As the focus of this work is on a sensible TES, two sensible TES technologies are introduced and explained more in detail in the following subsection.

1.2 Sensible Thermal Energy Storage

Sensible TES systems rely on the first law of thermodynamics, see Eq. (1). Thermal energy is stored by simply raising the material's temperature.

$$Q = \int_{T_{min}}^{T_{max}} m \cdot c_p \cdot \mathrm{d}T \tag{1}$$

These kinds of TES are the most common TES, as it is a rather simple technology. For example, buffer tanks using water as heat storage medium (HSM) are installed in numerous households. In the field of electricity generation, especially at CSP plants, molten salt replaced thermal oil as state of the art HSM. Only two tanks, a HEX and some conveying technology are therefore needed.

The so called sandTES-technology, which is key part of this work, uses particles as HSM. As no phase change occurs, the sandTES-technology is also a sensible TES, although combinations with phase change materials are considered. The particles, e.g. quartz sand can be stored in silos. The particle-based HEX uses fluidization technique for the particle transport inside the HEX.

Besides the sandTES-technology several other TES concepts are in development. Two of them, which already entered the market, will be briefly introduced:

A fixed-bed regenerator uses solid materials like crushed rocks as HSM. To charge or discharge the TES a heat transfer medium (HTM) is needed, in this case air, which is simply blown through a fixed-bed to exchange heat. One major disadvantage of this technology is the high auxiliary power consumption due to the high volumetric flow of the air. To reduce the auxiliary power consumption, the pressure drop through the bed

has to be minimized, which is achieved by decreasing the flow length [14]. In the case of Storasol's fixed bed regenerator, see Fig. 2 (a), the path of the air through the bed is minimized by maximizing the flow cross section. To still get a rather compact layout, the fixed bed is split into several parallel chambers. This furthermore leads to a more flexible plant operation, as the number of parallel chambers and with it the thermal output, can be controlled by valves. Figure 2 (b) shows the pilot plant of Storasol's fixed-bed regenerator, located at University of Bayreuth in Germany.

At the moment Storasol's fixed-bed regenerator is designed for temperatures up to 600 °C, using particles like quartz sand with a sauter diameter of 3 mm as HSM [29]. The volumetric heat capacity of quartz sand is in the range of 1.4 $\frac{\mathrm{MJ}}{\mathrm{m^3 \cdot K}}$ with a heat conductivity of 0.7 $\frac{\mathrm{W}}{\mathrm{K \cdot m}}$. This low heat conductivity claims small particle diameters, which leads to a higher pressure drop through the bed. Due to the large total surface of the numerous particles the terminal temperature difference between air and fixed bed are low (in the range of a few centigrade).

Due to the appearing thermocline at these fixed-bed regenerators and depending on the design and operation parameters, not all parts of the regenerator can be charged and discharged to the maximum and minimum temperatures, respectively, which affects the overall energy density. As high volumetric air flows are required for transporting the thermal energy, huge air piping is needed, leading together with valves and insulation to additional costs. However, highest temperatures can be reached at a less complex system.

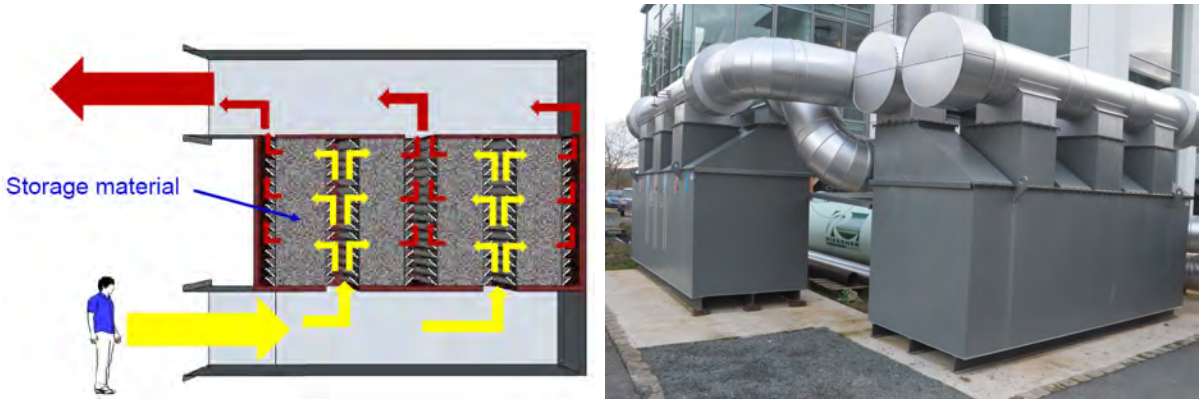

(a) Principle Storasol's fixed-bed regenerator [30] (b) Storasol pilot plant at University of Bayreuth

Figure 2: Fixed bed regenerator

Another attractive novel TES system for high temperature application is based on concrete. The company EnergyNest, located in Norway, developed in cooperation with HeidelbergCement a specialized concrete, called heatcrete. This heatcrete is supposed to fit for high temperature application, although the longevity performance has to be validated first. Tube bundles with e.g. thermal oil as HTM are placed in a cylinder of heatcrete, see Fig. 3 (a). A highly modular design aims at decreasing the costs.

However, due to thermal extension and stress, and the endurance of the HTM, the maximum temperature at this concept is limited at about 450 °C [13]. Due to a high volumetric heat capacity of 2 to 4 $\frac{\mathrm{MJ}}{\mathrm{m^3 \cdot K}}$ the limited temperature range can be compensated. If a direct heat exchange with a working fluid like water/steam is not feasible, thus a HTM is

needed, also the high heat conductivity of about 1.5 to 2.5 $\frac{\mathrm{W}}{\mathrm{m \cdot K}}$ cannot compromise the doubled terminal temperature difference. A pilot plant of this TES located at Masdar Institute in Abu Dhabi is already commissioned, see Fig. 3.

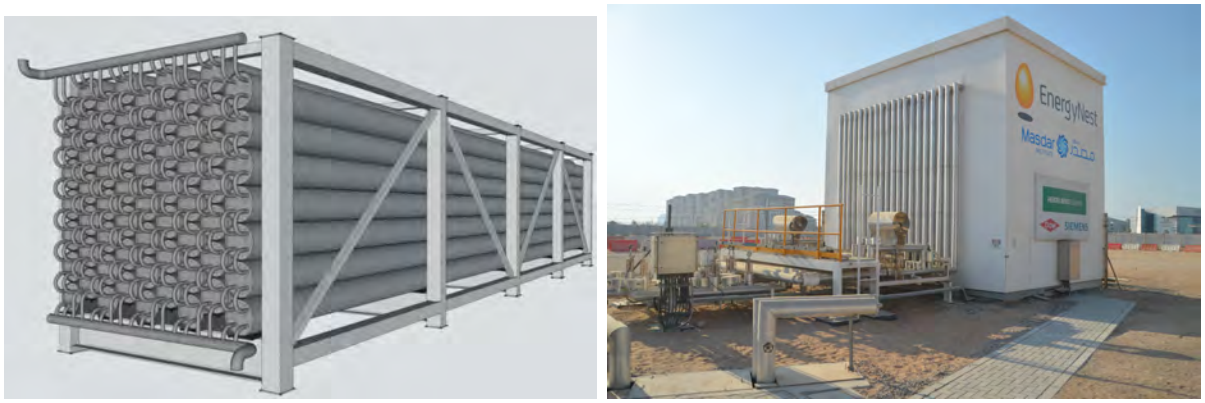

(a) Sketch of one EnergyNest module [13] (b) EnergyNest's pilot plant at Masdar Institute

Figure 3: EnergyNest's Heatcreate TES

Reflecting the previous TES technologies with all assets and drawbacks, there is room for new ideas and developments. The sandTES-technology, which this work is about, is envisaged to overcome several issues of the two technologies sketched above, like temperature limits, auxiliary consumption or ability for direct heat exchange with the working fluid.

1.3 Scope of the work

In this work, the basics of the sandTES technology are introduced. The principles of the concept and the key technologies are explained in detail. At first the benefits of using particles as HSM are outlined by investigating crucial parameters like energy density and costs. Second, the basic process of a standard two-tank TES-System, applied for the sandTES-concept, is explained. The key technologies making the sandTES-system uniquely efficient are explained in detail.

For experimentally validating simulations as well as for proofing the concept including the key technologies, the design and erection of a semi-industrial 280 $\mathrm{kW_{th}}$ pilot plant has been part of the work. A detailed description of this pilot plant's set-up is followed by first measurement results. These results are the most significant for a reliable and optimized further plant design.

Finally, various application cases concerning thermal power plants are suggested and analyzed in detail. The enhancement of flexibility and dynamics of coal-fired power plants is suggested to be improved by integrating a sandTES-system. Several options for implementing the TES in the power plant process for charging as well as for discharging are examined.

To lower the levelized cost of electricity (LCOE) of CSP plants, the replacement of the storage cycle and of the power cycle can be beneficial. Variants applying a sandTES-system as a cost-effective alternative to state of the art TES are analyzed.

2 SandTES Technology

The sandTES-technology is developed at the Institute for Energy Systems and Thermodynamics of TU Wien. As mentioned before, the main goal is to gain a TES system, which fits for highest temperatures - beyond the current maximum of about 560 °C of molten salt - and achieves enhanced energy densities at still low cost. All these aspects can be covered by solids.

This chapter introduces the fundamentals of the sandTES-technology, which are crucial for understanding the experimental investigations and the application analysis. More detailed theoretical background is provided by Schwaiger [26].

2.1 Heat Storage Media

Using particles as sensible heat storage medium (HSM) in a simple two tank system not only allows to exceed previous temperature limitations, but also reaching higher energy densities. Table 1 shows the key data of the most common sensible HSM and heat transfer media (HTM) in comparison to the most promising powders for use in a sandTES-system.

Table 1: Comparison of sensible heat storage media [2–5, 7, 8, 28]

Property	Unit	SiO_2	Al_2O_3	SiC	VP1	Na	SS
Minimum Temperature	°C	50	50	50	50	98	222
Maximum Temperature	°C	800	800	800	400	700	565
(Bulk) Density	kg/m^3	1265	1900	1605	894	836	1825
Mean Heat Capacity	kJ/m^3K	1357	2112	1699	1837	1110	2761
Energy Density	MJ/m^3	1038	1586	1276	514	614	824
Specific Cost	€/t	30 ÷ 90	1150	1200	6700	2800	1200
Levelized cost	€/MJ	37 ÷ 110	1378	1509	11653	3812	2658

The minimum temperatures are defined with 50 °C by means of an application-oriented perspective, excluding those media with an even higher minimum temperature. The first three columns show the data of the powders quartz sand (SiO_2), corundum (Al_2O_3) and silicon carbide (SiC), each with a mean particle diameter of about 80 microns. Therminol VP-1 is a widespread thermal oil used as HTM (and HSM) in industry and at power plants. Liquid sodium (Na) is envisaged as high temperature HTM e.g. at CSP plants, due to its high heat conductivity and the resulting lower thermal losses. As state of the art HSM - commonly used in CSP plants - the binary molten salt Solar Salt (SS), a mixture of 40 % KNO_3 and 60 % $NaNO_3$ (weight), is the current main competitor to novel particle-based TES-systems.

As it can be seen in Tab. 1, the material cost per thermal energy is much lower for the powders, especially for quartz sand, which is a strong argument for applying a particle-based TES, especially at large-scale applications. Due to the high temperature ranges also the energy densities are rather high, despite the low heat capacities. This can lead to a cost reduction for various plant components like storage tanks, heat exchangers or conveyors as long as high temperature steels can be avoided.

Figure 4 shows the volumetric heat capacities and the volumetric enthalpies of the same media presented in Tab. 1 in dependency of the temperature. The non-continuous line for quartz sand is a result of the quartz inversion at about 570 °C. Again, from an application-oriented point of view a minimum temperature was chosen for the volumetric enthalpies, if the real minimum temperature of the medium is not higher.

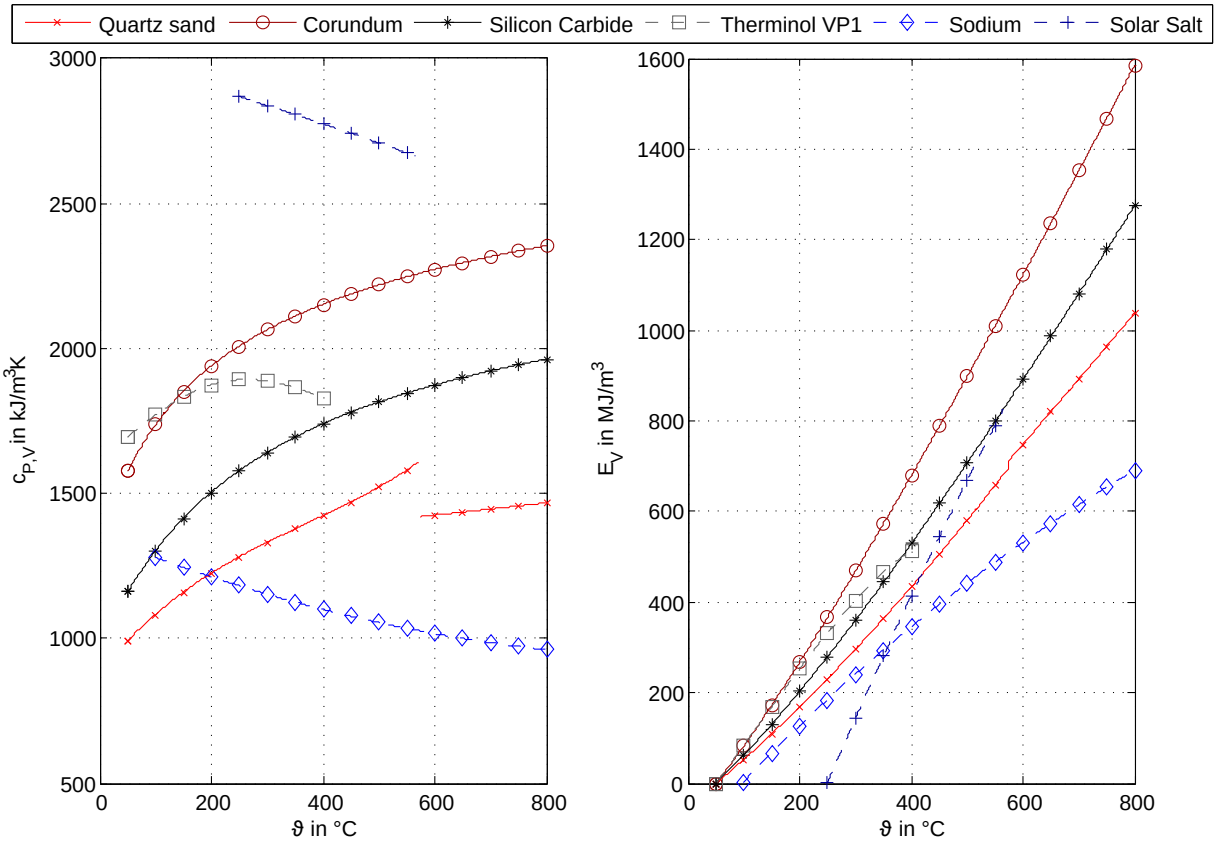

Figure 4: Volumetric heat capacity and energy density of various HSM [7,8,28,33]

In terms of energy density, corundum and silicon carbide even surpass Solar Salt, making them promising HSM.

2.2 Plant Setup

To introduce the principles of the sandTES concept, a simplified process flow sheet is shown in Fig. 5. The main components are the two tanks, at least one HEX and some conveyors. The HEX is pictured in top view in Fig. 5. As described in the next section in detail, fluidization technique is used for transporting the particles inside the HEX. Additional equipment for handling the fluidization gas - mostly air - is needed. At least blowers, recuperators, filters and induced draft fans have to be installed.

The charging process starts e.g. with a filled cold silo. The cold particles get fed to the inlet of the HEX by some conveyor e.g. a screw-conveyor. By running in horizontal direction through the U-shaped HEX, the particles get heated up by a working fluid,

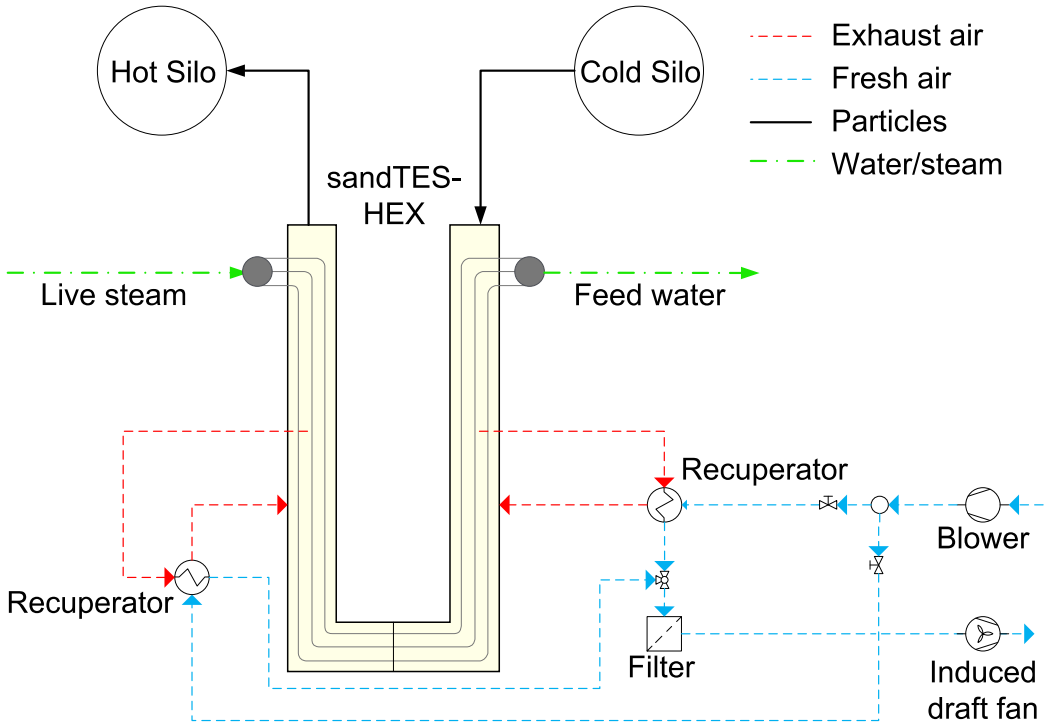

Figure 5: Simplified process flow sheet of the sandTES concept

which is contained in the tube bundle. At the end of the HEX, the hot particles fall down into e.g. a bucket conveyor and get transported upwards into the second silo.

On demand, all the flow directions of HSM and HTM simply can be reversed, to discharge the TES. Although the sandTES-technology provides bidirectional HEXs in which the flow directions of the working fluid and the particle suspension can be reversed, most of the applications analyzed in this study rely on two separate and specialized HEX.

The plant setup is completed by the blowers for fluidizing the fluidized bed HEX. Recuperators are used to minimize heat losses by the hot exhausted fluidization gas. At the end, the exhausted air leaves the system through a particle filter and an induced draft fan.

In Fig. 6 a typical sandTES setup, in this example for implementation at a thermal power plant for enhancing the plant flexibility, is shown. As it can be seen, a common two tank system with one HEX is applied. Depending on the application scenario and the given boundaries like maximum and minimum temperatures, different setup variations seem preferable. This especially concerns the conveying technology. For filling the tanks, thus transporting the particles vertically upwards, bucket conveyors or pan conveyors are preferred. However, bucket conveyors suffer from a rather low maximum temperature of about 300 °C, while pan conveyors need plenty of space, as a vertical transportation is not possible. Pan conveyors mostly are tilted in an angle of 30° to 60° to the horizontal. Recently a novel type of particle elevator was introduced, which is based on insulated bins, allowing components like the bearings to remain cold. This would suggest no need for tilted conveyors at high temperatures. If transportation by gravity is not suitable,

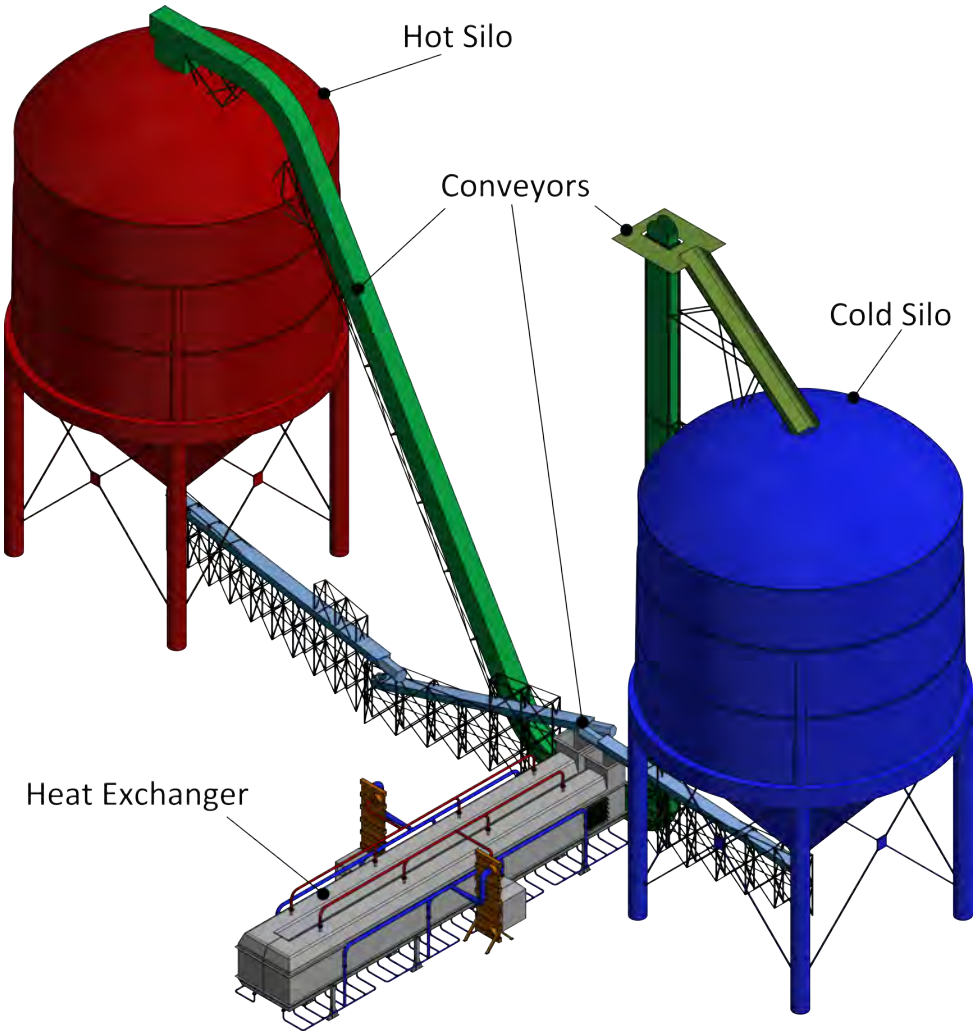

Figure 6: Typical sandTES setup [25]

horizontal transportation of the particles by screw-conveyors or vibrating troughs are needed.

2.3 Heat Exchanger

As mentioned above, the key part of the sandTES-technology is the particle-based HEX. The main challenge is to move the particles inside the HEX with as low as possible auxiliary power consumption. Furthermore, the heat transfer should proceed in an exergetically efficient way. Taking into account of these two claims a counter current HEX seems preferable, using fluidization technique for the particle transport. By fluidizing a particle bed, thus blowing e.g. air from the bottom to the top of the bed, the resulting particle-air suspension gets fluid-like behaviour. By inserting a particle mass flow on the one end and removing the same mass flow at the other end of the HEX, a height difference between in- and outlet results. With only this height difference between in- and outlet as the driving force, the particle-air suspension flows (similar to fluids) through a horizontal channel.

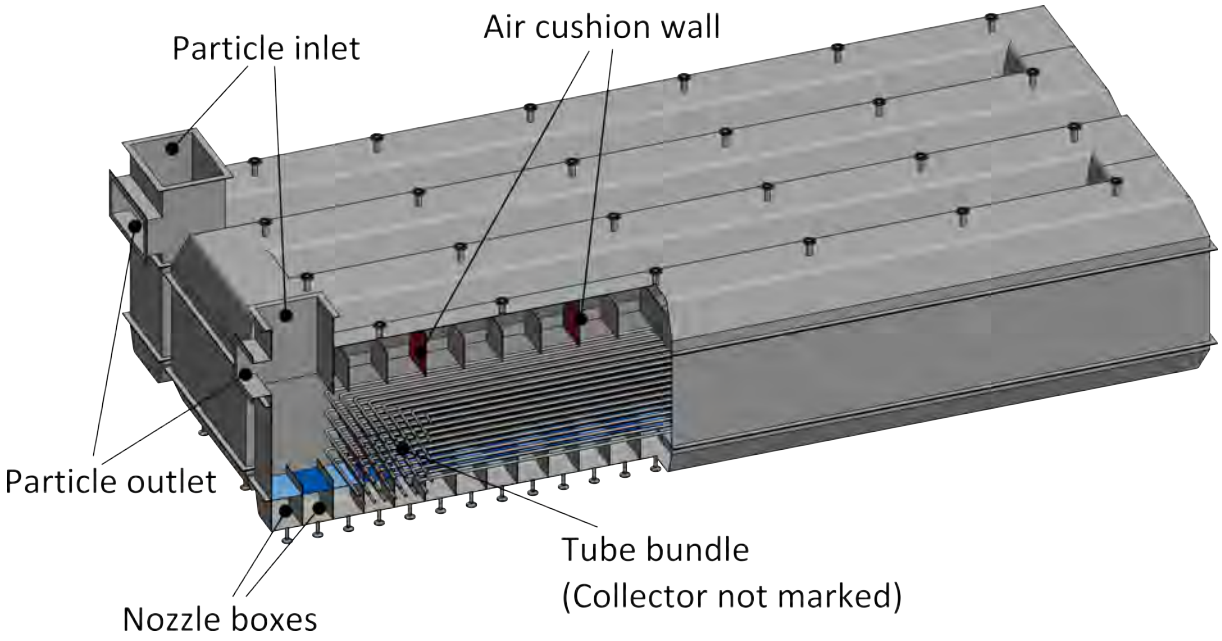

Figure 7: Principle sketch of a sandTES-HEX

An additionally inside the channel installed tube bundle, containing the according working fluid, leads to the postulated particle-based countercurrent HEX. Compared to a cascaded stirred tank as the common alternative, the heat transfer is exergetically more efficient [26]. A principle sketch, showing the HEX-construction with the channel as well as the tube bundle can be seen in Fig. 7.

So called wind boxes - simple tubes connected to the nozzle boxes at the bottom - provide air for fluidizing the bed. Each wind box is fed by one separate blower and recuperator. Every mixing box - a collector tube at the top used for leading away the exhausted air - has its own recuperator and induced draft fan. The nozzles and the according nozzle boxes are a constructive unit of the nozzle distributor floor, which is explained in the next section. Valves above the HEX are part of the air cushion technology, which is introduced at the end of the section.

To minimize the auxiliary consumption of the fluidized bed HEX, a low pressure drop through the bed and low mass flows are required. Figure 8 shows the typical pressure drop characteristic of a particle bed, depending on the mass flow of a fluid pushed from the bottom to the top.

At the first part of the graph, called the fixed bed area, the pressure drop through the bed Δp_b rises linearly with the increasing velocity u_{act} of the fluid. This can be seen at the modified Ergun Eq. (2) with the densities of the bed material ρ_p and the fluidization gas ρ_f, the porosity Ψ, the mean particle diameter d_p and the height of the bed ΔH_{fb} [32].

$$\Delta p_b = \left(\frac{17.3}{Re_p} + 0.336\right) \cdot \frac{\rho_f u_{act}^2 \Delta H_{fb}}{d_p} (1 - \Psi) \Psi^{-4.8} \tag{2}$$

The porosity is thereby defined as the fluid voidage fraction, see Eq. (3).

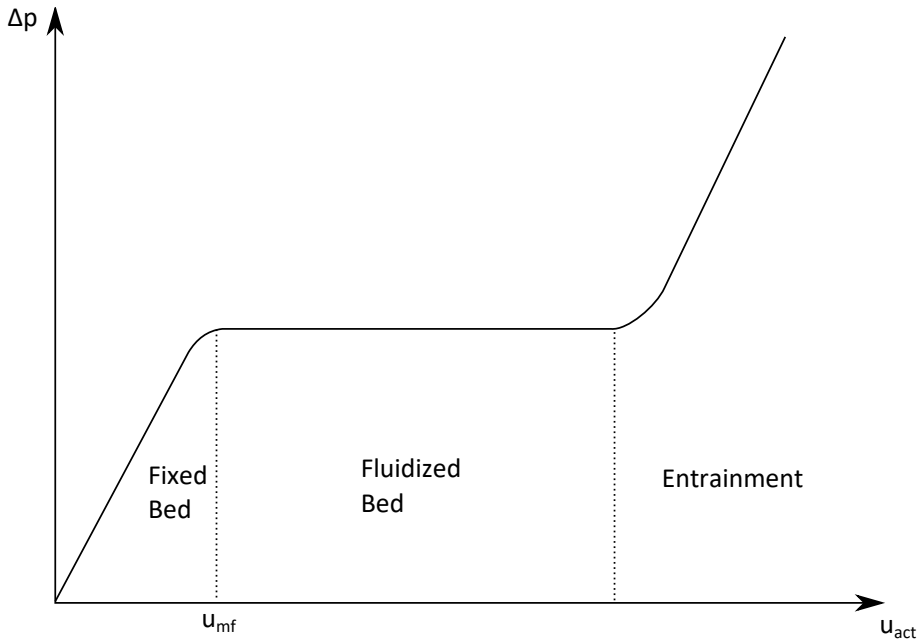

Figure 8: Pressure drop through a particle bed depending on the fluidization gas velocity

$$\Psi = 1 - \frac{V_p}{V_{fb}} = 1 - \frac{\rho_{fb}}{\rho_p} \tag{3}$$

The particles Reynolds number is calculated with the density ρ_f, the superficial velocity u_{act}, the kinematic viscosity ν_f of the fluid, and the mean particle diameter d_p as the characteristic length, see Eq. (4). A Reynolds number $Re_p <= 1$ characterizes a laminar flow, $Re_p > 1$ a turbulent flow.

$$Re_p = \frac{u_{act} d_p \rho_f}{\nu_f} \tag{4}$$

The next part of the graph in Fig. 8, called the fluidization area, is characterized by a constant pressure drop, despite an increasing fluid velocity. This area starts at the so called minimum fluidization velocity u_{mf}. The flow resistance of the fluid flow equals the weight of the bulk minus the buoyancy. The pressure drop through the fluidized bed Δp_{fb}, can be quantified with Eq. (5).

$$\Delta p_{fb} = (1 - \Psi)(\rho_p - \rho_f) g \Delta H_{fb} \tag{5}$$

The last part of the graph in Fig. 8 is characterized by again rising pressure drop. In this entrainment area particles get transported out of the fluidized bed by the fluidization fluid.

Compared to common fluidized beds known from power or chemical industries, the fluidization gas velocities in sandTES application remain in the range slightly above the minimum fluidization velocity. This minimum fluidization velocity again is depending on

various parameters, see Eq. (6). Several correlations are available, all based on the type of Ergun's equation, with C_1 and C_2 as experimental validated constants [32].

$$Re_{p,mf} = \sqrt{C_1^2 + C_2 * Ar} - C_1 \tag{6}$$

The Archimedes number therein is the ratio of the buoyancy force of the particles to the viscous forces of the fluidization gas, see Eq. (7).

$$Ar = \frac{d_p^3 \rho_f (\rho_p - \rho_f) g}{\nu_f^2} \tag{7}$$

For the considerations in this work, the particle diameter is the by far most important parameter for quantifying the minimum fluidization velocity. Low particle diameters lead to low fluidization velocities and overall to a low auxiliary power consumption.

Relying on Eq. (6) and several data for the constants C_1 and C_2, the following correlations are suggested in Yang [32].

Equation (8) shall be used at $Ar < 10^3$.

$$u_{mf} = 7.5 \cdot 10^{-4} \frac{(\rho_p - \rho_f) g d_p^2}{\nu_f} \tag{8}$$

Equation (9) fits best for $Ar > 10^7$.

$$u_{mf} = 0.202 \sqrt{\frac{(\rho_p - \rho_f) g d_p}{\rho_f}} \tag{9}$$

For characterizing the fluidization regime with a dimensionless number, the fluidization grade is introduced, see Eq. (10), with u_{act} as the superficial velocity and u_{mf} as the minimum fluidization velocity.

$$\mu = \frac{u_{act}}{u_{mf}} \tag{10}$$

For the sandTES-HEX a bubbling fluidized bed is preferred, to ensure a sufficient vertical mixing of the bed and thus a homogeneous temperature distribution in every cross section along the HEX. The particle diameters therefore have to be chosen according to Geldart's classification out of the groups A or B, see Fig. 9.

Geldart divides powders in four groups, depending on their particle diameter and the density difference of particles and fluid. Group A is characterized by a dense phase expansion before the bubbling fluidization while increasing the fluidization grade. Similar to that, group B directly starts with bubbling fluidization at the minimum fluidization velocity. The group C represents cohesive particles, which are very difficult to fluidize. In group D only stable spouted beds can be realized.

Coming back to the flow behaviour of the fluidized bed, the before mentioned height difference between HEX in- and outlet leads to an inclined bed surface along the flow axis

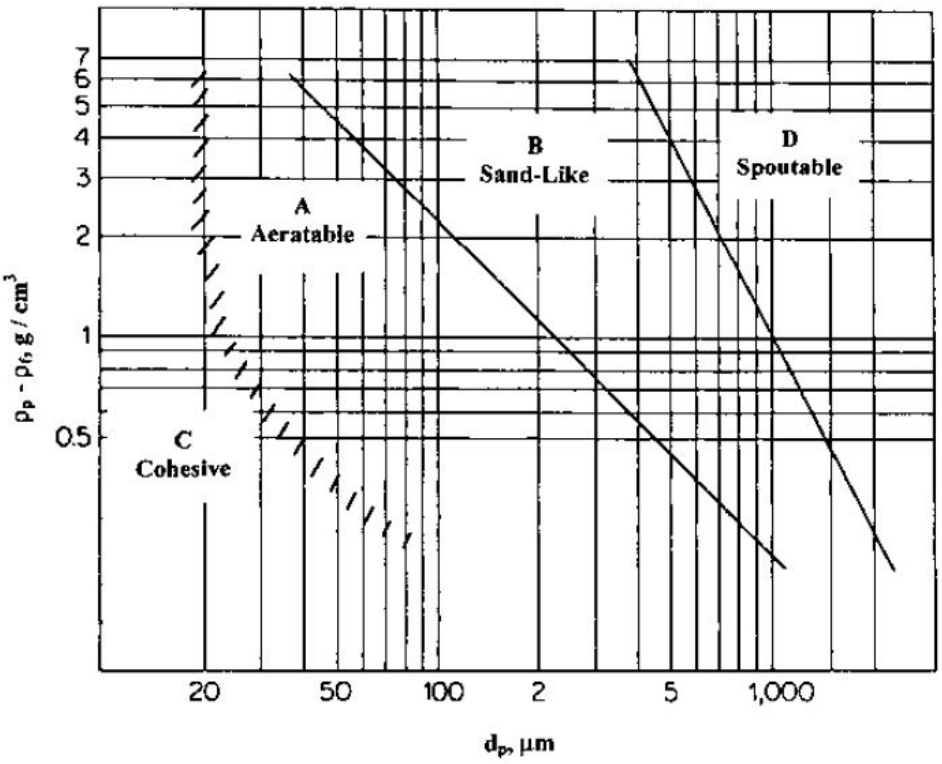

Figure 9: Geldart's classification of powders [32]

of the HEX. The associated height gradient depends on several fluidized bed parameters and of course the HEX geometry. The most significant fluidized bed parameters are the bed material with its particle size distribution, the fluidization velocity and the fluidization fluid. Regarding the HEX geometry the accumulated contact surface of the HEX walls and the tube bundle as well as fixtures or barriers influence the incline of the bed surface. Similar to fluids, the particle-air suspension inside the HEX-channel can be characterized with a (fictive) viscosity, which of course influences the mentioned inclination.

Looking at Fig. 10 a simplified scheme of a segment of a sandTES-HEX can be seen, with the sloped fluidized bed level and the tube bundle. Furthermore nozzles at the bottom, the key part of the nozzle distributor floor, are sketched as well as controlled valves at the top, implementing the air cushion technology.

Both these further on introduced key technologies are based on Eq. (11), with the pressure drops of the nozzles at the bottom Δp_{Nozzle}, of the fluidized bed in vertical direction Δp_{fb}, and of the controlled valves at the top Δp_{Valve}, which altogether have to be constant in every cross section of the HEX.

$$\Delta p_{HEX} = \Delta p_{Nozzle} + \Delta p_{fb} + \Delta p_{Valve} = const. \tag{11}$$

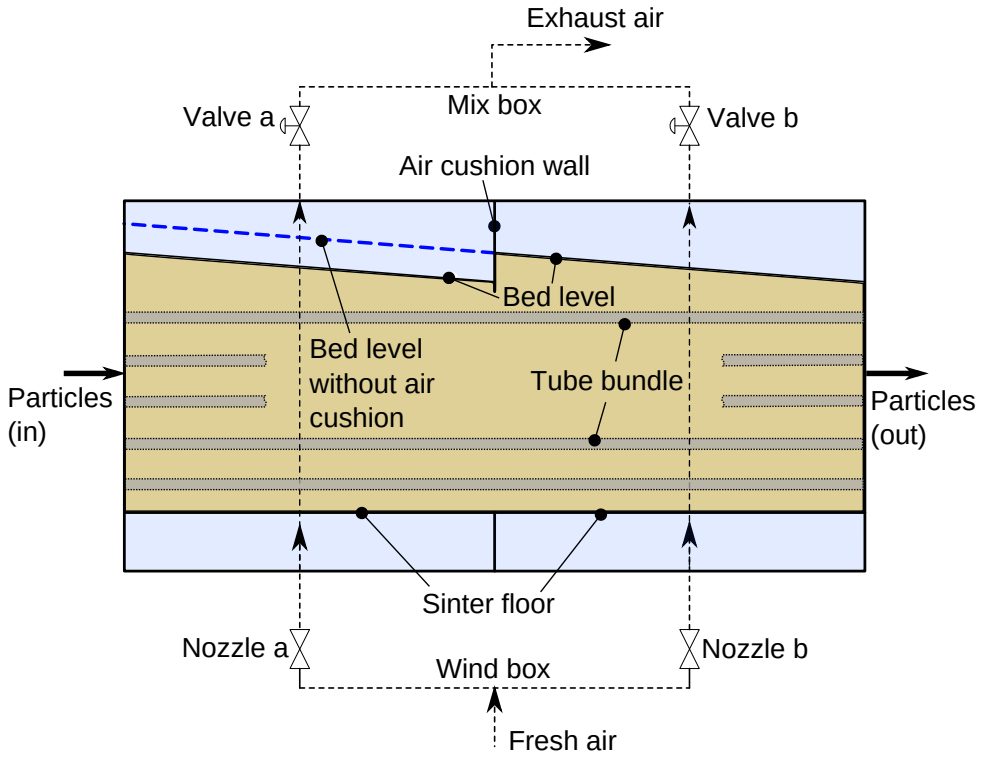

Figure 10: Sectional view of a sandTES-HEX [22]

2.3.1 Nozzle distributor floor

Looking back on Eq. (5), the vertical pressure drop through the bed is, at constant porosity and densities, only depending on the height of the bed. Obviously, as a result of the inclined bed surface, this vertical pressure drop differs along the flow axis of the HEX. The fluidization gas tends taking the easiest way. Because of the characteristics of fluidized beds (see Fig. 8) with a constant pressure drop independent of the fluidization velocity, the majority of the air mass flow would pass through the sections with lower bed height near the particle outlet (right hand side in Fig. 10). In the other cross sections of the fluidized bed, with air velocities below the minimum fluidization velocity, the bed would collapse. Thus, an odd air distribution along the flow axis of the HEX would be the result, leading to an unstable fluidization.

To ensure an even air distribution along the flow axis, it is necessary to change the overall pressure drop characteristic of the HEX Δp_{HEX}. For these first explanations, the pressure drop of the valves shall be neglected ($\Delta p_{Valve} = 0$), as it is only of importance for the air cushion technology.

The pressure drop Δp_{Nozzle} of orifice plates, for historic reasons referred to as nozzles, increases quadratic with increasing air velocities, see Eq. (12) with the pressure drop coefficient ζ and the superficial velocity at the corresponding nozzle u_{Nozzle}.

$$\Delta p_{Nozzle} = \zeta \frac{\rho_f u_{Nozzle}^2}{2} \tag{12}$$

Therefore, nozzles installed in series in front of the fluidized bed lead to the needed overall

pressure drop characteristic of the HEX, where the pressure drop in one cross section increases with an increasing air mass flow. Additionally, porous sintered plates, arranged in the so called nozzle boxes, slightly enhance the flow distribution with its pressure drop characteristic and retain the particles of plugging the nozzles.

2.3.2 Air cushion technology

Another issue accompanied by the inclined bed surface is the area above the tube bundle. Particles above the tube bundle are not participating at the heat exchange in a proper way. For enhancing the efficiency of the HEX as well as for reducing its size, these areas should be minimized. Another claim is to enhance the dynamics at reversing the flow direction of the fluidized bed. Therefore the air cushion technology was developed. An air cushion consists of gas tight chambers and the appropriate valves before the mixing box. Gas tight plates, which are immersed into the top of the fluidized bed, divide the upper section of the HEX in several chambers with different pressure levels, controlled by the valves.

Looking at Eq. (11), the focus is on the until now neglected pressure drop term of the valves ($\Delta p_{Valve} > 0$). To keep the overall pressure drop of the HEX constant, at least one of the terms of Eq. (11) has to decrease, if the additional pressure drop of the valves increases. This mainly concerns the pressure drop for the fluidized bed. Regarding Eq. (5), mainly the bed height in the appropriate section has to fall, to lower this pressure drop.

The number of nozzle boxes and air cushions in Fig. 10 was just chosen for illustrating the principles of both technologies. In reality, these two numbers differ from each other. Furthermore, an economic optimum has to be found.

3 Experimental Investigations

In the experimental part of this work, the focus is on proving the sandTES concept by measurements at the pilot plant, see Fig. 11. Especially for the core of the technology - the fluidized bed HEX - fundamental measurement results are required to find optimization criteria for future large-scale plant designs.

Figure 11: Overview of the pilot plant at Arsenal Vienna

The sandTES pilot plant basically is designed for two test phases. The first test phase concentrates on phenomena concerning the flow parameters and stability limits of the fluidized bed. In this phase, the pilot plant is run cold, thus without heating.

A second test phase deals with several heat transfer related parameters. For these hot tests a 280 kW_{th} thermal oil plant is envisaged for powering the sandTES HEX. Unfortunately this second test phase is not part of this thesis, as the final modifications of the pilot plant for hot test are not finished at the time of writing. However, future work will provide significant data of the temperature distribution inside the HEX as well as the corresponding heat transfer coefficients.

3.1 Pilot Plant Set-up

For a full proof of the sandTES concept, a pilot plant in a semi-industrial scale was erected at the institute's laboratory site. Figure 12 shows a scheme of the pilot plant with its main

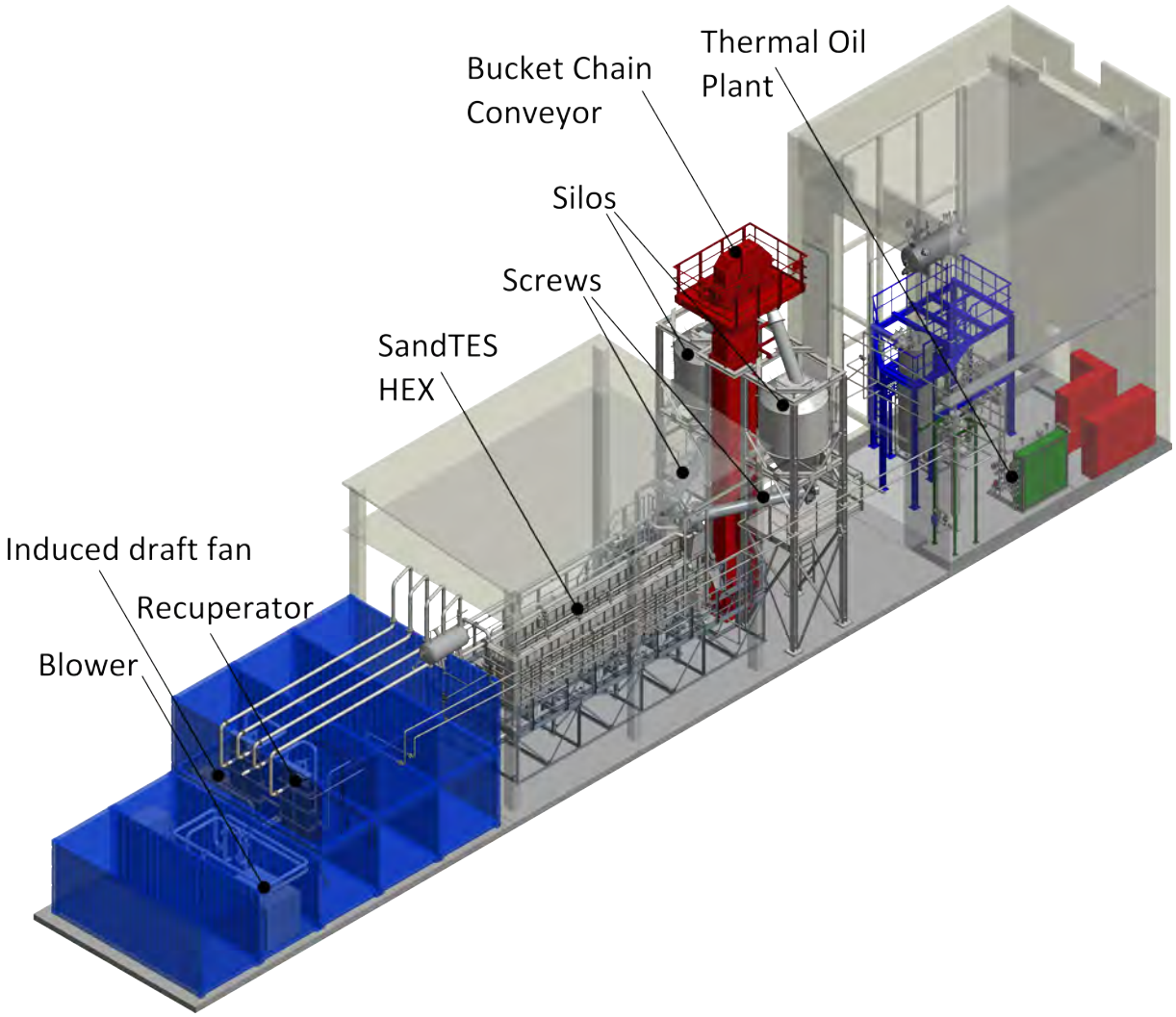

Figure 12: Overview of the sandTES pilot plant at Arsenal Vienna [22]

components. If not explicitly mentioned, all the main parts of the plant are made out of the unalloyed heat-resistant steel 1.0345 (P235GH) and are designed for a maximum temperature of 390 °C, limited by the maximum temperature of the thermal oil plant.

The heart of the plant, the fluidized bed HEX is installed beneath a roof in the center of the installation. Right next to the HEX, in Fig. 12 on the right-hand side, the conveying units, namely the bucket chain conveyor and the two screws, as well as the storage silos are positioned. The equipment needed for fluidization is located in the container-arrangement on the other side. Figure 13 shows a detail of the central pilot plant components, excluding the fluidization aggregates and the thermal oil plant. The dimensions of this components are in the range of 13 m height with a ground area of approximately 86 m^2.

Before explaining the key components of the plant in detail, its functionality is introduced by reference to Fig. 14. Similar to the explanations in the previous section, a two tank system, but with a bi-directional HEX, is applied. Only one bucket chain conveyor transports the particles into a silo, which can be selected by a switch. Each silo is connected to the corresponding particle-inlet of the HEX by a conveying screw, which is

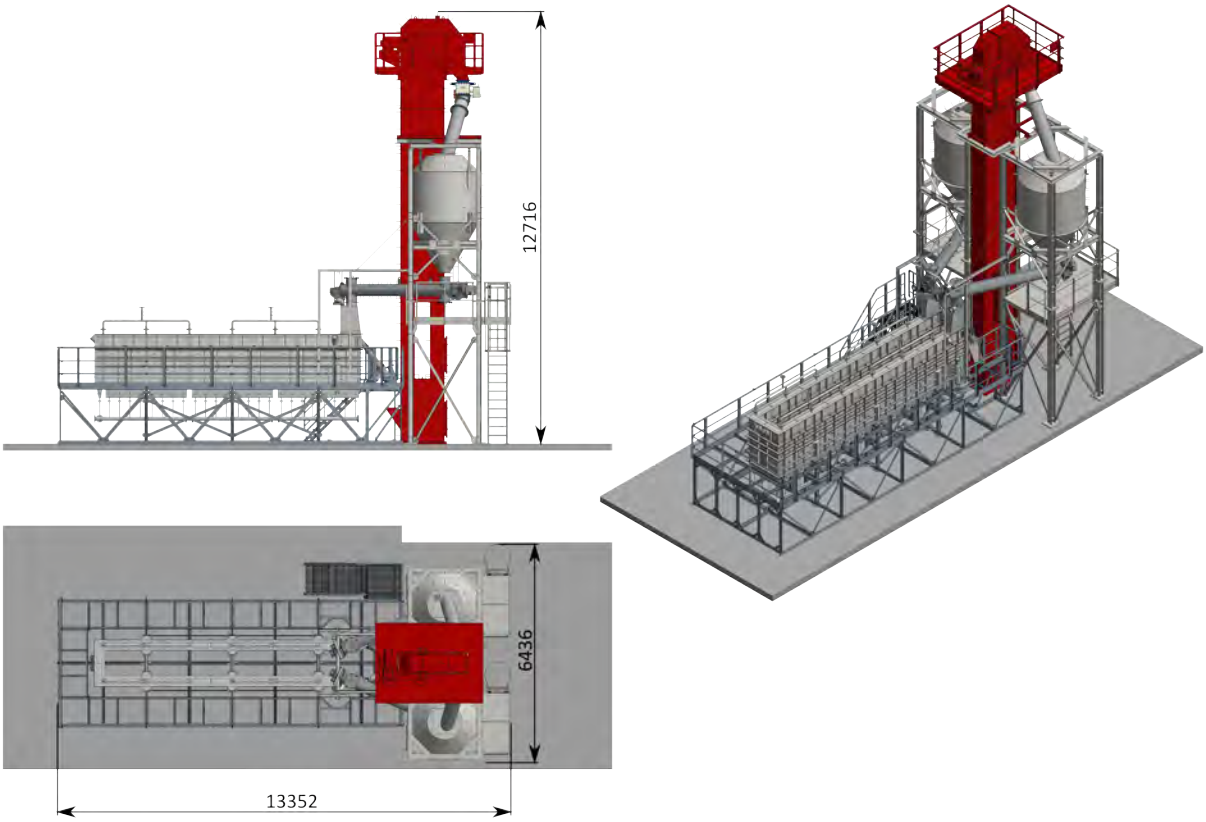

Figure 13: Detail of the sandTES HEX including conveyors and silos

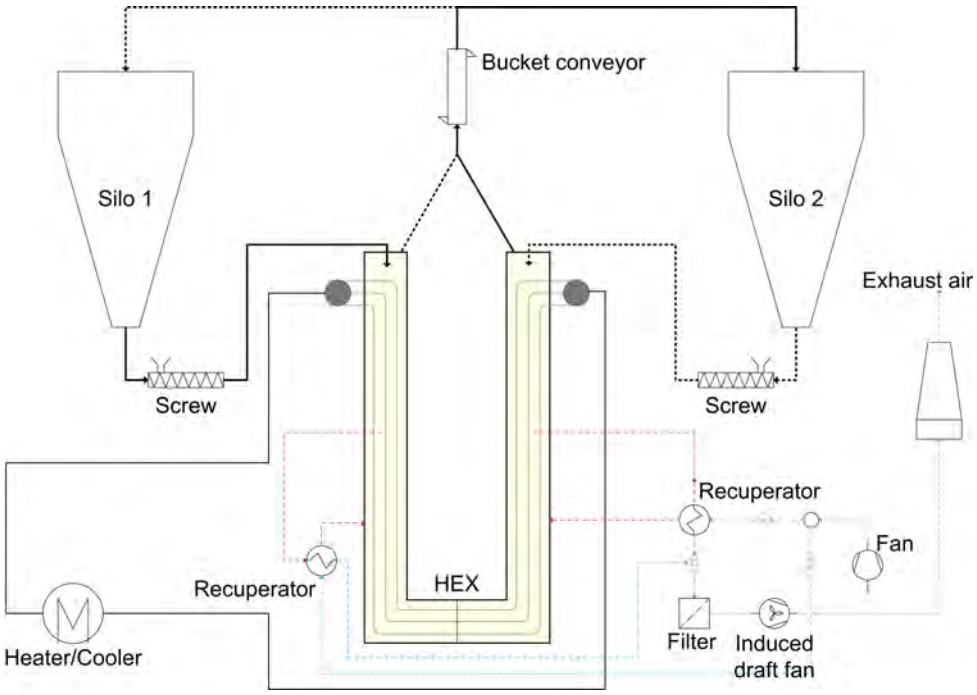

Figure 14: Process flow sheet of the sandTES pilot plant [23]

also responsible for controlling the particle mass flow. The emptying of the particles from the HEX outlet to the bucket chain conveyor is achieved by a simple chute.

The air supply of the HEX is divided into two wind boxes. Normally, two blowers are necessary, for assuring independent pressure and mass flow in each of these two feed lines. As the energy demand of the pilot plant is not crucial for the test purpose, a more energy consuming alternative was applied. Two orifices with appropriate valves lead to a sufficient result, but with one less blower. However, a port for a later upgrade of a second blower is applied in the piping. For recovering the heat from the exhausted fluidization gas, two recuperators constructed as plate heat exchangers, are installed. Afterwards, the exhausted air leaves the system through a combined filter and induced draft fan.

The key components of the pilot plant are introduced further on in detail. For the completeness of these following explanations, the basic information about the plant in its hot test configuration is provided too.

3.1.1 Heat Storage Medium

As described in the previous section, various solid materials are envisaged for the use in a sandTES system. Also for the pilot plant, various powders can be used for testing. At the beginning, quartz sand with a mean particle diameter of about 87 microns is applied. The sieve analysis is summarized in Table 2.

Table 2: Sieve analysis of the used particles

Fraction mm	Amount %	Pass through %
> 0.140	0.00	100.00
0.100 - 0.140	0.12	99.88
0.075 - 0.100	73.73	26.15
0.071 - 0.075	10.43	15.72
0.063 - 0.071	9.55	6.17
0.040 - 0.063	6.13	0.04
0.000 - 0.040	0.04	0.00

The most relevant data of the used quartz sand are listed in Table 3.

Table 3: Key data of quartz sand

Description	Unit	Value
Density	kg/m^3	2650
Melting Point	°C	1723
Quartz inversion	°C	574
Mean grain size	μm	87
Specific surface	cm^2/g	266

Due to the high energy density (also see Fig. 4) corundum seems to be a promising material and will be tested in later measurement series.

3.1.2 Heat Exchanger

The main focus of the experimental work is on the fluidized bed heat exchanger. A detailed image of the sandTES-HEX can be seen in Figure 15.

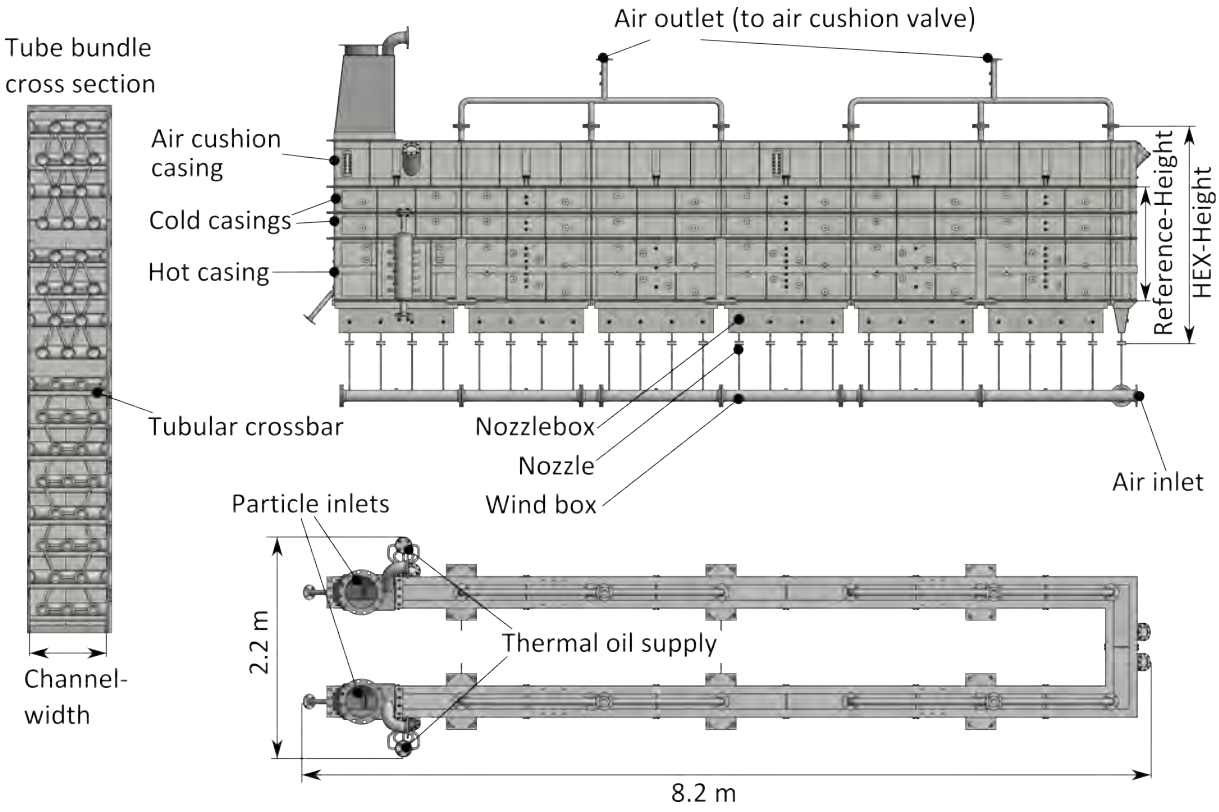

Figure 15: Overview of the pilot plant's HEX

Typical for the sandTES technology, the HEX basically consists of a channel, with a nozzle distributor floor at the bottom and some air piping at the top. The design maximum pressure was set to an excess pressure to the ambient of 300 mbar. Inside the channel, a tube bundle is applied, in this case with a staggered alignment. This staggered alignment prevents the fluidization air from simply passing through the bed vertically and enlarging the blind area above the tubes.

The axial length of the HEX is about 16 m, with a channel width of 150 mm, see Tab. 4. The minimum height of the whole HEX accumulates to 1650 mm, if the two cold casings, each containing 10 dummy tubes, are removed. Only the 20 tubes installed in the basis of the HEX, the hot casing, would remain. In contrast to the dummy tubes, these 20 tubes are proposed to be fed by thermal oil to be used for heating and cooling.

Including both the 250 mm high cold casings, the overall height of the HEX is 2115 mm. The cold dummy tubes just are built-in as hindrances to investigate the behaviour of the fluidized bed at various HEX heights.

For all the tubes, including the heated tubes as well as the dummy tubes, the same geometry pattern is applied. The corresponding data are listed in Table 4 too.

Table 4: SandTES-HEX geometry data [22]

Description	Unit	Value
Elongated length of HEX	m	16
Height of HEX	m	2.1
Width of HEX-channel	mm	150
Reference cross section	m^2	0.15
Number of wind boxes	–	1
Number of mix boxes	–	1
Number of nozzle Boxes	–	52
Nozzle diameter	mm	5
Number of air cushions	–	4
Outer tube diameter	mm	25
Wall thickness	mm	5
Tube number horizontal	–	3
Tube number vertical	–	16
Horizontal tube bundle pitch	mm	50
Vertical tube bundle pitch	mm	62.5

As it can be seen from Fig. 15, the tubes are fixed to each other by tubular crossbars. The complete tube bundle is mounted on the HEX sidewalls by horizontal tubular crossbars. To gain a segment of a quasi-infinite HEX, thus to reduce the influences of the walls, halved dummy tubes are additionally implemented at these sidewalls. These furthermore prevent the air from passing through the bed near the walls.

The nozzle distributor floor beneath the hot casing mainly consists of the wind boxes, orifices and the so called nozzle boxes. As already explained, a wind box is a simple tube, in this case with an outer diameter of 114.3 mm. Several outlets are running to the (here 52) orifices, which are spread along the flow axis. In the pilot plant case, the HEX with its two paths has the ability to be fed by one or alternatively two wind boxes. Above the orifices, the appropriate nozzle boxes are positioned. As a constructive unit, a nozzle winnow was designed, each containing four nozzle boxes, which can be seen in Fig. 16. This nozzle winnow has four, to each other gas tight separated chambers, with an air inlet pipe at the bottom and a porous sintered plate at the top.

The air cushion casing at the top consists of twelve to each other air tight chambers. The bottom of these chambers is open. The air cushion chamber walls, which are about 2 cm immersed into the fluidized bed, allow different air cushion pressures along the HEX.

As the particle inlet of the HEX is a neuralgic spot, the two ends of the HEX are not equipped with air cushions. Feeding particles inside a pressurized vessel is a challenging task, especially at altering temperatures. For this reason, the inlets on both ends of the HEX are not constructed as air cushion. In comparison to the air cushions, the pressure drop of the valve is substituted by an additional pressure drop through the fluidized bed. In other words, by leaving out the air cushion technology, the fluidized bed reaches its original height, with ambient pressure above the bed level.

On the top of each air cushion chamber, an outlet flange is assigned, running to the air cushion valve. After these valves, similar to the wind boxes, the so called mix boxes

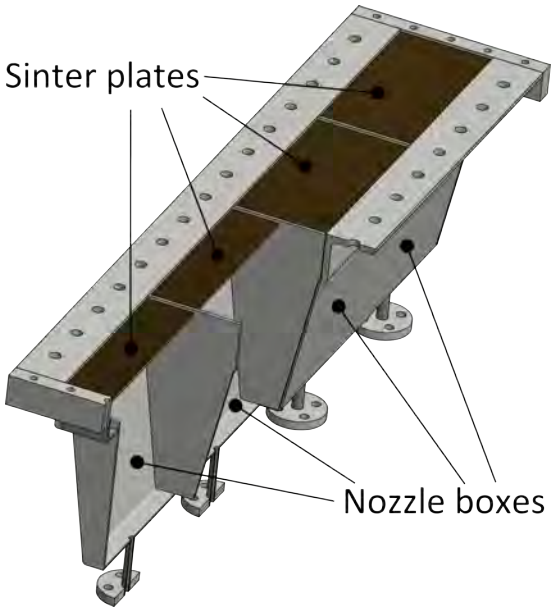

Figure 16: Detail of one pilot plant nozzle winnow

collect the fluidization air and direct it back to the recuperators. Again, two mix boxes are installed at the pilot plant, which also can be combined to one mix box.

Several vertically aligned hindrance plates at the bottom and the top of the HEX are installed for forcing the particles to flow as near as possible to the tube bundle. For installing the appropriate measurement equipment, numerous half-inch connectors are applied all over the HEX. The most relevant are the pressure sensors, which are provided with scavenging air, to prevent the connecting pipes from plugging. If all the other parameters can be specified, height differences of the fluidized bed can be calculated based on the appropriate pressure drops, again see Eq. (5). To directly monitor the bed height and validating the porosity, various sight glasses are built-in around the HEX.

When starting with the hot test phase, additional temperature sensors (Pt100) can be installed. The HEX, similar to the other hot operated components of the plant, are prepared for an insulation with a thickness of up to 200 mm.

3.1.3 Fluidization equipment

The fluidization equipment includes the blower, the recuperators, the induced draft fan, a filter, and of course the piping and valves. Figure 17 shows the main air components located in the container-arrangement. The induced draft fan already includes the cartridge filter.

Similar to the HEX, all the pipes needed for feeding as well as leading away the fluidization gas, are made out of the unalloyed heat-resistant steel 1.0345 (P235GH) with an outer diameter of 114.3 mm. The principle flow arrangement of the air piping again can be looked up in Fig. 14.

The same kind of half-inch connectors as at the sandTES-HEX for mounting the measurement equipment is spread all over the piping. Additionally to the pressure and

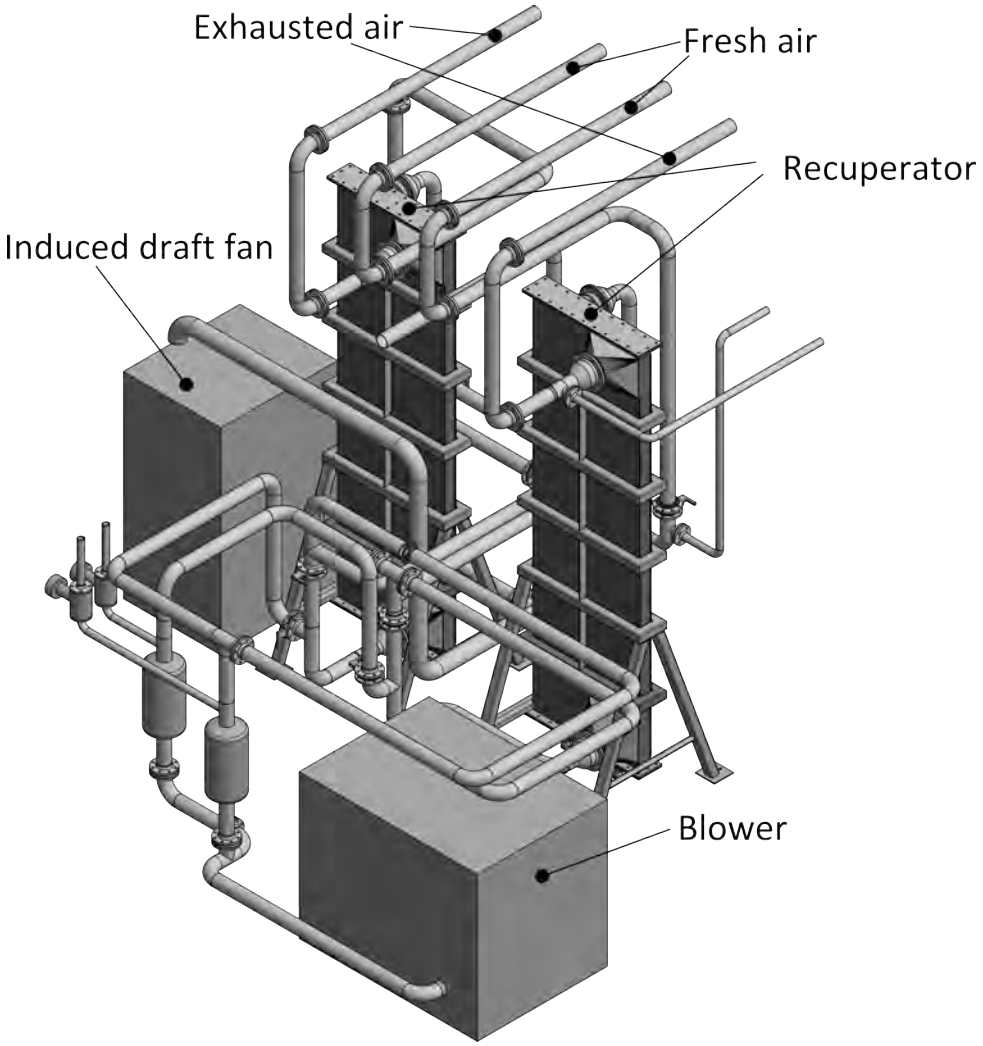

Figure 17: Overview of the main fluidization components

Table 5: Data of the measurement equipment [22]

Measurand	Principle	Type	Unit	Range	Accuracy
Pressure	Piezoelectric	Kalinsky DS2	mbar	$0 \cdots 250$	1.7 %
Pressure	Piezoelectric	Kalinsky DS2	mbar	$0 \cdots 10$	2.7 %
Temperature	Resistance thermom.	Pt100A 4L	°C	$-50 \cdots 400$	1 %
Air mass flow	Hot-wire anemom.	Höntzsch TA10	$(\mathrm{m/s})_\mathrm{n}$	$0.2 \cdots 60$	2.5 %
Mass	Load cell	Bosche S21N	kg	$0 \cdots 2000$	1 %

temperature sensors (Pt100), two mass flow sensors are applied near the blower, for quantifying the mass flow in both of the feed lines. These mass flow sensors basically are hot-wire anemometers, directly putting out a signal, which is proportional to the air mass flow.

The key data of all the used sensors of the pilot plant are listed in Tab. 5. The load cells are used for quantifying the particle mass in the silos.

In Tab. 6 the key data of the blower, the recuperators and the induced draft fan are

Table 6: Nominal data of the air components

Description	Unit	Blower	Recuperator	Induced draft fan
Quantity	-	1 (2)	2	1
Type	-	Rotary blower	Plate HEX	Cartridge filter
Mass flow	g/s	225	143	1078
Standard volume flow	$(m^3/h)_n$	626	397	3000
Pressure difference	mbar	500	8/7	15
Electric power	kW_{el}	18.5	–	3.0
Sound pressure level	dB(A)	70	–	72

summarized.

For feeding the pilot plant with the fluidization air, at least one blower is needed, wherefore an Aerzen-GM 10 S rotary blower is applied. Regarding the maximum mass flow rate, the implemented solution with two additional outlet valves in the feed lines for guaranteeing independent mass flows and pressures is sufficient for most of the tests. As mentioned before, a second blower can be upgraded at any time.

The two recuperators, built as plate heat exchangers out of stainless steel 1.4301 for preheating the fluidization air in the hot operation mode, have been supplied from GEA Ecoflex GmbH (now Kelvion PHE GmbH).

As explained before, the particle-inlets of the pilot plant have to end with ambient pressure, to avoid the problematic of feeding particles into a pressurized vessel. However, this is the reason, why an induced draft fan is needed, as the pressure drops of the piping, the recuperators and the filter have to be overcome. The Air-Jet DF4 from Air-Fresh-Service Industriefilter GmbH is a combination of a fan and a cartridge filter.

3.1.4 Conveyors

For transporting particles up from the HEX outlet to the silos, a bucket chain conveyer is installed, including a switch for choosing one of the silos to be filled. For emptying the silos and adjusting the particle mass flow, each silo is closed at the bottom by a conveyor screw. This principle was already illustrated by means of Fig. 14. The main data of the bucket chain conveyor and the two screws is presented in Tab. 7. A view of this conveyor arrangement can be seen in Fig. 13.

Table 7: Nominal data of the Conveyors

Description	Unit	Bucket chain conveyor	Screw Conveyor
Quantity	-	1	2
Maximum mass flow	kg/s	10	10
Maximum temperature	°C	400	
Electric power	kW_{el}	7.5	3
Conveying distance	m	10.0	3.0

The bucket chain conveyor operates with a constant rotational speed and is always ready for feeding the maximum mass flow up to the silos. As the screws are needed for controlling

the particle mass flow, these are supplemented by a frequency inverter. All the conveyor components have been delivered from EMDE Industrie-Technik GmbH.

3.1.5 Storage Silos

The design of the two storage silos was carried out relying on DIN 1055-6 (2005). With an outflow angle at the cone of 60° to the vertical, core flow cannot be reached. However, fixtures inside the silo improve the drain off behaviour of the particles. The design data of the storage silos, each one able to contain about 650 kWh_{th} of thermal energy at a temperature range of 25 to 390 °C, are listed in Table 8. In Fig. 13 the silos can be seen in the conveying arrangement.

Table 8: Design data of the silos

Description	Unit	Value
Quantity	-	2
Height bin	m	3.5
Inner diameter bin	m	2.0
Cone angle	°	60
Total Height	m	9.0
Sand capacity	t	8.0

Silos bridging can be a crucial issue, impacting the availability and performance of the whole plant. However, for fine powders it is not too much of a problem, as long as moisture can be avoided. Additionally, oil-free compressed air can be inserted at the cone, for loosening the sand bed inside the silo.

Each silo bin is hanging on its framework, connected by load cells for the mass measurement. The quantification of the mass flows fed into the HEX is achieved by measuring the particle mass inside the silos with these load cells in dependence of the time. For measuring the temperature distribution inside the silo's sand bed, several temperature sensors are applied at the silos. For maintenance a hatch on the top of the silo is installed.

3.1.6 Thermal Oil Plant

For the planned hot test phase, heater and cooler are needed. The thermal oil Therminol VP-1 is used as heat transfer medium inside the HEX's tube bundle. The key data of the installed thermal oil plant (see Fig. 18) are summarized in Tab. 9.

The thermal oil plant from HTT energy GmbH is powered by seven 40 kW_{el} electric heating elements, which together with several fittings and the primary pump are implemented in the primary circuit (right hand side of Fig. 18). Two water/thermal oil coolers for removing the thermal energy out of the system and relieving it to the ambient with air coolers on the roof, are installed in the secondary circuit (left hand side of Fig. 18). Furthermore, several fittings, the secondary pump and a reversion device are implemented in the secondary circuit. An expansion tank is applied at the highest point of all oil filled parts above the secondary circuit.

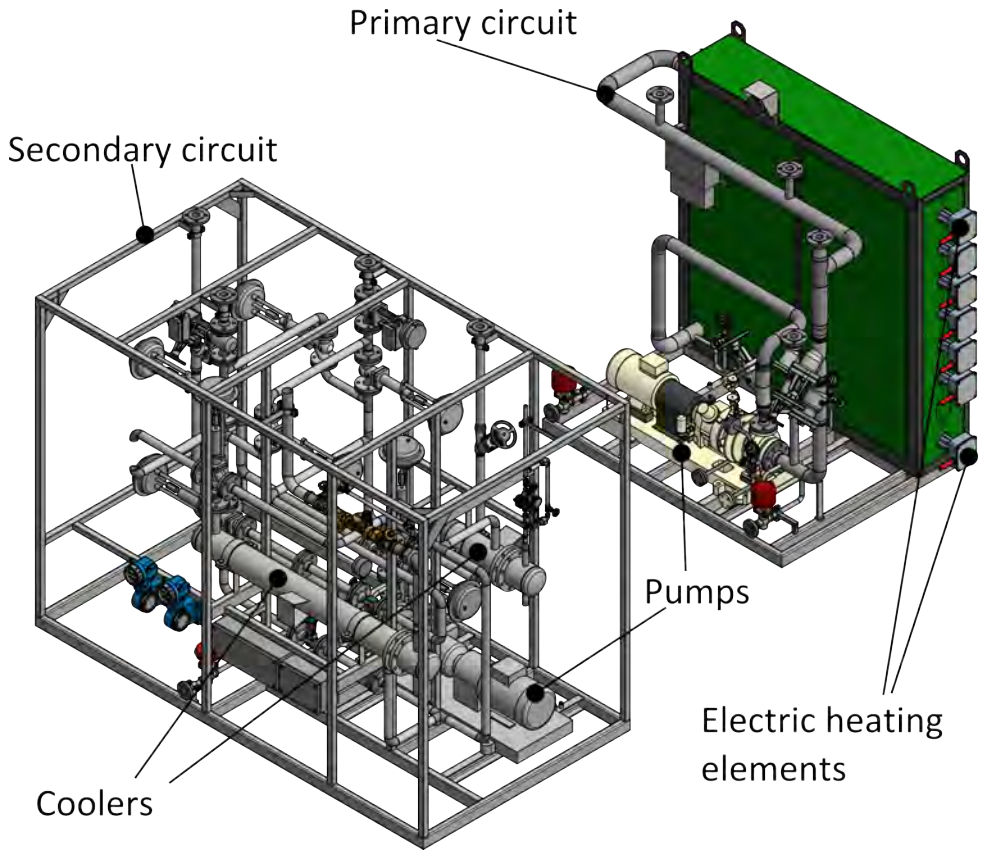

Figure 18: Overview of the thermal oil plant

Table 9: Key data of the thermal oil plant

Description	Unit	Value
Heat transfer medium	-	Therminol VP-1
Maximum temperature	°C	390
Heater power	kW_{th}	280
Cooler power	kW_{th}	200
Maximum operating pressure	bar	11
Maximum allowable pressure	bar	16
Mass flow	m^3/h	$0.6 \cdots 6$

3.1.7 Process Control System

For all measurements and for controlling the plant, a process control system (PCS) from Bernecker + Rainer Industrie Elektronik Ges.m.b.H. was installed. The used CPU X20CPU1585 is running independently from a dedicated PC with its operating system called Aprol. This operating system is used for controlling the plant and preparing the measurement data. A screenshot of the operating system can be seen in Fig. 19.

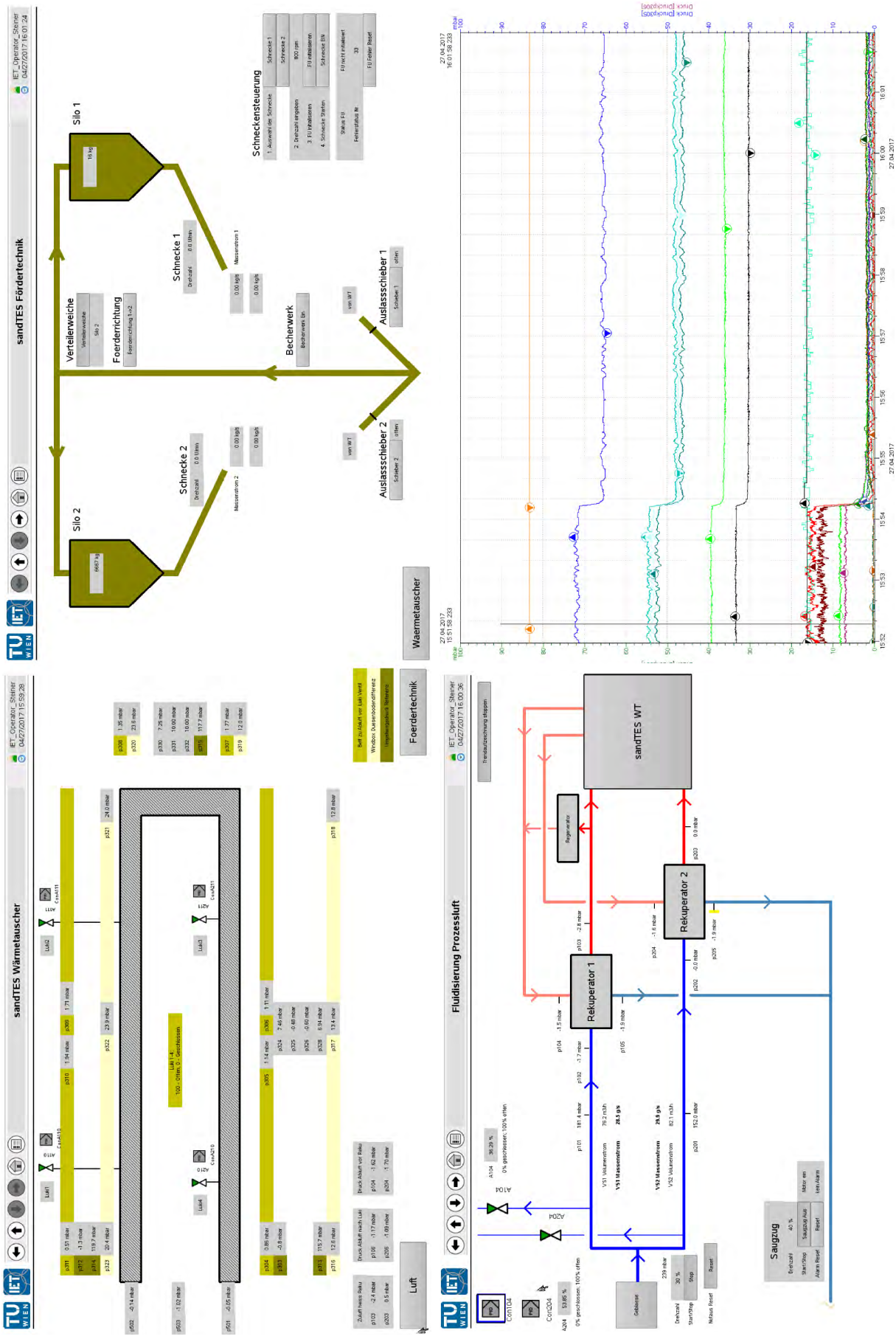

Figure 19: Screenshots of the APROL PCS

3.2 Measurement Results

Before presenting the main results of the pilot plant measurements, a short back view to previous test rigs and simulations is provided in **Paper 1** and **Paper 2**. The main achievement of the sandTES-technology and its HEX is a horizontal plug flow of the fluidized bed, which allows a counter current heat exchange with an appropriate tube bundle in a highly flexible way. For gaining first design parameters and proving the concept in small-scale, a plexiglass test rig was constructed. By performing tests with coloured sand, the key technologies and also the realization of the aforementioned plug flow could be validated. The mixing behaviour of the fluidized bed was observed with the desired outcome of sufficient vertical mixing and only limited horizontal mixing. These results are in good agreement to simulations performed with the commercial code Barracuda, which is based on the multiphase Particle-in-Cell method. These simulations lead to some early optimization ahead of the pilot plant design.

The first significant measurement results of the sandTES pilot plant are presented in **Paper 2**. As already introduced, the cold test phase provides crucial information about the flow behaviour of the fluidized bed inside the sandTES-HEX. The dependency of the height difference between in and outlet, thus the backlog, as well as the dynamic behaviour is the base of an optimized HEX design. **Paper 2** summarizes the actual experimental setup used for these cold tests. The key results and the conclusions drawn are presented.

The backlog measurements have been carried out by measuring the pressure drop through the fluidized bed at various fluidization grades μ and particle mass fluxes G_p. The pressure difference $\Delta p_{fb,io}$ was built of a measuring spot slightly above the nozzle distributor floor at both ends of the HEX and the corresponding pressure in the wind boxes above.

As a result a regress-function was found (see Eq. (13), which is valid in the range of about $\mu = 3.7 \cdots 5.5$ and $G_P = 0 \cdots 25 \frac{kg}{m^2 \cdot s}$.

$$\frac{\frac{\Delta p_{fb,io}}{mbar}}{\frac{l_{HEX}}{m}} = 0.60 - 0.07 \cdot \mu + 0.17 \cdot \frac{G_p}{\frac{kg}{m^2 \cdot s}} - 0.01 \cdot \mu \cdot \frac{G_p}{\frac{kg}{m^2 \cdot s}} \tag{13}$$

The corresponding measurement data are plotted in Fig. 20.

The marked measurement points represent the mean value of the backlog for both flow directions. Figure 20 (a) shows the backlog depending on the fluidization grade at various mass fluxes. Vice versa, Fig. 20 (b) shows the backlog depending on the mass flux at various fluidization grades. As expected, a higher fluidization grade leads to a lower viscosity of the fluidized bed and thus to a lower backlog. A higher mass flux obviously results in a higher backlog, as the flow velocity of the fluidized bed rises. The maximum backlog $\Delta p_{fb,io}$ at the examined operating points is below $4 \frac{\text{mbar}}{\text{m}}$, which is in the same range as at previous test rigs [10]. It has to be mentioned, that these tests are strongly depending on the fluidization regime, which relies on the nozzle distributor floor design. The current tests have been performed with one wind box, one mix box and inner nozzle diameters of 5 mm.

In Fig. 20 (a) for the values at $G_p = 0$ can be seen, that a slight backlog results, despite the missing particle mass flow. Thus, also at a theoretically even bed level, a difference of the pressure drop $\Delta p_{fb,io}$ occurs, which is a result of imperfections in the HEX construction.

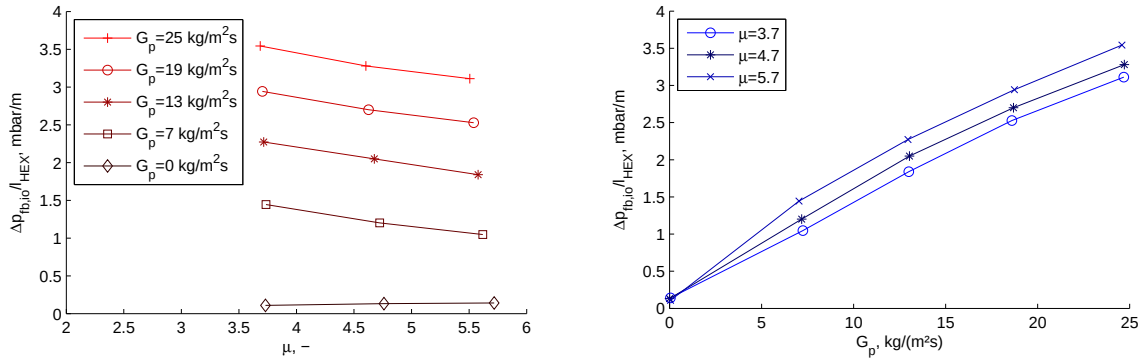

(a) Dependency of the fluidziation grade

(b) Dependency of the mass flux

Figure 20: Backlog measurements

The maximum mass flux of 25 $\frac{\text{kg}}{\text{m}^2 \cdot \text{s}}$ in these test series can be further increased. However, the increasing bed level at the inlet leads to a higher risk of entrainment over the exhaust gas piping and thereby limits the operating performance.

Paper 2 also provides a rough estimation of the load change characteristics. The time span for reaching a steady state was measured at certain operating conditions. It was thereby proven, that the flow direction can be reversed immediately and the corresponding steady state can be reached within a few minutes. For speeding up these reversing processes, it seems preferable to run with increased fluidization grades, as thereby a higher viscosity can be expected. More detailed measurements for improving the HEX dynamics are envisaged.

In future, tests with removed cold casings as well as with different HSM (e.g. corundum) are planned. Finally hot tests shall follow, for completing the measurements by investigating heat transfer coefficients and temperature distributions.

4 Application Concepts

In this section several application scenarios for the sandTES technology are introduced, with a focus on thermal power plants. **Paper 3** and **Paper 4** deal with enhancing the load flexibility of coal-fired power plants (CFPP). **Paper 5** and **Paper 6** address the cost reduction of CSP plants. All application scenarios are based on the demand of a low-cost TES with enhanced temperature range.

Former work also treated ACAES in combination with sandTES [26]. Industrial applications, especially in the energy intensive high temperature sector like steel production, are a promising field of application and have to be examined in detail in future work.

4.1 Coal-fired Power Plants

Most of the electricity worldwide is generated by CFPP, as coal is a cheap primary energy source and geographic limitations are not crucial. The number of plants worldwide is still rising due to the increasing population and energy demand per head. In Europe only a few new CFPP projects are planned, as renewable technologies have been strongly enforced during the past years. The increasing number of renewables leads to a highly volatile electricity generation and subsequently to a demand for storage and highly flexible conventional power plants. Since no storage technology is available for directly compensating for the load- and demand peaks in this order of magnitude, the enhancement of the flexibility of conventional power plants seems to currently be the appropriate choice.

Several CFPP have been designed for base load, hence only for a limited number of load changes at rather low load change rates. One approach for enhancing the load change characteristics is to integrate a TES into the process of a thermal power plant. These concepts also offer a chance for preserving the lifespan of the power plants. Thus, the integration of TES can be economical beneficial on the electricity market and also by lowering the maintenance cost of the existing plant.

Supercritical state of the art CFPP reach live steam temperatures of 600 °C at a pressure of 285 bar, which results in gross efficiencies up to 47 %. At these plants, the low load of the boiler is in the range of 40 %, while the minimum load of the turbine is at about 25 % [20]. This gap is one possibility to be used for TES integration. Thus, the live steam of the power plant at its minimum boiler load, which is not put to the turbine, is used for charging the TES. Another approach for charging is to switch off the turbine and simply use the nominal load live steam as heat transfer medium for charging the TES. For discharging various options seem feasible, like replacing some preheaters with an appropriate TES-HEX. The direct steam generation for discharging suffers from the terminal temperature differences during heat transfer, wherefore the nominal live steam parameters cannot be reached.

Paper 3 and **Paper 4** are based on the Reference Power Plant North Rhine-Westphalia (RPP NRW). The implementation of a sandTES-system is examined in detail.

In **Paper 3** a concept based on charging a sandTES with live steam is examined. Live steam is branched before the turbine and condensed in the appropriate sandTES-condenser. For discharging, the thermal energy of the particles is used to preheat the

fresh air of the CFPP. This method resulted in the patent *Wärmekraftwerk* [24]. These air-preheaters are specialized particle-air HEX, which can be constructed as a fluidized bed HEX or a cyclone. This discharging method benefits from the independence of the live steam temperature and from not harming the water/steam cycle. However, the accompanying impacts on the combustion streams have to be investigated more in detail.

Figure 21 shows an overview of a simplified sandTES-setup implemented in a CFPP. A sandTES-HEX is used for charging, thus heating quartz sand by condensing live steam. The hot particles are stored in the hot silo (red coloured) to be afterwards used for air preheating. The air preheater, which is fed by the hot sand, is designed as a simple fluidized bed HEX.

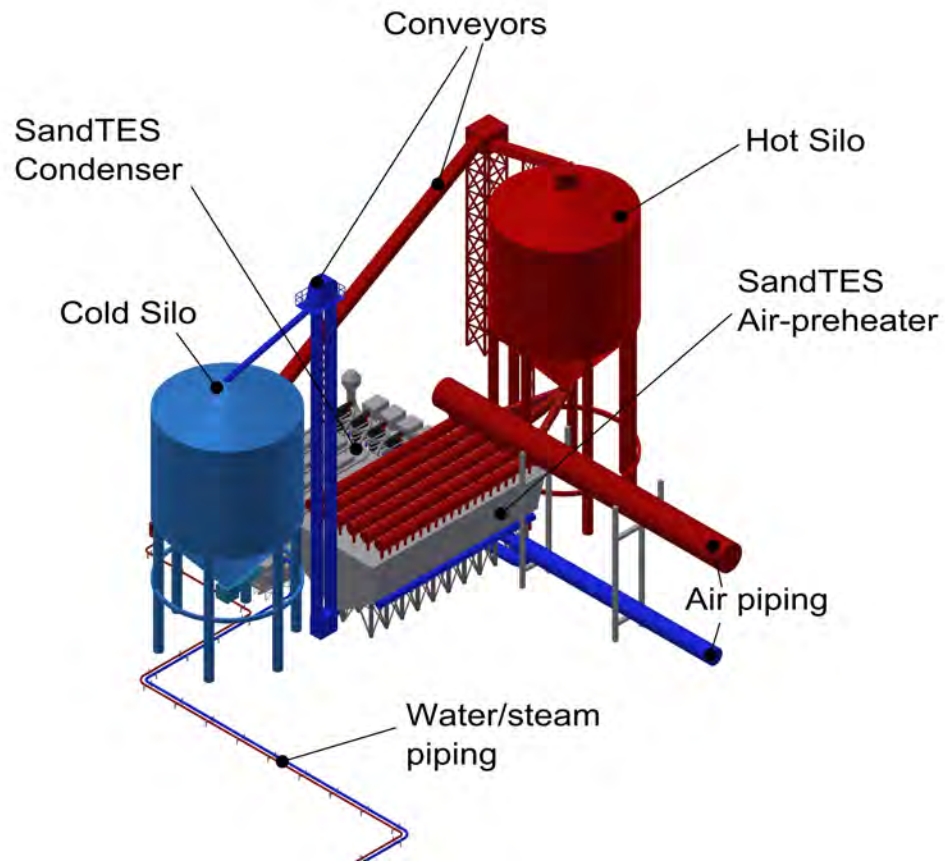

Figure 21: Overview of a sandTES-system integrated in a CFPP [15]

Paper 4 extends the results of **Paper 3**. Additionally, the charging is accomplished by using the plants electric output directly from the generator for heating the particles. Electric heating elements therefore replace the tube bundle inside a sandTES-HEX. The sandTES again is discharged by preheating the fresh air of the plant. Additionally a variant for directly generating live steam is presented. The benefit of using electric heating elements is the extensive independence of the regular power plant process. Furthermore, the maximum temperatures can exceed the live steam temperatures, offering a direct live steam generation at nominal parameters for discharging. High particle temperatures and

thus high energy densities also lead to small equipment of the TES, including the HEX and the silos. However, as the electric energy was generated with losses before, the overall storage efficiencies are rather low.

4.2 Concentrated Solar Power Plants

Concentrated Solar Power is a promising alternative to photovoltaics, as storage can be implemented quite cost-effective.

The most common CSP systems are parabolic trough and central tower plants. In Fig. 22 the parabolic trough CSP plant Shams 1, using thermal oil as heat transfer medium, is pictured. Figure 23 shows the modern CSP plant Crescent Dunes (CD), applying the central tower concept and a TES based on molten salt as HSM. The further considerations deal with the central tower concepts, as it fits to particle based TES more properly.

(a) Overview Shams 1 (b) Parabolic troughs of Shams 1

Figure 22: Overview of the CSP plant Shams 1

(a) Overview Crescent Dunes (b) Overview of the receiver and power island

Figure 23: Overview of the CSP plant Crescent Dunes [27]

A CSP plant mainly consists of the storage cycle and the power cycle. The storage cycle includes the receiver mounted on a 100 to 200 m high tower, which is located in the center

of the surrounding heliostats field. A heat transfer or heat storage medium is fed up to the receiver, where the concentrated beams from the solar field are used for heating up the medium. Direct steam generation in the receiver is unfavourable due to issues implementing a TES. On the ground, the HSM can directly be stored. Otherwise, the HTM is used to heat up the HSM, which can be stored in tanks.

The most common power cycles applied at CSP plants are water/steam Rankine cycles. In recent years also supercritical carbon dioxide cycles are discussed, which is taken into account in **Paper 6**. These power cycles can be fed by the HSM on demand, making the CSP technology a very attractive technology.

Paper 5 aims for implementing a sandTES-system into a CSP plant, with the same performance data as CD. This concerns mostly the thermal power coming from the solar field and the storage capacity. One approach is to directly heat particles like corundum in the receiver. In this case no HTM, but large and due to reradiation inefficient receivers are needed as well as conveying technology capable for transporting the particles up to the top of the receiver at highest temperatures.

The second approach is heating liquid sodium as HTM in the receiver for transferring the thermal energy to the TES system on the ground. Due to the high conductivity of liquid sodium, these receivers are very small, also compared to molten salt receivers. The losses at the receiver therefore are low, but an additional HEX on the ground is needed. Furthermore, liquid sodium is known to be a hazardous medium, especially at contact with water. A modular CSP plant from VastSolar [19] uses molten salt as HSM and liquid sodium as HTM. According to them, sodium fires can be handled rather easily, as long as water contact can be avoided.

These two concepts are compared to each other and to CD in **Paper 5**. The main result is, that the efficiency of particle receivers have to be strongly increased, to be advantageous even compared to CD.

As mentioned above, sCO2 cycles are often proposed as alternative to the wide spread water/steam Rankine cycles. **Paper 6** introduces a CSP plant similar to CD, but with the particle based sandTES and a sCO2 cycle. Once more, the sandTES technology is introduced in there to further on present a design example of the sCO2-corundum-HEX.

The sCO2 technology is a rather novel technology, which is expected to provide higher efficiencies and thus lower LCOE of the CSP plant. As these CSP plants commonly are erected in arid regions with rare water resources, the cooling needed at the power cycle is more difficult. Mostly air-coolers are applied, leading to higher minimum temperatures in the power cycle. More than water/steam cycles, sCO2 cycles suffer from these high cooler temperatures, which strongly affect the cycle's efficiency. Only at high maximum power cycle temperatures of about 660 °C and above the efficiencies of sCO2 cycles exceed the efficiencies of water steam power cycles at these arid conditions [21]. Thus, only the announced low capital cost of the sCO2 cycle are advantageous, which are also doubted more often [16].

5 Conclusion and Outlook

5.1 Conclusion

Much research in recent years has focused on the development of storage systems. For thermal processes, e.g. applied at power plants or at industrial plants, the direct integration of TES seems to be an attractive, cost-effective opportunity.

Especially in the field of high temperature storage, several novel systems are entering the market, since state of the art technologies suffer from various issues. Molten salt, which is the state of the art HSM in CSP plants, is limited by its maximum temperature. Furthermore, the usable temperature range is restricted by the freezing temperature of molten salt. For freezing prevention heat traces have to be installed, causing enlarged costs for the heat trace itself and auxiliary power when required.

Novel developments aim for using solids as HSM, due the high thermal persistence and the low costs. Fixed-bed regenerators are using air as HTM, which is heated or cooled by flowing through a bed of e.g. crushed rocks. The advantage of high achievable temperatures is compensated by the high auxiliary power consumption and large constructions of all components.

Another approach is using a specialized high temperature concrete as HSM. As HTM thermal oil can be used. However, the maximum temperatures are more restricted compared to the fixed bed regenerator, due to the HTM itself and thermal stress.

A novel TES technology from TU Wien, called sandTES, is based on particles like quartz sand as HSM. The sandTES technology applies a common two tank system, including two storage silos, some conveyors and the particle-based HEX. Capacity and power are decoupled, wherefore the capacity can be enlarged quite easily by just adding further silos. Quartz sand is not only a low cost product, but also offers maximum temperatures up to theoretically 1000 °C and above, with no relevant minimum temperature limit. High energy densities are the result of the great temperature range.

The HEX as the heart piece of the technology is based on fluidization technology. Fluids contained in a tube bundle can be heated or cooled by the sand in counter current, making the technology exergetically efficient. As a unique feature, the flow directions of the fluidized bed and the working fluid inside the tube bundle can be reversed. Low fluidization velocities limit the auxiliary power consumption, while heat losses by the fluidization air can be minimized by recuperation. Two key technologies, the nozzle distributor floor and the air cushion technology, are needed for guaranteeing a stable fluidization along the axis of the HEX and controlling the flow behaviour.

For a full proof of concept, a 280 kW_{th} pilot plant was erected at the institute's laboratory. Cold tests already approved the functionality of the technology, including both the key technologies. For a further reliable scale up of future plants, measurement results are needed to find optimization criteria. One crucial design parameter is the backlog, thus the height difference between in- and outlet, of the fluidized bed by flowing through the HEX, which was determined below 4 mbar/m at the relevant operating conditions. The dynamic behaviour was roughly estimated too, resulting in reversing durations of

the fluidized bed of a few minutes. All these measurements were performed at ambient temperatures without heating or cooling, as the focus was on the fluidization behaviour.

To figure out the requirements on the TES system, several application scenarios have been investigated, with a focus on power plants. Coal-fired power plants are struggling due to the rising number of renewables and the accompanying increased number of load changes for stabilizing the electric grid. Thus, for economic and technical reasons, the integration of a high temperature TES directly into the power plant process makes sense. At a common thermal power plant steam or electricity from the generator can be used for charging the TES system. Charging with steam limits the maximum TES temperature, which can be an issue, if live steam has to be generated at discharging. Electric heating elements allow a highly flexible, but overall less efficient way of charging the TES.

For discharging amongst others, preheaters can be fed, live steam can be generated, or even fresh air can be preheated. Discharging by high pressure preheaters seems to be most likely for retrofitting. The direct live steam generation with the sandTES system impacts the whole power cycle, if the live steam temperatures cannot be reached again. The fresh air preheating does not harm the water/steam cycle, but might force profound changes in the combustion streams.

A similar field concerns concentrated solar power. For generating electricity also thermal power plants, mostly applying water/steam cycles, are used. For a particle TES especially the central receiver technology seems preferable.

A CSP plant roughly consists of the storage cycle and the power cycle. Both are aimed to be optimized by raising the temperatures for lowering the LCOE. The maximum temperature at the moment is limited by the HSM, mostly molten salt. The particle-based TES technologies are predestined for this application.

In case of the sandTES-technology, a way of heating up the particles has to be found. This can be accomplished by directly heating these particles in a receiver, or applying an intermediate heat transfer cycle. A direct particle-receiver is very inefficient, due to the lower heat transfer coefficients. A large receiver surface with the corresponding losses due to convection and reradiation is the result. Furthermore, some conveying technology for transporting the particles up to the receiver at elevated temperatures is needed. An intermediate cycle, e.g. using liquid sodium as HTM, however requires one huge additional HEX at the ground. The maximum temperatures again are more restricted and liquid sodium is known as a hazardous medium, when contact with water cannot be avoided.

As novel power cycle the supercritical CO_2 cycle often is proposed as more efficient alternative to the common water/steam cycles. However, in arid regions, where water cannot be used for cooling, the high minimum power cycle temperatures affect the thermal efficiency of the sCO2 cycle much more, than of the water/steam cycle. Only at highest temperatures in the range of 650 °C and beyond, sCO2 cycles can be beneficial. The expected low cost for these sCO2 cycles are often doubted recently and still turbomachinery is under development. A combination of the claimed high temperature power cycles (sCO2 or water/steam) with the sandTES-technology can lead to the intended lower LCOE.

5.2 Outlook

For future work various cold and hot tests with the pilot plan are scheduled. The cold measurements are planned to be completed by investigating the particle segregation behaviour inside the sandTES-HEX, analysing the stability limits of the nozzle distributor floor, or examining the backlog of the fluidized bed depending on parameters like the bed height. The following hot measurements shall provide information about the temperature distribution inside the sandTES-HEX. Furthermore, the heat transfer coefficients measured in previous test rigs shall be validated. Conclusions about the dispersion of the particle-air suspension are expected by running transient hot tests.

Looking at the application cases for the sandTES-technology, a huge potential in energy intensive industry but also in chemical industry should be investigated. Also the analysis of the economic feasibility of a sandTES-implementation is of interest for taking the technology on the next level.

References

[1] A. Beck ; M. Koller ; H. Walter ; M. Hameter: Transient Numerical Analysis of Different Finned Tube Designs for Use in Latent Heat Thermal Energy Storage Devices. In: *Proceedings of the ASME 2015 9th International Conference on Energy Sustainability* (2015), Nr. ES2015-49145

[2] Alibaba.com: *Corundum.* https://german.alibaba.com/product-detail/white-korund-grain-f8-f220-60339243618.html?s=p. (2017)

[3] Alibaba.com: *KNO3-NaNO3.* https://www.alibaba.com/product-detail/Solar-Thermal-Power-Plant-Solar-salt_1985588242.html. (2017)

[4] Alibaba.com: *Silicon Carbide.* https://german.alibaba.com/product-detail/black-silicon-carbide-859283625.html?s=p. (2017)

[5] Alibaba.com: *Sodium.* https://german.alibaba.com/product-detail/99-7-sodium-metal-634608116.html?s=p. (2017)

[6] BMWFW: *Energiestatus Österreich 2015: Entwicklung bis 2013.* (2015)

[7] Boerema, N. ; Morrison, G. ; Taylor, R. ; Rosengarten, G.: Liquid sodium versus Hitec as a heat transfer fluid in solar thermal central receiver systems. In: *Solar Energy* 86 (2012), Nr. 9, S. 2293–2305. http://dx.doi.org/10.1016/j.solener.2012.05.001. – DOI 10.1016/j.solener.2012.05.001. – ISSN 0038092X

[8] Chase, M. W. Jr.: NIST-JANAF Themochemical Tables, Fourth Edition. In: *J. Phys. Chem. Ref. Data, Monograph 9* (1998)

[9] Clemencon, R.: The Two Sides of the Paris Climate Agreement: Dismal Failure or Historic Breakthrough? In: *The Journal of Environment & Development* 25 (2016), Nr. 1, S. 3–24. http://dx.doi.org/10.1177/1070496516631362. – DOI 10.1177/1070496516631362. – ISSN 1070–4965

[10] D. Busse ; D. Kieffer: *Active Fluidization Storage sandTES.* Wien, TU Wien, Bachelor Thesis, (2014)

[11] Drury, E. ; Denholm, P. ; Sioshansi, R.: The value of compressed air energy storage in energy and reserve markets. In: *Energy* 36 (2011), Nr. 8, S. 4959–4973. http://dx.doi.org/10.1016/j.energy.2011.05.041. – DOI 10.1016/j.energy.2011.05.041. – ISSN 03605442

[12] E. Christensen: *VGB Facts and Figures - Electricity Generation 2015|2016.* (2015)

[13] EnergyNest: *Rethink Energy Storage (Brochure).* (2016)

[14] F. Mayrhuber ; H. Walter ; M. Hameter: Experimental and numerical investigation on a fixed bed regenerator. In: *Proceedings of SEEP2017, Bled, Slovenia* (2017)

[15] Lang, F.: *Integration eines thermischen Energiespeichers in ein Kohlekraftwerk.* Wien, TU Wien, Bachelor Thesis, (2017)

[16] M. Meybodi et al.: Techno-economic Analysis of Supercritical Carbon Dioxide Power Blocks. In: *Proceedings of the SolarPaces 2016 Conference (AIP)* (2016)

[17] M. Sterner ; I. Stadler: *Energiespeicher.* Berlin, Heidelberg : Springer Vieweg, (2014). – ISBN ISBN 978–3–642–37379–4

[18] Ma, T. ; Yang, H. ; Lu, L.: Feasibility study and economic analysis of pumped hydro storage and battery storage for a renewable energy powered island. In: *Energy Conversion and Management* 79 (2014), S. 387–397. http://dx.doi.org/10.1016/j.enconman.2013.12.047. – DOI 10.1016/j.enconman.2013.12.047. – ISSN 01968904

[19] N. Bartos ; J. Fisher ; A. Want: Experiencies From Using Molten Sodium Metal As A Heat Transfer Fluid In Concentrating Solar Thermal Power Systems. In: *Proceedings of the 2015 ASIA-PACIFIC SOLAR RESEARCH CONFERENCE* (2015)

[20] N. Latk, M. Syrbe, U. Gampe: Erste Untersuchungen zur Niedriglastfahrweise einer Dampfturbine großer Leistung. In: *VGB PowerTech - International Journal for Electricity and Heat Generation* (2015)

[21] P. Steiner ; K. Schwaiger ; M. Haider: CSP-Systems based on sCO2-Power Cycles and Particle based Heat Storage. In: *1st European Seminar on Supercritical CO2 (sCO2) Power Systems* (2016), Nr. Presentation

[22] P. Steiner ; K. Schwaiger ; M. Haider ; H. Walter: Flow Characteristics of a Fluidized Bed Heat Exchanger used for High Temperature Thermal Energy Storage. In: *Applied Energy* (2017), Nr. Submitted 2017

[23] P. Steiner ; K. Schwaiger ; M. Haider ; H. Walter ; M. Hämmerle: Increasing Load Flexibility and Plant Dynamics of Thermal Power Plants via the Implementation of Thermal Energy Storages. In: *Proceedings of the ASME 2016 Power and Energy Conference* (2016), Nr. PowerEnergy2016-59181

[24] P. Steiner ; M. Haider ; K. Schwaiger ; H. Walter ; M. Haemmerle: Wärmekraftwerk. In: *Patent* (2017), Nr. granted

[25] Ramsauer, C.: *Auslegung und Design eines thermischen Speichers für einen Wärmeknoten.* Wien, TU Wien, Bachelor Thesis, (2017)

[26] Schwaiger, K.: *Development of a novel Particle Reactor/Heat-Exchanger Technology for Thermal Energy Storages.* Wien, TU Wien, PhD Thesis, (2016)

[27] SolarReserve ; SolarReserve (Hrsg.): *Media Gallery.* http://www.solarreserve.com/en/global-projects/csp/crescent-dunes. (2016)

[28] Solutia Europe S.A./N.V.: *THERMINOL VP-1 Datasheet* (2013)

[29] Storasol: *Entwicklung der STORASOL-HTTESS-Speichertechnologie.* (2014)

[30] Storasol: *STORASOL GmbH High Temperature Thermal Energy Storage HTTES: Technology for the future and today.* (2015)

[31] UNFCCC: *Adoption of the Paris agreement: FCCC/CP/2015/L.9/Rev.1.* (2015)

[32] Yang, W. (Hrsg.): *Handbook of fluidization and fluid-particle systems.* Bd. 91. Chemical Industries, (2003)

[33] Zavaico, A.: Solar Power Tower Design Basis Document: Revision 0. In: *Sandia National Labs Report* (2001), Nr. SAND2001-2100

List of Papers

Paper 1

P. Steiner, K. Schwaiger, H. Walter, M. Haider: *Active Fluidized Bed Technology used for Thermal Energy Storage*; Proceedings of the ASME 2016 Power and Energy Conference, PowerEnergy2016, Charlotte, North Carolina, USA, 2016

Paper 2

P. Steiner, K. Schwaiger, M. Haider, H. Walter: *Flow Characteristics of a Fluidized Bed Heat Exchanger used for High Temperature Thermal Energy Storage*; Submitted to Applied Energy, 2017

Paper 3

P. Steiner, K. Schwaiger, M. Haider, H. Walter, M. Hämmerle: *Increasing Load Flexibility and Plant Dynamics of Thermal Power Plants via the Implementation of Thermal Energy Storages*; Proceedings of the ASME 2016 Power and Energy Conference, PowerEnergy2016, Charlotte, North Carolina, USA, 2016

Paper 4

P. Steiner, M. Haider, K. Schwaiger: *Flexibilisierung und Mindestlastabsenkung kalorischer Kraftwerke mittels Einbindung thermischer Hochtemperatur-Energiespeicher*; Tagungsband Kraftwerkstechnisches Kolloquium, Dresden, Germany, 2016

Paper 5

P. Steiner, K. Schwaiger, M. Haider, H. Walter: *System Analysis of Central Receiver Concepts with High Temperature Thermal Energy Storages: Receiver Technologies and Storage Cycles*; AIP conference proceedings: SolarPaces2016, Abu Dhabi (UAE), 2016

Paper 6

P. Steiner, K. Schwaiger, H. Walter, M. Haider, M. Hämmerle: *Fluidized Bed Particle Heat Exchanger for Supercritical Carbon Dioxide Power Cycles*; Proceedings of the ASME 2016 International Mechanical Engineering Congress and Exposition, IMECE2016, Phoenix, Arizona, USA, 2016

Paper 1

P. Steiner, K. Schwaiger, H. Walter, M. Haider

Active Fluidized Bed Technology Used for Thermal Energy Storage

Proceedings of the
ASME 2016 Power and Energy Conference PowerEnergy2016
June 26-30, 2016, Charlotte, North Carolina

Proceedings of the ASME 2016 Power and Energy Conference
PowerEnergy2016
June 26-30, 2016, Charlotte, North Carolina

PowerEnergy2016-59053

ACTIVE FLUIDIZED BED TECHNOLOGY USED FOR THERMAL ENERGY STORAGE

Peter STEINER
TU-Wien
Institute for Energy Systems and Thermodynamics
Getreidemarkt 9/302
A-1060 Vienna, AUSTRIA

Karl SCHWAIGER
TU-Wien
Institute for Energy Systems and Thermodynamics
Getreidemarkt 9/302
A-1060 Vienna, AUSTRIA

Heimo WALTER
TU-Wien
Institute for Energy Systems and Thermodynamics
Getreidemarkt 9/302
A-1060 Vienna, AUSTRIA
Email: heimo.walter@tuwien.ac.at
Contact Author

Markus HAIDER
TU-Wien
Institute for Energy Systems and Thermodynamics
Getreidemarkt 9/302
A-1060 Vienna, AUSTRIA

ABSTRACT

A higher number of research institutions work on solutions for energy storage systems. Therefore a large number of differing approaches in competition among each other to develop storage technologies. At the TU-Wien, Institute for Energy Systems and Thermodynamics a novel thermal energy storage concept based on an active fluidized bed technology - the so called sandTES-heat exchanger technology – has been developed. The present paper describes the basic idea behind the key technology and the design methodology of a test rig in semi-industrial scale. In addition the results of selected preliminary experimental and numerical investigations are presented and discussed.

INTRODUCTION

The administrations of many countries have made resolutions that the energy efficiency of power plants as well as industrial processes, the utilization of waste heat and the development and use of the renewable energy potential must be intensified. This results in a fairly long-term transformation of the energy markets of these countries. For example, the share of renewables in the primary energy demand in Germany has increased from 1.3% in 1990 to 11.7% in 2013 and the plans are to increase it further to 50%, or even 100%, by 2050 [1].

The increase of the renewable energy share on the energy (electricity) production has on the one hand the consequence that conventional power plants must operate more flexibly and often under low load conditions (which should be dropped down in future to lower values if possible). On the other hand the energy supply is becoming more volatile. Nevertheless, the renewable energy sources used for the production of electricity must be integrated into the existing power grid. Compared to conventional power plants the renewable energy sources are different in scale and availability. This results in a difficult integration into the power grid and thus, an expansion of infrastructure is necessary [2]. As mentioned in [3], in a medium time frame, the planned development of wind and solar power plants will not reduce the need for heat and power production in fossil as well as biomass-fired thermal power plants. This is necessary, because at the moment conventional power plants are driven by demand to maintain power grid base load stability. Otherwise the transition to the renewable energy sources in the power grid will pose problems concerning system stability like power balance stability, voltage stability, primary control stability or inter area oscillations [4]. On the other hand the increasing generation of electricity by wind and photovoltaic plants reduces the economics of thermal power

plants and therefore the operation of thermal power plants cannot be shown economically in the future.

To fulfill all necessary requirements for a stable power grid and, associated therewith a stable overall energy supply in the future, an economical way to store the excessive electrical load as well as the excessive (waste) heat is needed. One solution can be to transform the excessive electrical power to heat and store the heat in thermal energy storage (TES) systems (this technology is referred to as power-to-heat, see e.g. [5]) or to produce hydrogen or methane (referred to as power-to-gas technology, see e.g. [6]). As mentioned in [7] the possibility to store electricity in a thermal energy storage device is more suitable because it is cheaper to store heat than electricity. Consequently, thermal energy storage devices can help to store energy for a later use. The following requirements are aimed:

- a good heat transfer between the storage material and the heat transfer fluid,
- a mechanical and chemical long-term stability,
- not flammable and not toxic,
- a high reversibility between charging and discharging cycles,
- low thermal losses,
- low change in volume,
- high energy density,
- high specific heat capacity,
- low cost,
- low corrosivity and
- low environmental impact factors.

Thermal energy storage systems can be subdivided into sensible and latent heat thermal energy storage devices. At the moment increased efforts are being made in research and development on both technologies to improve existing and develop new thermal energy storage technologies as well as components, see e.g. [8-17].

Feasible storage materials are needed for storing thermal energy at high temperatures in TES systems for industrial applications, such as make steam cycles for power generation or industrial processes more flexible or to homogenize batch mode operations of e.g. electric arc furnaces. Systems using packed beds of ceramic bricks or other ceramic bodies have been analyzed for high-temperature storage up to approximately 800°C as described in [17] and [18]. These storage system configurations are simple but the storage materials are expensive. However, to reduce the costs for TES systems at high temperature level a low-price and widely available material is required. Silica sand can be a potential material for such a TES system.

The advantage of silica sand as storage material is that it can be heated up from ambient to high temperature levels and silica sand is a low-cost and widely available material. Particles, such as silica sand can be used in active storage cycles; thus the total storage volume can be used, the operation pressure for the storage system can be ambient pressure and the heat exchanger pressure loss is independent from the storage capacity. As a further important advantage of silica sand or another similar storage material, e.g. corundum, silicon carbide, ash, bauxite or magnesium oxide, is that the storage medium can be used also as heat transfer medium.

In reference [17] a concept for a sand-air heat exchanger for the use in solar power towers with open volumetric receivers is presented. This heat exchanger is designed in a cross-flow arrangement for the heat transfer media sand and air. A narrow-width design is chosen to reduce the pressure drop in the moving packed bed. For the charging process hot air enters the heat exchanger through a porous wall, passes through the falling sand flow and leaves the heat exchanger at a lower temperature level also through a porous wall in direction to the storage device. For discharging the heat the sand must flow through an additionally installed fluidized bed cooler.

The experimental results on a lab scale heat exchanger with the dimensions 0.5 m height, 0.05 m width and 0.1 m depth have shown that optimal sand grain size with respect to heat transfer and heat exchanger auxiliary energy demand is in the range of 2-3 mm. The results presented in [17] have also shown that with increasing grain size of the sand the effectiveness of the heat exchanger decreases while a decreasing grain size the pressure drop increases if the air velocity is decreased. This increasing pressure drop leads to a substantially higher auxiliary energy demand or a larger heat exchanger dimension.

The authors in [17] have also concluded that the fluidized bed cooler is the limiting element of their system because a larger grain size leads to increased erosion on the heating surfaces so that the grain size is probably limited to a value of 1 mm.

A power cycle for a concentrating solar power plant (CSP) using circulating fluidized-bed technology for heat exchange and packed particles for thermal energy storage is presented in [19]. The charging process described in [19] moves sand from the cold silo with the help of a bucket elevator into a particle receiver. Within the particle receiver a gravity-driven particle flow is given and the sand particles heated up by solar fluxes leave the receiver in direction to the hot sand silo. For discharging, the sand particles leave the hot silo at its bottom and enter a particle feeder (not described in detail in [19]) which fed the circulating fluidized-bed. Inside the fluidized-bed reactor the heat is transferred to the surrounding evaporator walls and the cold particles leave the circulating fluidized-bed through a cyclone in direction to the cold silo. The authors concluded that the fluidized-bed TES can hold hot particles of > 800°C with >95% exergetic efficiency, storage effectiveness, and thermal efficiency.

In reference [20] and [21] different power cycles for a CSP based on fluidized-bed technology are presented. The focus in [20] was to describe the economic and performance benefits of these CSP system designs while in [21] the priority was on the system description; especially the description of the different power cycles possibilities like air-Brayton combined cycle, natural gas combined cycle and natural circulation as well as

supercritical Rankine power cycles. For the discharging of the stored heat an atmospheric fluidized bed cooler is used. Only for the air-Brayton combined cycle a pressurized fluidized-bed system was utilized.

At the TU-Wien, Institute for Energy Systems and Thermodynamics a novel thermal energy storage concept based on an active fluidized bed technology - the so called sandTES-heat exchanger technology - was developed (see e.g. [9], [10]). This technology enables a charging and discharging of heat from/to the heat transfer fluid to/from a fine bulk powdered storage material such as silica sand, bauxite or corundum. The present paper focuses on a description of the novel heat exchanger technology, the semi-industrial test loop and, the future investigations scheduled with the test loop.

THE SANDTES TECHNOLOGY

General description of the system

The main reason for developing the sandTES heat exchanger technology has been to dispose a scalable thermal energy storage design which can be operated at high temperature level. A further relevant aspect for the design of the technology is that it can be used in a wide range of applications like solar power plants, improving the flexibility of Rankine cycles and industrial processes. In a first step sand is used as storage material because sand fulfills many of the material requirements described above. But it is also considered to make investigations with other storage materials like e.g. corundum or magnesia.

The sandTES heat exchanger technology is based on a combination of a counter current heat exchanger (HEX) and the fluidized bed technology.

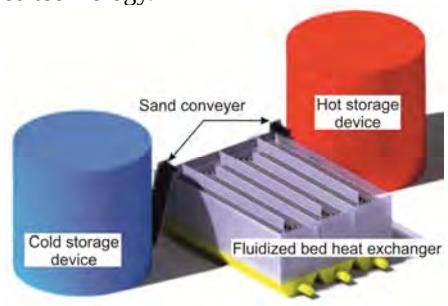

Figure 1: Sketch of the sandTES storage system

Figure 1 shows a simplified sketch of the overall sandTES storage concept. During the charging process cold sand leaves the cold storage unit and is fed into the fluidized bed heat exchanger with the help of e.g. a screw conveyor or an alternate solids conveying system. The sand within the HEX is fluidized by air which enters the heat exchanger at its bottom and leaves it at the top. The fluidized sand is heated up by the heat transfer fluid which flows inside a tube bundle. The sand itself moves from the cold bunker through the HEX in direction to the hot bunker while the heat transfer fluid flows in the opposite direction. Thereby a counter current HEX is realized. This arrangement maximizes overall mean temperature differentials between the solids and the heat transfer medium allowing for a reduction in total heating surface area for a given amount of heat duty. The hot sand leaves the HEX at the hot side of the HEX and is transported via appropriate bulk conveying technology.

For discharging the stored heat, the flow direction of both - the sand as well as the heat transfer fluid - is changed so that also a counter current HEX is realized.

One of the main advantages of the sandTES technology is that it is usable for a wide range of applications like e.g. improving the flexibility of thermal power plants (sub- as well as supercritical) [10] and [22], in CSP cycles [23], [24] or adiabatic compressed air energy storage cycles [25].

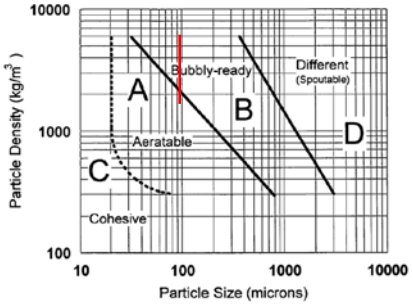

Figure 2: Geldart classification of powder [26]

It is well known that the auxiliary energy needed for the operation of a fluidized bed increases with rising particle diameter of the bed inventory. Therefore the particle diameter used in the sandTES HEX is in the range of approx. 50 to 100 µm. As long as the particle bulk is fluidizable regarding the Geldard classification, smaller particles are favorable. Nevertheless particles at 100 µm are aimed, since sieving efforts become too costly beyond this size. Based on the Geldart classification, which is presented in Fig. 2, the working regime of the sandTES HEX is within the bubbly-ready region B but close to region A (marked with the red line). The operation of a fluidized bed close to region A results in the need of a minimum air mass flow for fluidization and thus in a minimum of auxiliary energy.

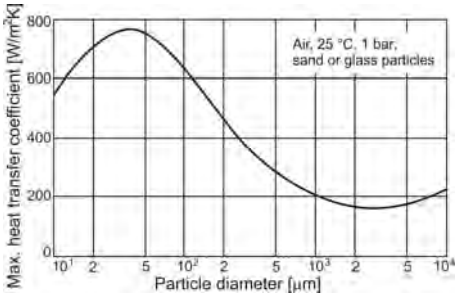

Figure 3: Maximum heat transfer coefficient between immersed surface and fluidized bed versus particle diameter [27]

The operation of a fluidized bed with small particle diameters results in the additional advantage that the maximum heat transfer coefficient between immersed surface and fluidized bed is large. This advantage is also described in [19] and [20]. As it can be seen in Fig. 3, for a particle of approx. 50 to 100 µm the maximum heat transfer coefficient is in the range of approx. 600 W/m^{2}K to 700 W/m^{2}K.

sandTES HEX design technology

A simplified sketch of the sandTES HEX to understand the main physical idea behind the concept is depicted in Fig. 4 (For simplification reasons only two air-cushions are plotted in Fig. 4).

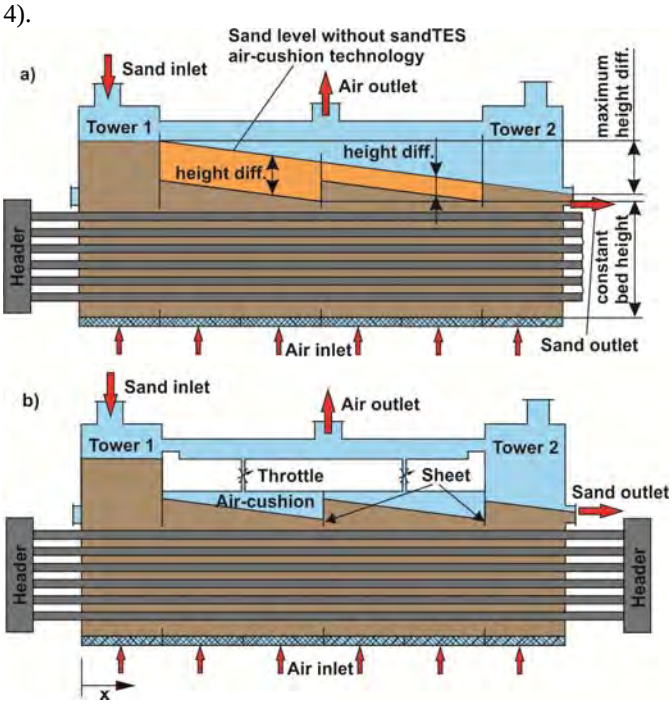

Figure 4: sandTES air-cushion principle

It is generally known that for a fluid transport within e.g. a tube or channel a pressure difference between the inlet and the outlet of the flow region is necessary. In case of the sandTES HEX a viscous sand suspension should be transported without any mechanical power engine horizontally over a larger distance (approx. 20 m in case of the test rig HEX, see Fig. 7). The flow of this viscous sand suspension itself can be classified as a Bingham fluid. The required driving force (pressure gradient) for such a fluid flow is depending on the viscosity of the sand suspension. With increasing viscosity, the pressure gradient necessary to achieve the fluid flow increases too, based on the increasing flow resistance. The pressure and thus the level of the fluidized bed are increasing in the up-stream direction of the particle flow.

Applying the principle of a free fluid flow to the sandTES HEX will result in the circumstance that the sand height at the HEX inlet is much higher than at the outlet. As mentioned above the sand level difference between inlet and outlet increases with increasing bed length and increasing viscosity of the sand suspension. This situation is shown in the sketch in Fig. 4a where only the upper part of the sandTES HEX without the air-cushion technology is presented. In case of a free fluid flow through the sandTES HEX the maximum difference in height, as it is shown in Fig. 4a, will be formed (for simplification reason a linear decrease of the sand level is assumed in the figure). This large difference in height has the disadvantage that a large unused air space is given above the sand level; the pressure difference of the fluidized bed between inlet and outlet increases with increasing HEX length and a limitation of the flexibility of the HEX is given by changing the flow direction (After changing the flow direction the distribution of the sand is inversely arranged. The maximum sand height is located in Tower 2 and the minimum in Tower 1). As a further consequence the heat exchanger design is also huge and thus the investment cost increases.

The pressure gradient acting as driving force is related to the level differences of the fluidized bed. The local pressure at the bottom of the fluidized bed can be calculated as sum of the air pressure above the sand level and the pressure drop through the fluidized bed. According to [28] the horizontal pressure gradient can be calculated with

$$\frac{\partial p_{fb}}{\partial x} = (1-\varepsilon)(\rho_p - \rho_f)g\frac{\partial h(x)}{\partial x} \qquad (1)$$

The term on the left hand side describes the pressure change along the HEX length; the first term at the right hand side (1-ε) describes the porosity and the remaining term the buoyancy force. As it can be seen from Eq. (1) the pressure gradient depends only on the sand height. This sand height can be subdivided in a constant bed height (see Fig. 4a) and a resulting triangle height. This triangle height causes the unfavorable HEX design. Therefore it would be more favorable for the design of the HEX if it is possible to reduce the height of the triangle without a loss of operability. This reduction can be done with the sandTES HEX technology which will be described in the following.

At the sandTES HEX technology the total HEX length is subdivided in partial length (sub heat exchangers) with the help of sheets. If we use the constant bed height as basis, then we can see in Fig. 4a that the maximum possible reduction of the sand height within the partial length depends on the position within the HEX. This possible reduction of the sand height is characterized in Fig. 4a by the orange colored surface (labeled as height diff. in Fig. 4a). However, the pressure reduction must be compensated by any other method to reach the needed total pressure difference. This is done with the so called air-cushions and is demonstrated in Fig. 4b. A single air-cushion is separated by sheets from the neighboring air-cushions (the sheet extends down into the fluidized bed as shown in Fig. 4b) and the fluidization air can leave the air-cushion only through the throttle which is located at the top of the air-cushion. This

throttle controls the air pressure within the air-cushion which compensates in turn the difference of the sand height of the triangle while the pressure difference between the wind box and the mixing box is constant over total length of the sandTES HEX (see Fig. 5). For further details see [28] and [29].

Fig. 5 shows the situation for the charging process. As it can be seen in Fig. 5 the sandTES HEX consist of a wind box, a nozzle-distributor-floor, a sinter floor, a fluidized bed (including the tube bank for the heat transfer fluid (HTF)), an air-cushion and a mixing box. Between the wind box and the nozzle-distributor-floor orifices and between the air-cushion and the mixing box throttles are arranged.

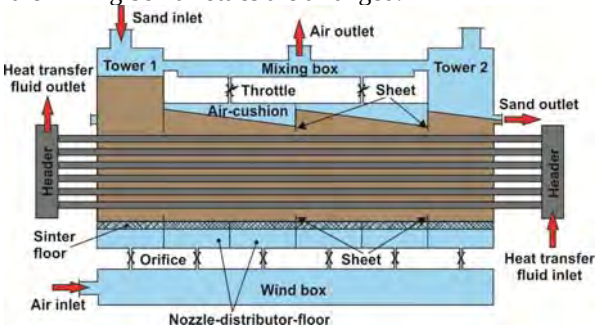

Figure 5: Sketch of the sandTES HEX design (charging mode)

The total length of the sandTES HEX is subdivided into the sections Tower 1 and 2 as well as a higher number of air-cushions. These sections are separated by sheets which extend into the fluidized bed. Tower 1 and 2 are used for charging and discharging of the sand mass flow based on the flow direction of the storage material. The air-cushions are necessary to separate the different air pressure levels over the HEX length (further more details see next sentences below).

The pre-heated fluidization air flows into the wind box and is distributed through the parallel arranged orifices to the different nozzle-distribution-floors. Due to the horizontal pressure gradient enabling the particle flow, the pressure at the bottom of the reactor is not constant. This leads to a none-uniform distribution, is stabilized by the special nozzle-distribution-floor. After passing the fluidized bed the warmed-up fluidization air flows through the air-cushion and the throttles in direction to the mixing box. Within the mixing box the air mass flow from the different air-cushions are mixed. From the mixing box the heated air leaves the sandTES HEX in direction of the recuperator where the heat carried by the fluidization air is used to pre-heat the sucked fluidization air from the ambient.

sandTES test loop layout

In Fig. 6 a general overview about the different mass flows within the test loop layout is presented. As heat source as well as heat sink for the sandTES test rig a thermal oil plant is used. The heat transfer fluid used is Therminol VP1 which can be heated up to 390°C. The thermal power of the plant is within the range of 5 to 280 kW_{th} and the volume flow rate of Therminol VP1 can be changed between 1 and 6 m^3/h (for more details see [30]). It is also possible to change the flow direction of the oil during the operation. This is necessary to obtain the counter current flow in the sandTES HEX during charging and discharging.

The fluidization air is sucked from the ambient with the help of a blower. To minimize the thermal looses within the sandTES HEX the fluidization air is preheated in a recuperator before entering the HEX. The exhaust air leaving the sandTES HEX is cooled down in a recuperator, followed by an air cleaning in a dust filter. The cleaned exhaust air leaves the test rig through a chimney.

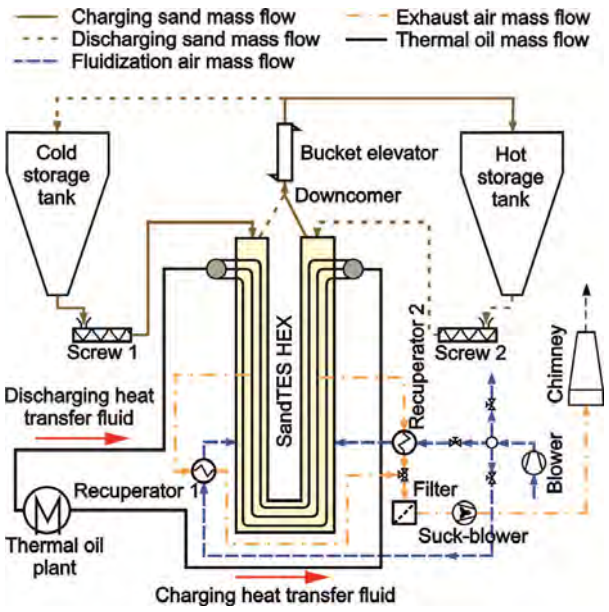

Figure 6: Process overview of the sandTES test loop layout

During the charging process the storage material mass flow leaves the cold storage tank and is transported into the sandTES HEX with the help of a screw conveyor. After entering the HEX the storage material is fluidized, is heated up by a heat exchange with the heat transfer fluid (HTF) and flows towards to the outlet of the HEX. The heated storage material particles leave the HEX through a downcomer in direction of the bucket elevator. The bucket elevator transports the storage material particles into the hot storage device. For the discharging process the flow direction is changed and the cold storage tank will be filled up.

Tab. 1 shows selected operation conditions of the test facility. The fluidization grade presented in Tab. 1 is defined as the ratio of the air velocity in the fluidized bed to the minimum fluidization velocity. Thus, the fluidization grade needs to be higher than 1 at every point of the HEX. This fluidization grade was selected to describe the fluidization conditions because the air flux distribution along the HEX is not uniform and depends

on the local air flux coming from the nozzle-distributor-floor (see Fig. 5) and the thermodynamic conditions of pressure and temperature. The values within the brackets depicted in Tab. 1 represent the operation conditions for a fluidization grade of 5.

Description	Values
Sand mass flow	0 to 10 kg/s
Air mass flow	40 to 100 g/s (200 g/s; depends on the fluidization grade)
Fluidization grade	4 (5)
Oil temperature	Up to 390 °C
Heating power	280 kW
Cooling power	200 kW
Capacity of the storage tank	8000 kg
Gauge pressure	0 to 300 (500) mbar
Blower capacity	0,3 to 1 kW (2 kW; depends on the fluidization grade)

Table 1: Selected operation conditions

A three dimensional construction drawing with the main dimensions of the sandTES HEX is presented in Fig. 7. The sandTES HEX design of the test loop was done in such a way that the HEX height can be changed flexible. This is necessary on the one hand to make investigations at different sand heights and fluidization grades. On the other hand the charging and discharging process can be done only at a lower bed height because the thermal power of the energy source is limited to 280 kW_{th} and, also the maximum volume flow of the plant is limited to 6 m^3/h. Therefore the geometrical dimensions of the tube bundle are also restricted. However, the tube bundle of the test rig consists of 20 tubes in a staggered arrangement in which three (two) tubes per row are in parallel (see Fig. 7). To avoid formations of layers along the vertical axis of the HEX wall half dummy tubes are implemented. The width of 0.15 m of a HEX arm is a result of the heat exchanger tube pitch.

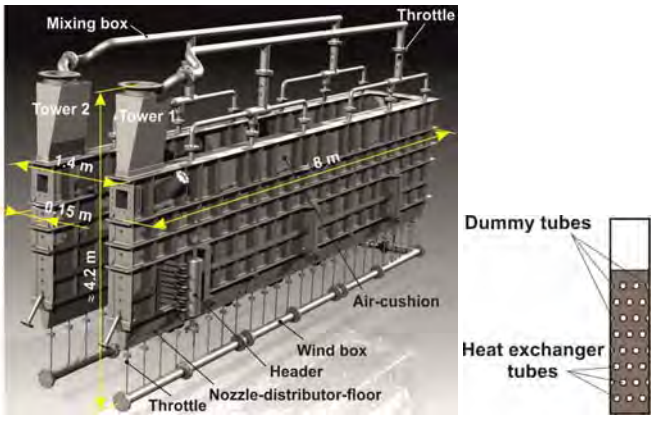

Figure 7: Construction drawing with dimensions of the sandTES HEX test rig and cross section through the HEX

In Fig. 8 a general overview about the sandTES test loop is presented. The sandTES test rig was designed as an outdoor facility. The outdoor facility consist of the sandTES HEX itself, the cold and hot storage tanks and the bucket elevator. The thermal oil plant, which is used as heat source and sink for the test loop, the used recuperator, blower and the control center are erected as indoor facilities.

In Fig. 9 images of the existing sandTES HEX and test loop are depicted. The main dimensions of the outdoor sandTES pilot plant is given with a length of approx. 10 m, a width of approx. 4 m and a height of approx. 12 m. On the left hand side of Fig. 9b blue container can be seen. These containers are used for housing the recuperator, the blower and the control center.

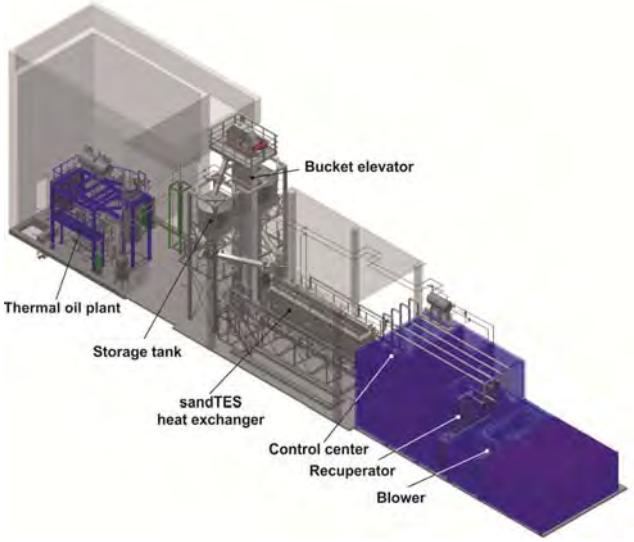

Figure 8: Sketch of the sandTES pilot plant facility

a) sandTES HEX b) sandTES HEX test loop

Figure 9: Existing sandTES HEX pilot plant (Feb. 2016)

INVESTIGATIONS TO THE sandTES TECHNOLOGY

Preliminary experimental and numerical investigation

Before starting the design of the test loop numerical and experimental investigations have been done for proofing the concept and to get a basic understanding of the sandTES technology. A special attention was paid on the mass flow distribution and the mixing of the sand feed stream with the

storage material within the heat exchanger because they are very important for the operation mode of the sandTES HEX.

In Fig. 10 a Plexiglas test rig used for the analysis of the mixing behavior of the fluid particles within the sandTES HEX is presented. This test rig is a small version of the heat exchanger design implemented in the pilot plant and consists of a nozzle-distribution floor and the tube bundle (unheated horizontal arranged Plexiglas tubes). The sand mass flow enters the test rig at the top on the left side and leaves the test rig at the right side. To make the mixing behavior visible colored sand (red) is used for the feed mass flow, while for the bed inventory (before starting the experiment) uncolored sand is used. At the right-hand side of Fig. 10 the result of the investigation is presented. The figure shows the sand distribution at the top, middle and bottom layer. As it can be seen, the red sand is well distributed over the whole height of the heat exchanger.

Figure 10: Plexiglas test rig for studying the mixing behavior in a sandTES HEX; left: test rig; right: results

This result is in good agreement with the numerical simulations presented in Fig. 11 which was calculated with the commercial software Barracuda. Barracuda can be used for the simulation of multiphase particle-gas flows and is based on the multiphase Particle-in-Cell (MP-PIC) method. This method allows a description of the particle phase based on a particle probability function which is based on [31] and [32]. For describing the multi-physics of the gas and particle phases an Eulerian-Lagrange approach is used. As mentioned in [33] the Eulerian description is used to approximate the gas phase as a continuum and the velocity, temperature, and density fields are solved using the appropriate conservation and constitutive laws. For the particles the Lagrangian phase is used. The fluid dynamics is described by averaged Navier-Stokes equations which are solved for a strong coupling of fluid and particle phase in three dimensions. Additionally an relaxation-to-the-mean term to represent damping of the particle velocity fluctuations due to particle collisions [32]. Mass, momentum, and energy of the two-phase mixture are conserved by exchange terms in the gas phase mass, momentum, and energy equations, respectively [34]. The mass and momentum equations for the fluid-phase are averaged forms of the detailed fluid-phase mass and momentum equations of Anderson and Jackson [35].

For more details on the mathematical background please refer to [31] - [35]. In [33] also a comparison between the FLUENT and the Barracuda code and also simulation results are presented.

Selected results of the numerical investigations done for the sandTES HEX are presented in Fig. 11 and 12.

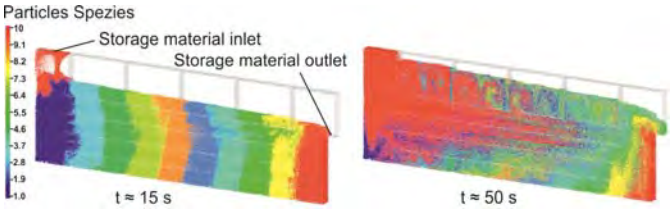

a) Distribution of the storage material close to simulation start

b) Mixing of the feeding storage material in the HEX ≈ 50 s after simulation start

Figure 11: Mixing behavior of the storage material within the sandTES HEX

Fig. 11 shows the mixing behavior of the storage material within the sandTES HEX at different time points. The bed material of the HEX within the individual nozzle-distribution-floors is colored different. The image at the left hand side of Fig. 11 shows the situation close to the simulation start. At this time the red storage material feed stream starts to enter the fluidized bed heat exchanger while the bed material starts to move in direction to the HEX outlet. The picture on the right hand side of Fig. 11 displays the storage material distribution within the HEX approx. 50 s after simulation start. As it can be seen, the storage material feed mass flow is well distributed over the heat exchanger height and flows not only at the top of the fluidized bed in direction to the HEX outlet.

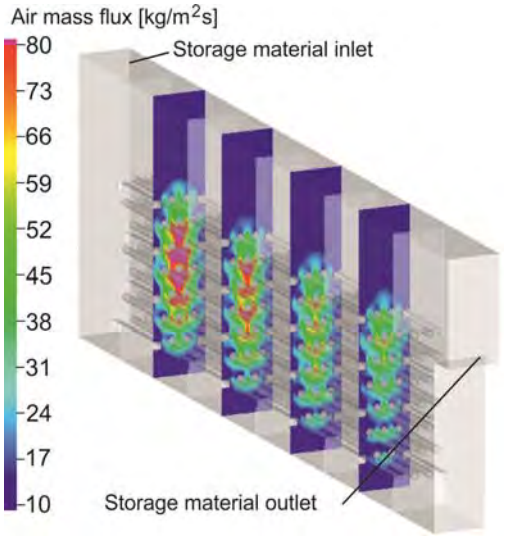

Figure 12: Time-averaged air mass density distribution within the sandTES HEX

As a further result of the Barracuda simulations the time-averaged air mass flow density of the suspension within the sandTES HEX is presented in Fig. 12. The air mass flow density is shown in cross-sectional planes along the length of the sandTES HEX. The air mass flow density decreases starting from the sand inlet in direction to the sand outlet based on the uneven air mass flow distribution along the HEX. It can be also seen in Fig. 12 that within a single cross-section plane the highest mass flux is given around the tubes arranged in the middle of the HEX. The flow stratification along the wall is hindered which is a result of the HEX design with the dummy tubes located at the HEX walls. Therefore a good heat transfer between the tube bundle and the sand should be given.

Beside the numerical investigations done with the software Barracuda the development of an in-house design software for the sandTES HEX has been performed. The calculation code is written and is integrated into the commercial software Matlab. With the help of this in-house design software it is possible to make dimensioning calculations for a sandTES HEX within a user friendly environment. The software allows in a first step a rough outlining of the HEX followed by an accurate design which includes the calculation of all governing effects. The software provides sketches of the HEX-design and all major components and generates automated process flow sheets. A detailed description of the mathematical models used within the in-house software can be found in [28].

Experimental research program

After completion of erection and commissioning of the sandTES test loop within the first two month of 2016 the research program will be immediately started.

In the first phase of the research program experimental investigations without charging and discharging of heat should be done. In the focus of this study is for example:

- the back pressure at different heat exchanger height and mass fluxes,
- the influence of the fluidization grade on the sand mass flux,
- the required degree on uniformity of the fluidization air distribution over the HEX length,
- the influence of the fluidization air distribution on the system stability and
- the influence of segregation effects on the sand transport through the sandTES HEX

After completion of the investigations done with the cold sandTES HEX, the laboratory test loop will be rebuilt for the experimental investigations with charging and discharging of heat. In a first step the following influence factors and operation conditions will be analyzed:

- heat transfer between the tube bundle and the sand,
- heat transfer depending on the particle diameter,
- the influence of the fluidization air distribution on the system stability,
- the influence of segregation and dispersion effects on the sand transport through the sandTES HEX,
- identifying of the effective auxiliary power for the operation of the sandTES HEX technology and
- overall full and part load behavior of the sandTES HEX

The investigations will be done not only for the storage material sand. In further investigations a change of the storage material to corundum will be done. Compared with sand silicon oxide and corundum shows a larger specific heat capacity and thus it will help to reduce the storage mass at constant thermal power.

CONCLUSION

The design of a novel thermal energy storage system based on a combination of the fluidized bed technology with a counter current heat exchanger, the so called sandTES HEX, is described. The functional principle of the technology is specified in detail. To reduce the height of the storage material for the fluid flow within the heat exchanger so called air-cushions are inserted.

The design of the sandTES HEX test rig has been completed to measure the thermal and flow performance of the HEX. The thermal capacity of the test rig is 280 kW_{th}. The goal of the test rig is to demonstrate the performance of the technology but also to have a facility for studying heat transfer, segregation and dispersion effects on the sand transport, overall full and part load behavior and system stability.

Selected preliminary experimental and numerical results are presented and discussed. The results of these investigations have shown that the innovations within the sandTES HEX technology will work with satisfaction.

NOMENCLATURE

g	Gravitation [m/s^2]
h	Height [m]
p	Pressure [Pa]
x	Length [m]

Greek letters

ε	Porosity [-]
ρ	Density [kg/m^3]

Subscripts

p	Particle
f	Fluid
fb	Fluidized bed

ACKNOWLEDGMENTS

The K-Project GSG-GreenStorageGrid (Grand no. 836636) is funded in the framework of COMET - Competence Centers for Excellent Technologies by the Federal Ministry of Transport, Innovation and Technology, the Federal Ministry of Science, Research and Economy, the Vienna Business Agency, the Federal Province of Lower Austria and by the Federal Province of Upper Austria. The program line COMET is administered by the Austrian Research Promotion Agency (FFG). The authors would like to thank also the project partners Valmet GesmbH., EVN AG, ENRAG GmbH. and Primetals Technologies GmbH. for the pleasant and constructive working relationship.

The author would like to thank also the sandTES research team for the helpful support and the numerous discussions. Also the installation crew shall be mentioned, for their effort at erecting the sandTES pilot plant.

REFERENCES

[1] Scholz, R., Beckmann, M., Pieper, Ch., Muster, M. and Weber, R., 2014, “Considerations on providing the energy needs using exclusively renewable sources: Energiewende in Germany”, Renewable and Sustainable Energy Reviews Vol. 35, pp.109–125.

[2] Report from the commission to the European parliament, the council, the European economic and social committee and the committee of the regions, 2013, Renewable energy progress report, report number SWD(2013) 102 final.

[3] Thorwarth, H., 2014, “Future developments within the scope of the Energiewende”, VGB PowerTech, No. 8, pp. 37-41 (in German).

[4] Weber, H., 2014, “Supply security upon the transition to the regenerative sources of power supply, VGB PowerTech, No. 8, pp. 26-31 (in German).

[5] Pieper, Ch., Sykora, N., Beckmann, M., Böhning, B., Hack, N. and Bachmann, T., 2015, “The economic operation of Power-to-heat plants in the German electricity balancing market”, Chemie Ingenieur Technik, Vol. 87, No. 4, pp. 390–402 (in German).

[6] Varone, A. and Ferrari, M., 2015, “Power to liquid and power to gas: An option for the German Energiewende”, Renewable and Sustainable Energy Reviews, Vol. 45, pp. 207-218.

[7] Thess, A., Trieb, F., Wörner, A. and Zunft, S., 2015, “Challange heat storage“, Physik Journal, Vol. 14, pp. 33-39 (in German).

[8] Tay, N. H. S., Belusko, M. and Bruno, F., 2012, “An effectiveness-NTU technique for characterising tube-in-tank phase change thermal energy storage systems”, Applied Energy, Vol. 91, pp. 309-319.

[9] Haider, M., Schwaiger, K., Holzleithner, F. and Eisl, R., 2012, “A Comparison between Passive Regenerative and Active Fluidized Bed Thermal Energy Storage Systems”, Journal of Physics: Conference Series, Vol. 395, pp. 1-8.

[10] Schwaiger, K., Haider, M., Walter. H., Puigpinos, M. and Prötsch, A., 2012, “Thermal storage of superheated steam in a combined sensible/latent TES”, in Proceedings of the Solarpaces 2012, Marrakech, Morocco, September 11-14.

[11] Urschitz, G., Brier, J., Walter, H., Mertz, R., Bleicher, F. and Haider, M., 2015, “New design of a bimetallic finned tube for the use in latent heat thermal energy storage units”, in Proceedings of the ASME 2015 9th International Conference on Energy Sustainability, San Diego, California, USA; 28.06.2015 - 02.07.2015; Paper-No. PowerEnergy2015-49143

[12] Beck, A., Koller, M., Walter, H. and Hameter, M., 2015, “Transient numerical analysis of different finned tube designs for the use in latent heat thermal energy storage devices”, in Proceedings of the ASME 2015 Power and Energy Conference, San Diego, California, USA, 28.06.2015 - 02.07.2015; Paper-No. PowerEnergy2015-49145

[13] Walter, H., Beck, A. and Hameter, M., 2015, “Transient numerical analysis of an improved finned tube heat exchanger for thermal energy storage system”, in Proceedings of the ASME 2015 Power and Energy Conference, San Diego, California, USA, 28.06.2015 - 02.07.2015; Paper-No. PowerEnergy2015-49144.

[14] Li, G., 2016, “Sensible heat thermal storage energy and exergy performance evaluations”, Renewable and Sustainable Energy Reviews, Vol. 53, pp. 897-923.

[15] Anderson, R., Bates, L., Johnson, E. and Morris, J. F., 2015, “Packed bed thermal energy storage: A simplified experimentally validated model”, Journal of Energy Storage, Vol. 4, pp. 14-23.

[16] Zanganeh, G., Khanna, R., Walser, C., Pedretti, A., Haselbacher, A. and Steinfeld, A., 2015, “Experimental and numerical investigation of combined sensible–latent heat for thermal energy storage at 575 °C and above”, Solar Energy, Vol. 114, pp. 77-90.

[17] Warerkar, S., Schmitz, St., Goettsche, J., Hoffschmidt, B., Reißel, M. and Tamme, R., 2011, “Air-Sand Heat Exchanger for High-Temperature Storage”, Journal of Solar Energy Engineering, Vol. 133, No. 2, pp. 021010-1 – 021010-7.

[18] Fricker, H., 2002, “Regenerative Thermal Storage in Atmospheric Air System Solar Power Plants,” Proceedings of the 11th International Symposium on Concentrated Solar Power and Chemical Energy Technologies, A. Steinfeld, ed., Zurich, Switzerland.

[19] Ma, Z., Glatzmaier, G. C. and Mehos, M., 2014, “Development of Solid Particle Thermal Energy Storage for Concentrating Solar Power Plants that Use Fluidized Bed Technology”, Energy Procedia, Vol. 49, pp. 898-907.

[20] Ma, Z., Mehos, M., Glatzmaier, G. C. and Sakadjian, B. B., 2015, “Development of a Concentrating Solar Power System Using Fluidized-bed Technology for Thermal Energy Conversion and Solid Particles for Thermal Energy Storage”, Energy Procedia, Vol. 69, pp. 1349-1359.

[21] Sakadjian, B., Hu, S., Maryamchik, M., Flynn, T., Santelmann, K. and Ma, Z., 2015, “Fluidized-bed Technology

Enabling the Integration of High Temperature Solar Receiver CSP Systems with Steam and Advanced Power Cycles", Energy Procedia, Vol. 69, pp. 1404-1411.

[22] Steiner, P., Schwaiger, K., Hämmerle, M., Walter, H., and Haider, M., 2016, "Increasing load flexibility and plant dynamics of caloric power plants via the implementation of thermal energy storages", in Proceedings of the ASME 2016 Power and Energy Conference PowerEnergy2016, Charlotte, North Carolina, USA; June 26-30; Paper-No. PowerEnergy2016-59181.

[23] Schwaiger, K. and Haider, M., 2014, "Active Fluidization Storage Applications for CSP", Energy Procedia, Vol. 49, pp. 973-982.

[24] Schwaiger, K., Haider, M., Hämmerle, M., Steiner, P., Walter, H. and Obermaier, M., 2015, "Fluidized Bed Steam Generators for Direct Particle Absorption CSP-plants", Energy Procedia, Vol. 69, pp. 1421-1430.

[25] Hämmerle, M., Haider, M., Willinger, R., Schwaiger, K., Eisl, R. and Schenzel, K., 2015, "Saline cavern adiabatic compressed air energy storage using sand as heat storage material", Proceedings of the 10th Conference on Sustainable Development of Energy, Water and Environment Systems, Sept. 27–Oct. 2, Dubrovnik, Croatia, paper no.: SDEWES2015-0583

[26] Yang, W.-Ch., 2003, "Handbook of fluidization and fluid-particle systems", Vol. 91 of chemical industries, Marcel Dekker, Inc., New York.

[27] Verein Deutscher Ingenieure, 2010, "VDI heat atlas", Verein Deutscher Ingenieure, VDI-Gesellschaft Verfahrens-technik und Ingenieurwesen (GVC), 2nd Edition, Springer Publishing Company, Heidelberg.

[28] Schwaiger, K., 2016, "sandTES fluidization concept: an enhanced particle transport, heat-exchanger and thermal energy storage technology", PhD at TU-Wien (in completion state)

[29] Schwaiger, K., Haider, M. and Hämmerle, M., 2015, Patent "Fluidized bed reactor", Patent No.: AT 515683 B1.

[30] Urschitz, G., Walter, H. and Hameter, M., 2014, "Experimental investigation of a finned mono tube - latent heat energy storage (LHTES)", in Proceedings of the ASME 2014 8th International Conference on Energy Sustainability ES2014, Boston, Massachusetts, USA; 30.06.2014 - 02.07.2014, pp. 1-8.

[31] Andrews, M. J. and O'Rourke, P. J., 1996, "The multiphase particle-in-cell (MP-PIC) method for dense particulate flows", International Journal of Multiphase Flow, Vol. 22, No. 2, pp. 379-402.

[32] Snider, D.M., 2001, "An incompressible three dimensional multiphase particle-in-cell model for dense particle flows", Journal of Computational Physics, Vol. 170, pp, 523-549.

[33] Ryan, E. M., DeCroix, D., Breault, R., Xu, W., Huckaby, E. D., Saha, K., Dartevelle, S. and Sun, X., 2013, "Multi-phase CFD modeling of solid sorbent carbon capture system", Powder Technology, Vol. 242, pp. 117-134.

[34] Snider, D.M., Clark, S. M. and O'Rourke, P. J., 2011, "Eulerian–Lagrangian method for three-dimensional thermal reacting flow with application to coal gasifiers", Chemical Engineering Science, Vol. 66, pp, 1285-1295.

[35] Anderson, T.B. and Jackson, R., 1967, "Fluid mechanical description of fluidized beds-equations of motion", Industrial and Engineering Chemistry Fundamentals, Vol. 6, No. 4, pp. 527-539.

Paper 2

P. Steiner, K. Schwaiger, M. Haider, H. Walter

Flow Characteristics of a Fluidized Bed Heat Exchanger used for High Temperature Thermal Energy Storage

Journal of Applied Energy
(Submitted 2017)

Flow Characteristics of a Fluidized Bed Heat Exchanger used for High Temperature Thermal Energy Storage

Peter Steiner[a,*], Karl Schwaiger[a], Markus Haider[a], Heimo Walter[a]

[a] *TU Wien, Institute for Energy Systems and Thermodynamics, Getreidemarkt 9/E302, A-1060 Vienna, Austria*

Abstract

The rapid rise of highly fluctuating renewables leads to challenges for power plants and power grids. Thermal Energy Storage (TES) is envisaged for enhancing the low load capabilities and plant dynamics of thermal power plants. As state of the art Heat Storage Media (HSM) like molten salt are rather expensive and furthermore limited due to their temperature range, particles are proposed as a promising alternative.

In a two tank TES system the handling of these particles, especially inside the Heat Exchanger (HEX), is a challenging task. The so called sandTES-technology uses a fluidized bed HEX, which allows a horizontal plug flow of the particle-air suspension, resulting in a highly efficient counter current HEX.

In this work a 280 kW_{th} sandTES pilot plant is described. The key measurement results, which are indispensable for a reliable and optimized design, are presented and discussed in detail.

Keywords: Fluidized Bed, Thermal Energy Storage, Particles, Heat Exchanger, Reactor

1. Introduction

Much research in recent years has focused on Thermal Energy Storage (TES). The increasing amount of renewables like photovoltaics or wind power, with

*Corresponding author
Email address: peter.p.steiner@tuwien.ac.at (Peter Steiner)

their fluctuating electricity generation, leads to technical and economical challenges for electricity suppliers. Conventional power plants (mostly thermal power plants) are more often required to run in low load and the number as well as the rate of load changes exceeds the original design values. The integration of a TES into the process of a thermal power plant results in enhanced low load capabilities, increased load change rates and improved service life [1].

Apart from the electricity generation sector, various industrial processes have a huge potential to reduce energy losses by buffering thermal energy, which results not only in economical but also environmental advantages.

Compared to TES systems, other storage types, like chemical or mechanical storage, suffer from high costs, issues concerning the scale up or low energy densities. Conventional large scale technologies like pumped storage hydro power are not feasible in many parts of the world.

TES can be divided in latent, thermochemical and sensible storage. Latent TES suffer from poor heat conduction of the storage material, leading to large Heat Exchanger (HEX) surfaces with e.g. complex finned tube geometries [2]. Furthermore the capacity and power of such systems are difficult to decouple. Thermochemical TES are preferable for long time storage, but they are in an early stage of development.

Sensible TES are state of the art e.g. in Concentrated Solar Power (CSP) plants, where nowadays molten salt is used as Heat Storage Medium (HSM). The flexibility of CSP plants can be easily enhanced by integrating a TES directly into the thermal process. For competing against conventional power plants, much research in this field currently is focused on lowering the Levelized Cost of Electricity (LCOE) of these CSP plants. For example, the U. S. Sunshot Initiative aims for an LCOE of 3 US-cents per kWh in 2030, starting from 27 US-cents per kWh in 2010 [3].

The key approach for decreasing the LCOE seems to be the development of a novel TES system, using HSM which are not only low-cost products, but also fit for higher temperatures beyond the current maximum of about 560 °C of molten salt [4]. Especially particles like quartz sand or corundum are often

proposed as HSM. These particles are relatively cheap materials with no relevant temperature limitations. The high achievable maximum temperature allows not only higher energy densities of the storage cycle, but also higher maximum temperatures and thus higher efficiencies of the power cycle [5, 6].

The storage cycle of a CSP plant consists of the Receiver and the TES. Similar to common heat transfer media (HTM), particles are envisaged to be heated up directly in the appropriate particle receiver to be stored in a silo afterward. Several receiver technologies are currently in development, reaching from indirect to direct absorption receivers [7, 8, 9, 10]. If the HEX is not integrated into the tower, a separate particle-fluid HEX is needed.

Apart from CSP technology Adiabatic Compressed Air Energy Storage (ACAES) has a huge potential as large scale energy storage, due to the high round trip efficiency of about 70 % [11, 12]. At ACAES plants air gets compressed and stored at an increased pressure level to be expanded later on demand. The heat resulting from the compression process can be stored with a TES. A pressurized fixed bed regenerator could be used as pressurized vessel and regenerator [13]. Alternatively, an active high temperature TES, thus a two-tank TES system where the HSM is moved from one to the other tank, could be applied.

A common two-tank TES system consists at least of the tanks or silos, a HEX and some conveyors. Regarding the heat losses at the storage bins, a temperature drop below 1 °C at the tank is published at the modern molten salt based CSP plant Crescent Dunes [14]. Due to the low heat conductivity of particles like quartz sand compared to molten salt, even lower heat losses can be expected for the particle bulk in the silos.

The HEX is needed for transferring the thermal energy from the particles to a working fluid (e.g. water/steam, air) or the other way around. Several research facilities worldwide are working on the development of efficient particle-fluid HEX. For increasing the HEX efficiency, thus reducing the terminal temperature difference, counter current HEX are generally suggested. An early project aimed for implementing a moving bed HEX, with particles falling downwards while interacting with a tube bundle, which contains the working fluid [15].

The enhanced heat transfer coefficients led many projects to the use of fluidization technique. A simple approach is a cascade of several tanks each containing a fluidized bed. A horizontal particle flow can be achieved, which allows a more easy control of the mass flow. These cascaded tanks with their fluidized beds inside can be assumed as stirred tanks, each with a nearly constant temperature. By connecting every outlet to the inlet of the next tank, a horizontal flow of the particles can be achieved. However, the non-continuous temperature profile results in higher terminal temperature differences, lowering the efficiency despite the possible counter current flow [16].

To close the gap in development of an efficient particle-fluid HEX, a novel TES system, called sandTES, was developed at the Institute for Energy Systems and Thermodynamics (IET) of TU Wien. The key component of the two tank TES system is the HEX, which also uses fluidization technique for handling the particles. Therein a horizontal plug flow of the particle-air suspension gains a highly efficient counter current HEX. Previous studies suggest exergetic efficiencies in the range of 93 %, including losses due to auxiliary, heat transfer and exhaust air [17]. Of course these efficiencies are strongly depending on the application case.

For proving the concept and validating several performance data like the efficiency of the TES or heat loss while long-term storage, a 280 $\mathrm{kW_{th}}$ pilot plant was put in operation in August 2016 at the IET's laboratory.

In this article the principles of the sandTES technology are outlined. Furthermore, the pilot plant and the overall measurement set up are introduced. Finally the first results of the cold test phase are presented and their consequences on large scale designs are discussed.

2. SandTES Technology

In this section the sandTES principles and key technologies are introduced. More detailed information can be found in [16, 18, 19].

2.1. Materials

As mentioned in the introduction, molten salt suffers from rather low maximum temperatures of about 560 °C. Molten salt furthermore is restricted by its freezing temperature at about 250 °C. Particles like quartz sand or corundum are proposed as HSM. The slightly lower energy density, particularly of quartz sand, is overcompensated by the huge applicable temperature range and the low costs.

2.2. Fluidization technique

The handling of these particles, especially inside the HEX is a challenging task. Mostly fluidized bed HEX are envisaged, due to the high achievable heat transfer coefficient. The effort for auxiliary power has to be kept low, wherefore the volumetric flow of the air and the according pressure drop through the fluidized bed have to be minimized. The pressure drop through the fluidized bed Δp_{fb} is depending on the bed height ΔH_{fb}, the gravity g, the porosity Ψ and the densities of the fluidization fluid ρ_f and the particles ρ_p, see Eq. 1.

$$\Delta p_{fb} = (1 - \Psi)(\rho_p - \rho_f) \cdot g \cdot \Delta H_{fb}. \tag{1}$$

It makes sense, to operate near the minimum fludization velocity, which is the velocity at the turn of a packed bed to a fluidized bed, because of a lower auxiliary power consumption. This minimum fluidization velocity decreases with the particles diameter. As an additional benefit, a low fluidization velocity also lowers the risk of erosion, which is a big issue at common fluidized beds in power plants.

As sieving these powders gets costly at some point, an economical optimum has to be found for a certain material. The considered particle diameters used for the sandTES system are in the range of 60 to 100 microns, which can be classified in between Geldart group A and B, where a bubbling fluidized bed can be expected. The bubbles are crucial for gaining a high heat transfer coefficient and a sufficient mixing in the vertical direction.

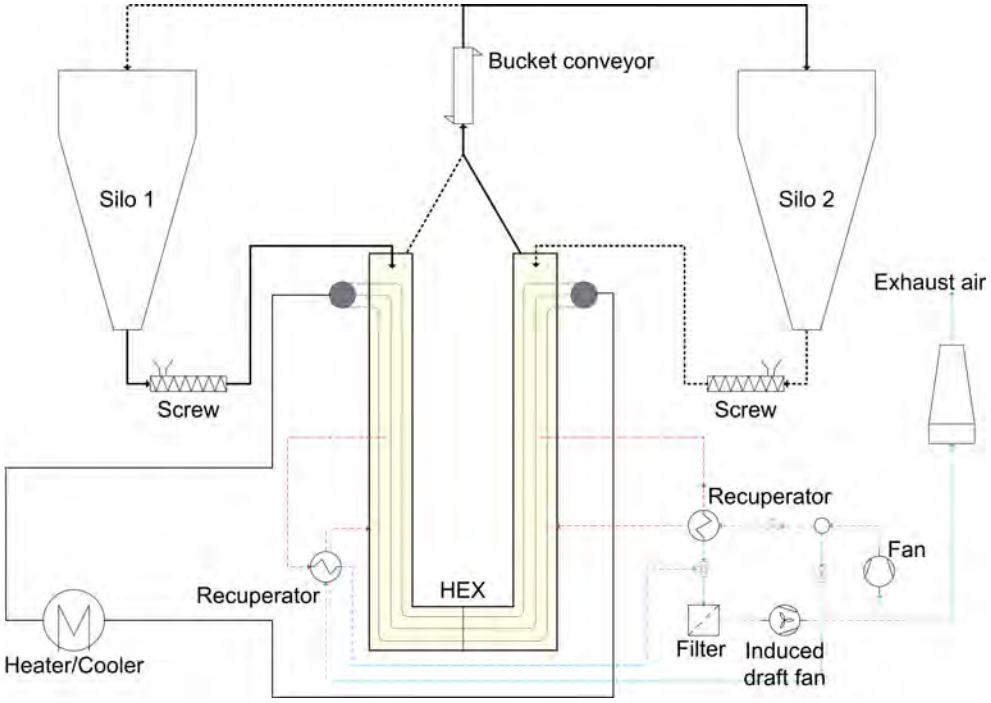

Figure 1: Process flow sheet of the sandTES pilot plant [1]

2.3. Process

As already mentioned, a two tank system is most common at sensible TES systems, thus also applies for the sandTES technology. Figure 1 shows a sandTES process flow sheet, in this case of the sandTES pilot plant.

In the middle the top view of the U-shaped HEX can be seen. Starting on the left hand side, the particles fall out of silo 1 down into a screw, where they get fed into the left HEX inlet. By fluidizing the particles inside the HEX, thus blowing air from the bottom to the top through the particle bed, the obtained particle-air suspension gets a fluid-like behavior. Similar to fluids, the particle-air suspension flows in the horizontal through the HEX, with only the height difference between in- and outlet as driving force. A horizontal tubebundle inside the HEX, containing any working fluid, can be used for exchanging heat in counter current. The working fluid can thereby be heated or cooled by the particles. In the case of the pilot plant, thermal oil (Therminol VP-1) is used as

working fluid, which is heated and cooled by a 280 kW_{th} thermal oil plant. In real life applications the working fluid could be e.g. water/steam from a thermal power plant or a heat transfer medium from a solar receiver. At the end of the HEX, the particles fall down into a conveyor and get transported upwards into silo 2. The directions of the particle and working fluid streams can be reversed, when one silo is emptied or filled, respectively.

As mentioned before, air is used as fluidization gas. To reduce heat losses via the fluidization air, recuperators are installed, to preheat the incoming air and cool down the exhaust air. An induced draft fan and the following filter complete the air flow.

2.4. Key technologies

The main challenge of a fluidized bed HEX achieving a horizontal plug flow, is a stable fluidization and a flexible operation behavior. Therefore two key technologies have been developed, which are briefly introduced [18].

The so called *nozzle distributor floor technology* is used for controlling the fluidization air distribution, while the *air cushion technology* is needed for controlling the height of the bed. Together they lead to a stable, efficient and highly flexible fluidized bed HEX, which enables a counter current heat exchange of the particle suspension and the working fluid.

Both mentioned key technologies are based on Eq. (2), which postulates, that the vertical pressure drop through the HEX Δp_{HEX} in a certain cross section is the sum of the pressure drops of the nozzle Δp_{Nozzle}, of the fluidized bed Δp_{fb} and of the air cushion valve Δp_{Valve}. The total pressure drop from the wind box to the mix box has to be constant in every cross section of the HEX along the particle's flow direction (HEX axis).

$$\Delta p_{HEX} = \Delta p_{Nozzle} + \Delta p_{fb} + \Delta p_{Valve} = const. \tag{2}$$

In Fig. 2 a simplified segment of a sandTES HEX with the horizontal tube bundle and the air piping, is shown. The flow direction of the particles (beige colored) is from the left- to the right-hand side.

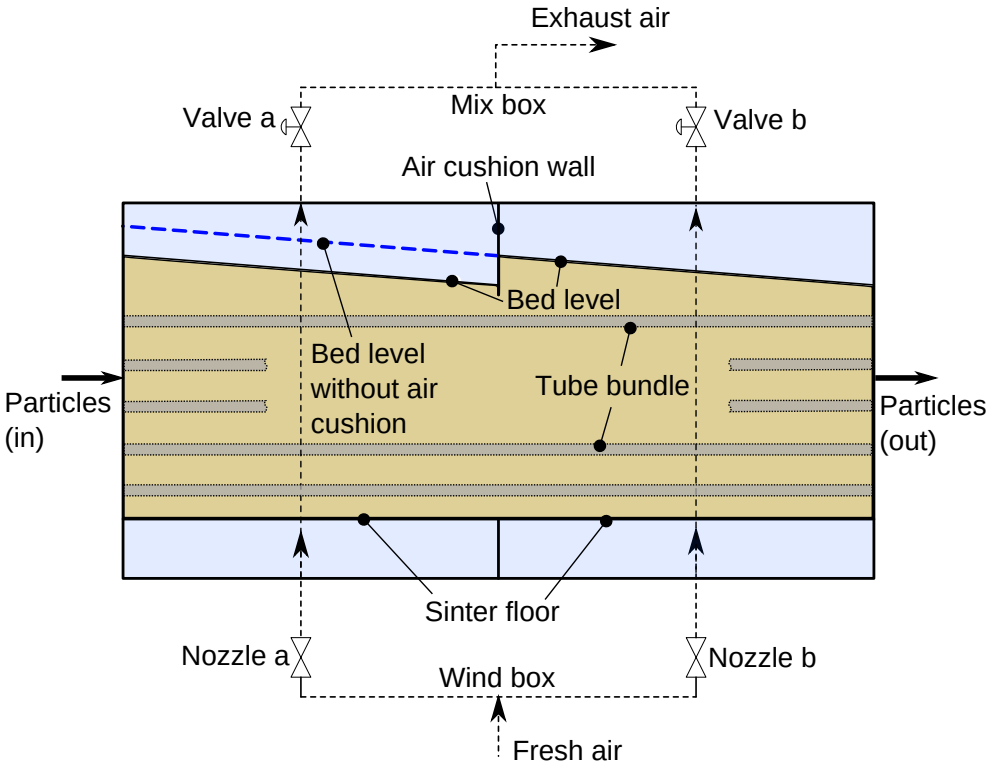

Figure 2: Segment of a SandTES-HEX

Air as the fluidization gas is fed to the wind boxes at the bottom from a single blower. After passing the HEX in the vertical direction, the air is collected at the top at the so called mix boxes.

For a first viewing, the nozzles and valves in Fig. 2 are ignored ($\Delta p_{Nozzle} = \Delta p_{Valve} = 0$). The bed level without air cushion in Fig. 2 continues on the left hand side, marked as the blue dashed line. As stated above, by inserting a particle mass flow on the one side of the HEX and removing it on the other side, the fluidized bed flows through the HEX channel with only the height difference between in- and outlet as the driving force. In fact the driving force is the local pressure of the fluidized bed above the nozzle distributor floor. Similar to liquids, a backlog results, due to the viscosity of the particle air suspension.

Referring to Eq. (1) it gets clear that the vertical pressure drop through the fluidized bed Δp_{fb} depends on the bed height, but not of the superficial velocity

u_{act}. Hence, this pressure drop through the fluidized bed is different in every cross section of the HEX along the particle's flow direction.

The fluidization gas aims to move along the path of least resistance, resulting in a highly unequal air distribution along the HEX axis.

Inserting the nozzles a and b after the wind box causes an additional pressure drop $\Delta p_{Nozzle} > 0$ with a quadratic dependency of the corresponding fluid velocity u_{Nozzle}, see Eq. (3) with ζ as the constant pressure loss coefficient.

$$\Delta p_{Nozzle} = \zeta \cdot \frac{\rho_f \cdot u_{Nozzle}^2}{2} \tag{3}$$

These nozzles smoothen the aforementioned uneven air distribution, by compensating for the different pressure drops through the bed. However, a high total pressure drop of the HEX leads to high auxiliary power consumption, wherefore an optimum has to be found.

The air distribution issue remains the same within one nozzle box, wherefore a number of nozzles is suggested. To keep the number of nozzles in an economic feasible range, the sinter floor, which consists of several porous sinter plates, is inserted below the fluidized bed. These sinter plates with pores in the range of 10 to 30 microns, induce a continuous vertical pressure drop along the HEX axis. The low superficial velocities of the fluidization gas resulting from the large sinter floor area lead to a laminar flow with a moderate stabilizing effect. Additionally, by retaining the fluidized bed, the sinter floor also prevents the particles from plugging the air piping.

The nozzles together with the sinter floor and the chamber in between make each up a so called nozzle box.

For long HEX channels, the slope (backlog) of the fluidized bed level leads to serious height differences between in- and outlet. Thus, great masses between the bed surface and the tube bundle below are not participating in the heat exchange, while requiring auxiliary power for fluidization.

The air cushion technology allows to push down the bed surface as far as reasonable: The top of the HEX is divided into two chambers, separated by

the gas tight air cushion wall, see Fig. 2. Together with the air cushion valves above, these chambers represent the so called air cushions.

Again referring to Eq. (2), an equal total pressure loss in every cross section along the HEX axis is postulated. Thus, an additional pressure drop of the air cushion valves $\Delta p_{Valve} > 0$ (similar to Eq. (3), but with variable ζ) forces one of the other terms of Eq. (2) to decrease, to satisfy that equation. The pressure drop through the fluidized bed has to decrease, wherefore any of the parameters Ψ, ρ_f or ΔH_{fb} of Eq. (1) could be exploited. The appropriate parameter is the bed height, wherefore a rising pressure drop of the air cushion valve leads to a sinking bed height. The pressure drop through the fluidized bed is thereby shifted to the pressure drop of the valve.

In Fig. 2 only two nozzles and two air cushions are shown for the sake of simplicity. Various combinations are possible and are the base of an optimized HEX design.

3. Experimental Investigations

As implied in the last section, various tests are necessary not only for proving the concept, but also for finding design and optimization criteria. The concept of the nozzle distributor floor and the air cushion technology had already been proven in small scale test rigs. The pilot plant, on which this section is based on, is the first semi-industrial scale sandTES-plant, allowing a reliable further scale up later on.

The above mentioned key technologies as well as the overall sandTES-concept could be validated successfully very soon after starting up the plant, leaving room for detailed measurements.

The envisaged test schedule is roughly divided into two phases: a cold and a hot test phase. The cold tests mainly deal with fluidized bed phenomena concerning the flow behavior of the bulk. Primary the height difference between in- and outlet is part of these first analysis, as this so called backlog is crucial for the HEX-design. Not only the HEX-height, but much more the nozzle distri-

butor floor and thus the auxiliary power consumption are mainly depending on this result. The second point of interest deals with the dynamics of the fluidized bed flow. The starting-, shutting down- and reversing-duration are important for compensating highly fluctuating load profiles. The hot tests finally aim to validate the heat transfer coefficients as well as the temperature distribution for this application.

In this article only the key results of the cold test phase are described. The experimental set up of the pilot plant is briefly introduced in the next section, followed by the measurement results and a detailed discussion.

3.1. Pilot Plant - Experimental Set Up

Figure 3 shows an overview of the whole sandTES pilot plant, consisting of the sandTES-HEX as the heart piece of the plant, one blower, a bucket chain conveyor, two silos with each a conveyor screw applied and an induced draft fan including the filter. For the hot tests, also a 280 kW_{th}-thermal oil plant is installed.

The applied two tank process has already been explained before. The key data of the plant components as well as the process parameters are summarized in Table 1.

The sandTES-HEX is fed with air as fluidization gas. As HSM quartz sand is used for these first measurements, although later on measurements are planned with corundum as HSM due to its higher energy density.

Figure 4 shows the sandTES-HEX in its basic set-up, while Table 2 provides the corresponding data. The reference cross section is based on the actual width of the HEX and the height between sinter floor and air cushion casing flange.

As a test rig, a modular and flexible design is essential especially for the sandTES-HEX. The HEX in its minimal set-up consists of the hot casing, 13 nozzle winnows below (each containing 4 nozzle boxes) and the air cushion casing at the top. For the cold tests two cold casings have been inserted in between the hot casing and the air cushion casing, leading to the total height of 2.1 m. The cold casings only contain tube dummies, being a flow resistance

Table 1: Key data of the pilot plant

Description	Unit	Value
Process temperatures	°C	$25 \cdots 390$
Maximum heating power	kW_{th}	280
Maximum cooling power	kW_{th}	200
Particle mass flow	kg/s	$0 \cdots 10$
Particle density	kg/m^3	2650
Mean particle diameter	μm	87
Total particle mass	kg	8000
Nominal power screw	kW_{el}	3.0
Nominal power bucket chain conveyor	kW_{el}	7.5
Air mass flow	g/s	$0 \cdots 225$
Nominal power blower	kW_{el}	18.5
Nominal power induced draft fan	kW_{el}	3

Table 2: SandTES-HEX geometry data

Description	Value
Elongated length of HEX	16 m
Height of HEX	2.1 m
Width of HEX-channel	0.15 cm
Reference cross section	$0.15\,m^2$
Number of wind boxes	1
Number of mix boxes	1
Number of nozzle Boxes	52
Nozzle diameter	5 mm
Number of air cushions	4
Number of tubes	40
Outer tube diameter	25 mm
Horizontal tube bundle pitch	50 mm
Vertical tube bundle pitch	62.5 mm

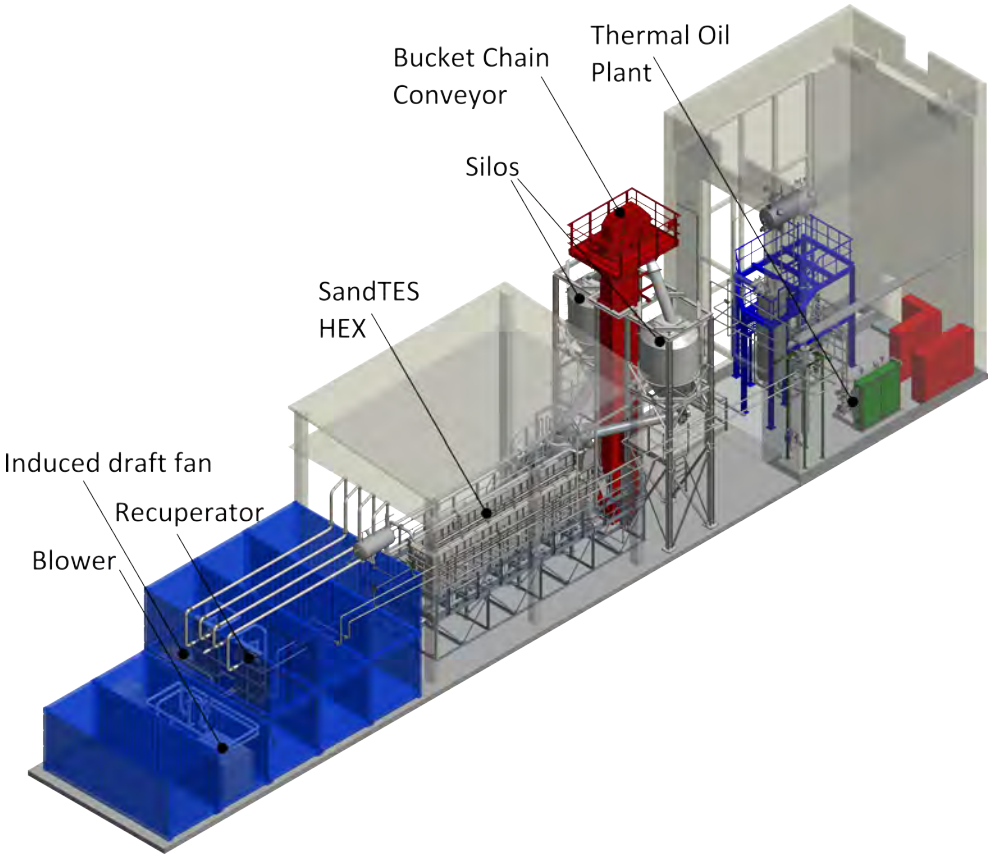

Figure 3: Overview of the sandTES pilot plant

in the fluidized bed. All tube bundles, in the hot as well as in the cold casing, are in a staggered alignment with an outer diameter of 25 mm and a pitch of 50 mm in the vertical and horizontal.

For an adequate resolution, numerous measurement spots are applied all over the HEX, at which pressure or temperature sensors can be applied. The used measurement equipment with the appropriate accuracy is summarized in Table 3. For the cold tests, two temperature sensors are applied in the wind box and are only used for determining the air density and thus the volumetric air flow. Several pressure sensors are applied only for controlling the plant. The air mass flow is determined by a Höntzsch TA10 hot-wire anemometer, which is mounted right after the blower. The particle mass in each silo is measured by

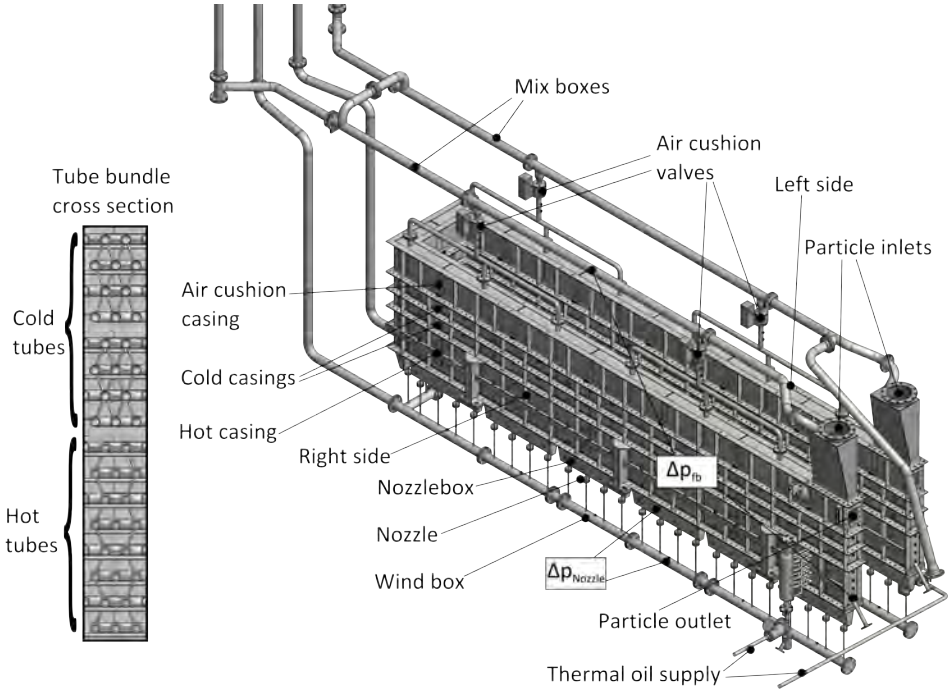

Figure 4: SandTES-HEX in the current measurement set-up

four Bosche S21N load cells, for further on calculating the particle mass flow.

For the following measurement results, pressure differences between the measurement spot in the fluidized bed and the pressure above the bed level Δp_{fb} have to be built, for quantifying the bed height. The appropriate sensors in the fluidized bed are positioned 6 cm above the nozzleboxes at both ends of the HEX as well as at the symmetrical plane. The pressure sensors above the bed are mounted in the wind boxes. Furthermore eight pressure sensors, applied along the axis of the HEX, are used for characterizing the air distribution by measuring the pressure loss Δp_{Nozzle} at selected nozzles.

3.2. Results

As mentioned before, for the cold tests the main measurement targets deal with the backlog, as it is one of the crucial design criterion for the sandTES-HEX.

For the stationary tests every measuring point was run for five minutes with

Table 3: Data of the measurement equipment

Measurand	Type	Unit	Range	Min. Accuracy
Pressure	Kalinsky DS2	mbar	$0 \cdots 250$	1.7 %
Pressure	Kalinsky DS2	mbar	$0 \cdots 10$	2.7 %
Temperature	Pt100A 4L	°C	$-50 \cdots 400$	1 %
Air mass flow	Höntzsch TA10	$(\mathrm{m/s})_\mathrm{n}$	$0.2 \cdots 60$	2.5 %
Mass	Bosche S21N	kg	$0 \cdots 2000$	1 %

a sample rate of 10 Hz. Figure 5 shows the pressure drop through the fluidized bed Δp_{fb} and of the selected nozzles Δp_{Nozzle} along the axis of the HEX at one particular stationary operating point ($\mu = 4.7$, $G_p = 25\,\frac{\mathrm{kg}}{\mathrm{m^2 \cdot s}}$, flow direction left to right). The dimensionless factor μ is the ratio of the actual air velocity u_{act} to the minimum fluidization velocity u_{mf}, see Eq. 4.

$$\mu = \frac{u_{act}}{u_{mf}} \tag{4}$$

The actual air velocity was measured in the wind box, while the minimum fluidization velocity was determined at 7 mm/s in previous test rigs with the same material, but without a tube bundle [20]. The mass flux G_p was calculated with a mean reference bed height and the resulting reference cross section presented in Table 2.

As it can be seen, at this particular operating point, the vertical pressure drop through the fluidized bed changes from about 195 mbar at the left end to about 140 mbar at the right end. Hence, the vertical pressure drop through the bed at the particle inlet is about 55 mbar higher, than at the particle outlet. Looking back to Eq. 2 and Eq. 3, an additional pressure drop is necessary to prevent all the air from passing through the bed at its lowest height on the right-hand side. This is achieved by the nozzle distributor floor, which can be seen at the dotted line in Fig. 5. Neglecting the pressure drop through the sinter plates, the pressure drop through the fluidized bed Δp_{fb} plus the pressure drop of the nozzles Δp_{Nozzle} should be the same in every cross section of the HEX,

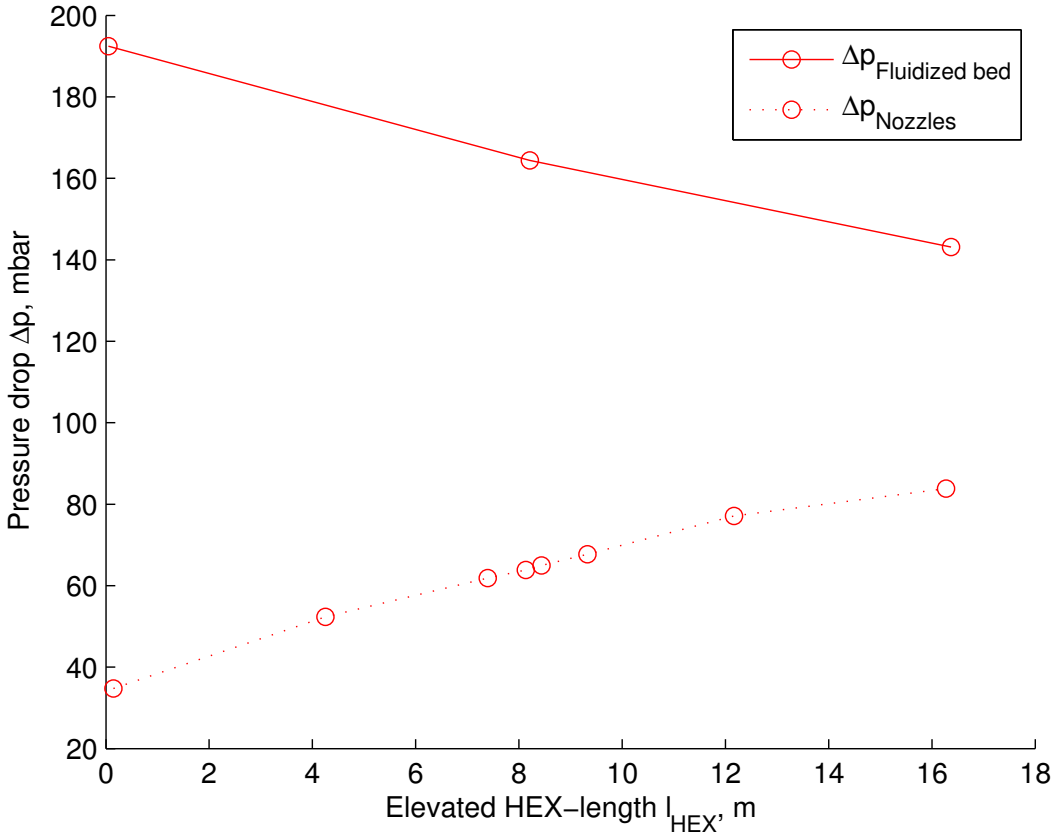

Figure 5: Pressure drop along the HEX-Axis

again see Eq. 2 and Fig. 5.

Reminding Eq. 1, the pressure drop through the fluidized bed Δp_{fb} depends on the corresponding height ΔH_{fb}, with the porosity Ψ as the only variable. For the porosity in the HEX a mean value of $\Psi = 0.54$ was measured, leading to a conversion factor of $f = 0.84 \, \frac{\text{cm}}{\text{mbar}}$.

Performing these stationary backlog measurements for several operating points, with various particle and air mass flows, leads to Fig. 6.

The vertical axis shows the difference $\Delta p_{fb,io}$ between the pressure drop through the fluidized bed at the particle inlet $\Delta p_{fb,i}$ and the corresponding pressure drop at the particle outlet $\Delta p_{fb,o}$ (for both flow directions) normalized

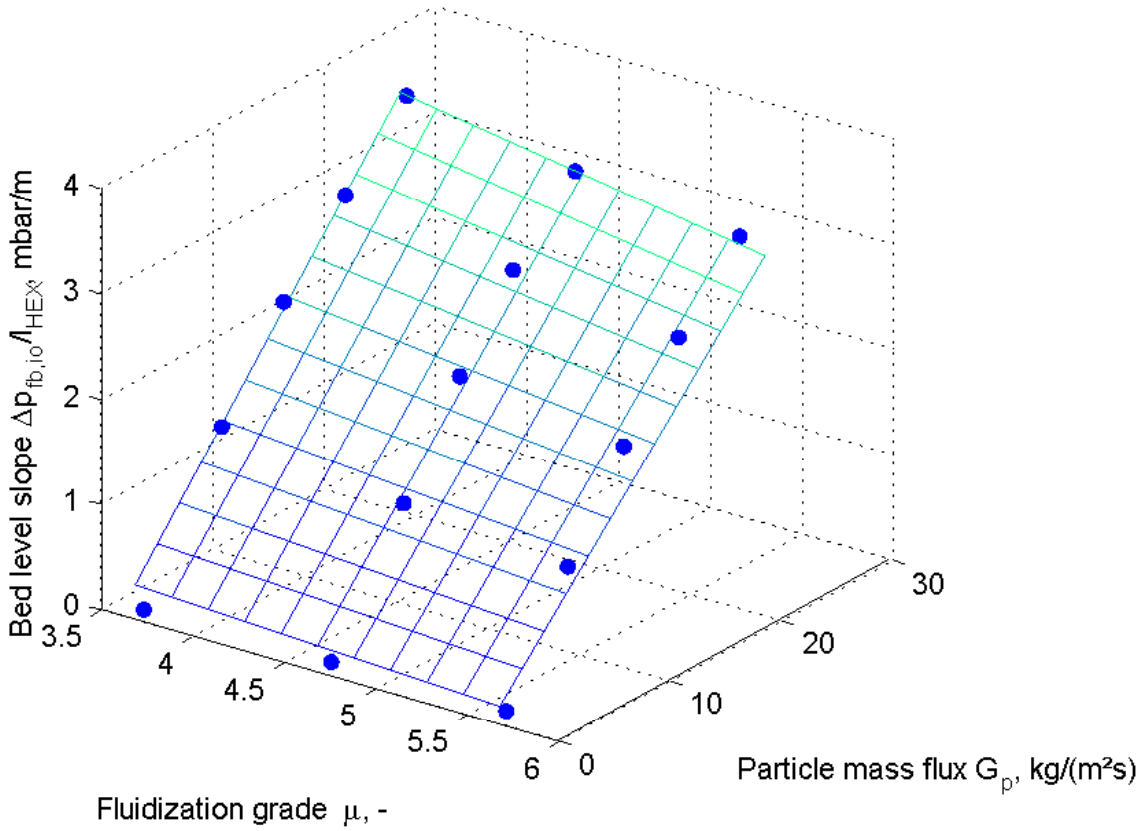

Figure 6: Backlog through the HEX

by the axial length of the HEX l_{HEX}, see Eq. 5.

$$\frac{\Delta p_{fb,io}}{l_{HEX}} = \frac{p_{fb,i} - p_{fb,o}}{l_{HEX}} \tag{5}$$

A regression of the mean values for both flow directions (blue dots in Fig. 6), carried out in Matlab, leads to Eq. 6, which is valid in the ranges $\mu = 3.7 \cdots 5.5$ and $G_P = 0 \cdots 25 \frac{kg}{m^2 \cdot s}$. The corresponding function is plotted in the same graph.

$$\frac{\frac{\Delta p_{fb,io}}{mbar}}{\frac{l_{HEX}}{m}} = 0.60 - 0.07 \cdot \mu + 0.17 \cdot \frac{G_p}{\frac{kg}{m^2 \cdot s}} - 0.01 \cdot \mu \cdot \frac{G_p}{\frac{kg}{m^2 \cdot s}} \tag{6}$$

These backlog measurements, as the most relevant stationary cold test results, are further on supplemented by dynamic cold tests.

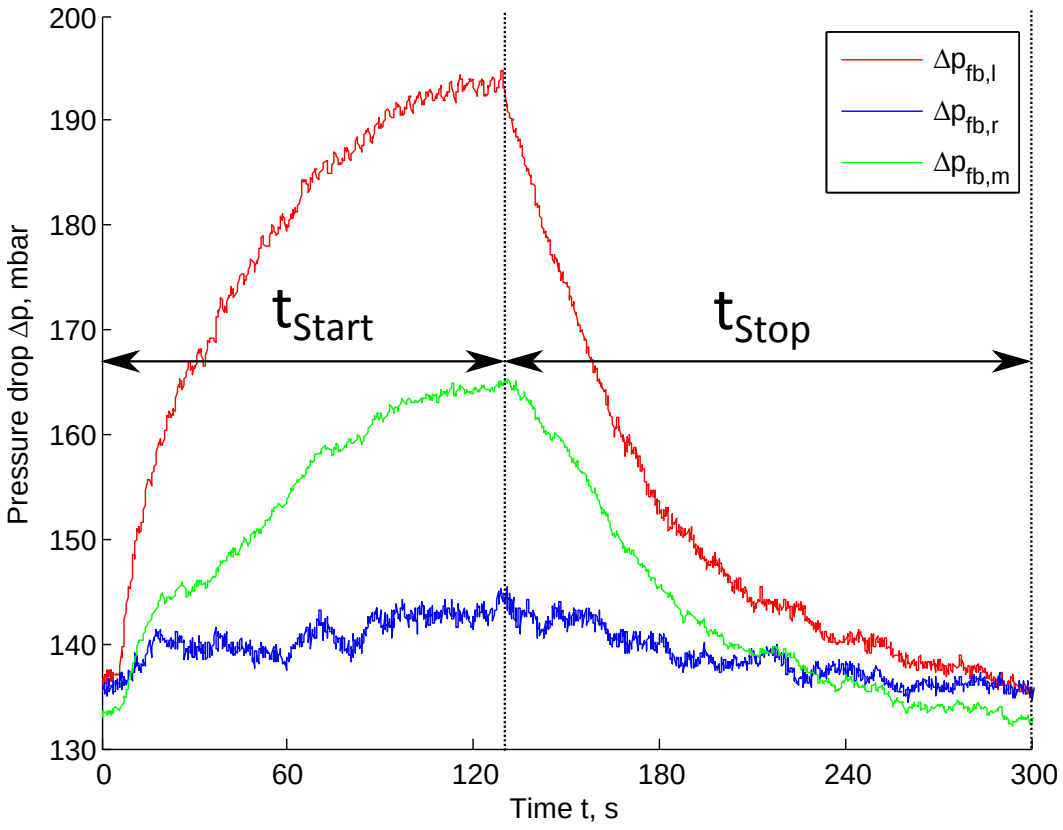

Figure 7: Start-/Stop measurements

Figure 7 again shows the vertical bed pressure drops Δp_{fb} on the left (l) and right (r) end as well as in the middle (m) of the HEX in a span of time t. In this test, starting at a stationary state with no particle mass flow, the conveyor screw gets switched on at a certain time. After reaching the maximum bed height at this operation point, the screw gets stopped.

The operation parameters are a constant particle mass flux with a value of $G_p = 25\,\frac{\mathrm{kg}}{\mathrm{m^2 \cdot s}}$ and a constant fluidization grade of $\mu = 4.7$. The time till the full bed height is reached is at about $t_{start} = 120\,\mathrm{s}$, the additional time till the starting state is reached again after shutting down the screw is at about $t_{stop} = 170\,\mathrm{s}$

At the same operation parameters a sequence of several reversing tests was performed. Figure 8 shows a section of this test series. At the beginning, the

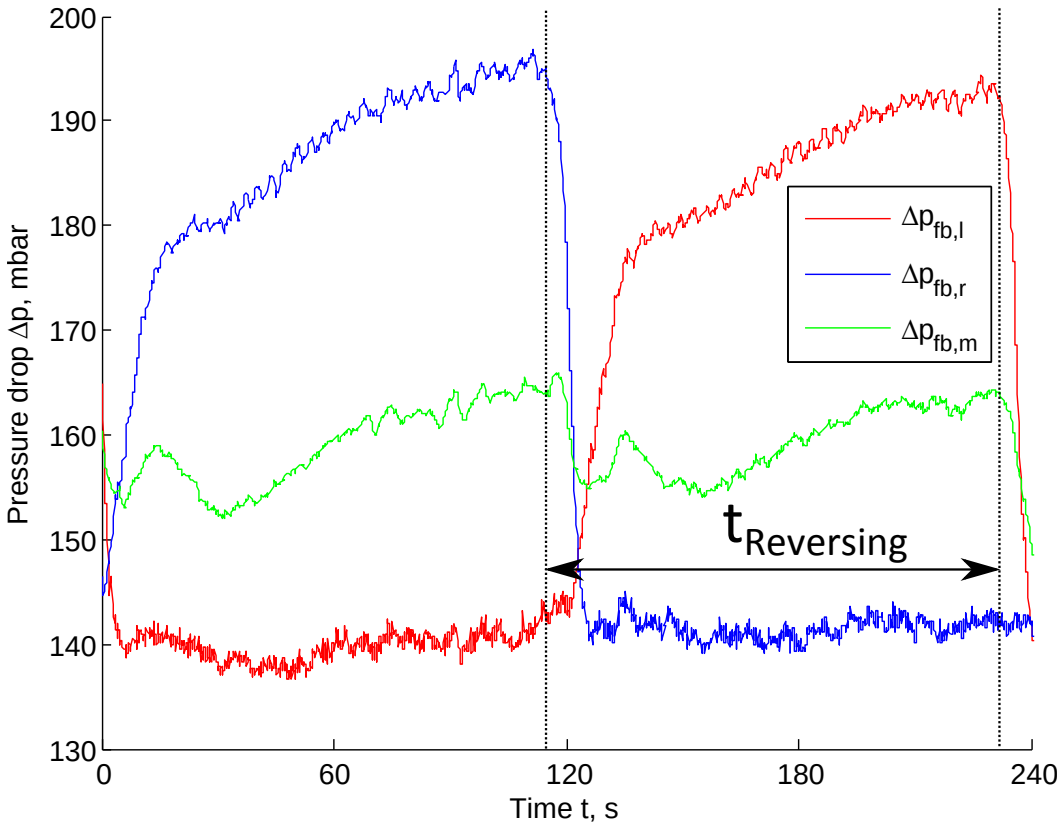

Figure 8: Reversing measurements

flow direction is just changed to right-to-left ($\Delta p_{fb,r}$ rising). An abrupt increase of the bed height at the right particle inlet is followed by a slow increase till the maximum bed height for this operation point is reached. After that, another reversing process takes place, which results in an abrupt pressure drop at the right HEX side ($\Delta p_{fb,r}$) and an fast increase of the pressure drop on the left side ($\Delta p_{fb,l}$) followed by a smooth further raise to its maximum value.

The maximum pressure drops of both flow directions as well as the reversing time $t_{Reversing}$ slightly defer, due to imperfections of the HEX construction.

The green line represents the bed height in the symmetry plane, which is not harmed that much during the reversing process. A delayed fall of the corresponding pressure drop can be seen, which is followed up by a smooth increase to the former bed height.

The time for this whole reversing process can be quantified with approximately $t_{Reversing} = 120\,\mathrm{s}$ at this operating point.

3.3. Discussion

As mentioned above, the particle mass flux G_p is a crucial design parameter. The higher the particle mass flux, the smaller the sandTES-HEX can be constructed at a given particle mass flow, as the flow cross section can be reduced. However, depending on the fluidization grade μ and the HEX geometry (tube bundle surface), the particle mass flux leads to a certain backlog $\Delta p_{fb,io}$, see Eq. 6. A higher fluidization grade and a lower particle mass flux lead to a lower backlog. For a proposed operating point of $\mu = 3.7$ and $G_p = 25\,\frac{\mathrm{kg}}{\mathrm{m^2 \cdot s}}$ a backlog of $\Delta p_{fb,io} = 3.5\,\frac{\mathrm{mbar}}{\mathrm{m}}$ results. Of course, the final operating point of a sandTES-HEX is part of the optimization in the design process and furthermore depending on economic boundaries.

The same applies for the dynamic behavior of the sandTES-HEX. As the fluidized bed is the more inertial compound compared to working fluids like water/steam or the thermal oil, the HEX dynamics are restricted by the particle's dynamics. As it can be assumed that the start-, stop- and reversing-durations decrease with a higher fluidization grade, a temporary raise of the fluidization grade for these operating modes seems reasonable.

4. Conclusion

The rapid rise of highly fluctuating renewables requires convenient storage solutions for guaranteeing a stable power grid. TES systems are frequently proposed, since their integration in the process of existing thermal power plants is advantageous. HSM like molten salt are rather expensive and furthermore restricted by their minimum and maximum temperature.

In recent years, several studies suggested particles like quartz sand or corundum as an appropriate alternative. Especially quartz sand, as a low cost material with a high temperature persistence fits for these applications.

However, the handling of solids is more defying. In a two tank system, conveyors like screws or bucket chain conveyors are needed, for transporting the particles between the tanks and the appropriate HEX.

The sandTES-technology is based on fluidization technique for transporting the particles inside the HEX. A horizontal plug flow of the particle-air-suspension is realized, for achieving a highly efficient counter current HEX.

In this work, the principles, including the sandTES key technologies like the nozzle distributor floor and the air cushion technology, are introduced. Furthermore, the pilot plant set up and the first measurement results are presented and discussed.

For the design of the sandTES-HEX, which is the key part of this TES-technology, the most relevant design parameters have been validated in a cold test phase. Besides the backlog, which correlates to the difference in height between particle in- and outlet, also the dynamic behavior was investigated. Equation 6 estimates the backlog, which is below 4 $\frac{\text{mbar}}{\text{m}}$ for the measured operating points and the present HEX geometry. The influence of the HEX geometry is planned to be investigated next, by removing the cold casings. The dynamic tests reveal a magnitude of a few minutes for changing the load case of the HEX.

This article deals with the fluidized bed related phenomena of the HEX, wherefore cold tests are sufficient. Hot tests, aiming for the temperature distributions and heat transfer coefficients inside the HEX, have already been performed with a similar test rig and are scheduled for further test series.

5. Acknowledgement

The K-Project GSG-GreenStorageGrid (Grand no. 836636) is funded in the framework of COMET - Competence Centers for Excellent Technologies by the Federal Ministry of Transport, Innovation and Technology, the Federal Ministry of Science, Research and Economy, the Vienna Business Agency, the Federal Province of Lower Austria and by the Federal Province of Upper Austria. The program line COMET is administered by the Austrian Research Promotion

Agency (FFG). The authors would like to thank also the project partners Valmet GesmbH., EVN AG, ENRAG GmbH. and Primetals Technologies GmbH. for the pleasant and constructive working relationship.

References

[1] P. Steiner, K. Schwaiger, M. Haider, H. Walter, M. Hämmerle, Increasing load flexibility and plant dynamics of thermal power plants via the implementation of thermal energy storages, Proceedings of the ASME 2016 Power and Energy Conference (2016) (PowerEnergy2016-59181).

[2] A. Beck, M. Koller, H. Walter, M. Hameter, Transient numerical analysis of different finned tube designs for use in latent heat thermal energy storage devices, Proceedings of the ASME 2015 9th International Conference on Energy Sustainability (2015) (ES2015-49145).

[3] DOE/EE-1501, The Sunshot Initiative: The SunShot Initiative's 2030 Goal: 3 US-cents per Kilowatt Hour for Solar Electricity(2017).

[4] D. Schlipf, P. Schicktanz, H. Maier, G. Schneider, Using sand and other small grained materials as heat storage medium in a packed bed httess, Energy Procedia 69 (2015) 1029–1038. doi:10.1016/j.egypro.2015.03.202.

[5] J. Spelling, A. Gallo, M. Romero, J. González-Aguilar, A high-efficiency solar thermal power plant using a dense particle suspension as the heat transfer fluid, Energy Procedia 69 (2015) 1160–1170. doi:10.1016/j.egypro.2015.03.191.

[6] P. Steiner, K. Schwaiger, M. Haider, H. Walter, System analysis of central receiver concepts with high temperature thermal energy storages: Receiver technologies and storage cycles, AIP Conference Proceedings (1850) (2016) 110015. doi:10.1063/1.4984489.

[7] A. Gallo, J. Spelling, M. Romero, J. González-Aguilar, Preliminary design and performance analysis of a multi-megawatt scale dense particle suspension receiver, Energy Procedia 69 (2015) 388–397. doi:10.1016/j.egypro.2015.03.045.

[8] A. C. Iniesta, M. Diago, T. Delclos, Q. Falcoz, T. Shamim, N. Calvet, Gravity-fed combined solar receiver/storage system using sand particles as heat collector, heat transfer and thermal energy storage media, Energy Procedia 69 (2015) 802–811. doi:10.1016/j.egypro.2015.03.089.

[9] L. Amsbeck, B. Behrendt, T. Prosin, R. Buck, Particle tower system with irect absorption centrifugal receiver for high temperature process heat, Energy Procedia 69 (2015).

[10] J. Christian, C. Ho, System design of a 1 mw north-facing, solid particle receiver, Energy Procedia 69 (2015) 340–349. doi:10.1016/j.egypro.2015.03.038.

[11] E. Drury, P. Denholm, R. Sioshansi, The value of compressed air energy storage in energy and reserve markets, Energy 36 (8) (2011) 4959–4973. doi:10.1016/j.energy.2011.05.041.

[12] A. Sciacovelli, Y. Li, H. Chen, Y. Wu, J. Wang, S. Garvey, Y. Ding, Dynamic simulation of Adiabatic Compressed Air Energy Storage (A-CAES) plant with integrated thermal storage – Link between components performance and plant performance, Applied Energy 185 (2017) 16–28. doi:10.1016/j.apenergy.2016.10.058.

[13] S. Freund, R. Marquardt, P. Moser, Adele adiabatic compressed air energy storage - status and perspectives, VGB PowerTech 5—2013 (2013) 66–70.

[14] SolarReserve, Media gallery.
URL http://www.solarreserve.com/en/global-projects/csp/crescent-dunes (2016)

[15] T. Baumann, S. Zunft, Development and performance assessment of a moving bed heat exchanger for solar central receiver power plants, Energy Procedia 69 (2015) 748–757. doi:10.1016/j.egypro.2015.03.085.

[16] K. Schwaiger, Development of a novel particle reactor/heat-exchanger technology for thermal energy storages, PhD Thesis, TU Wien, Wien (2016).

[17] M. Haider, K. Schwaiger, F. Holzleithner, R. Eisl, A comparison between passive regenerative and active fluidized bed thermal energy storage systems, Journal of Physics: Conference Series 395 (2012) 012053. doi:10.1088/1742-6596/395/1/012053.

[18] P. Steiner, K. Schwaiger, H. Walter, M. Haider, M. Hämmerle, Fluidized bed particle heat exchanger for supercritical carbon dioxide power cycles, Proceedings of the ASME 2016 International Mechanical Engineering Congress and Exposition (2016) (IMECE2016-67104).

[19] P. Steiner, K. Schwaiger, H. Walter, M. Haider, Active fluidized bed technology used for thermal energy storage, Proceedings of the ASME 2016 Power and Energy Conference (2016) (PowerEnergy2016-59053).

[20] M. Hämmerle, Auslegung und Konstruktion einer 200[kW]th-sandTES Pilotanlage, Master thesis, TU Wien, Wien (2013).

Paper 3

P. Steiner, K. Schwaiger, M. Haider, H. Walter, M. Hämmerle

Increasing Load Flexibility and Plant Dynamics of Thermal Power Plants via the Implementation of Thermal Energy Storages

Proceedings of the
ASME 2016 Power and Energy Conference PowerEnergy2016
June 26-30, 2016, Charlotte, North Carolina

Proceedings of the ASME 2016 Power and Energy Conference
PowerEnergy2016
June 26-30, 2016, Charlotte, North Carolina

PowerEnergy2016-59181

INCREASING LOAD FLEXIBILITY AND PLANT DYNAMICS OF THERMAL POWER PLANTS VIA THE IMPLEMENTATION OF THERMAL ENERGY STORAGES

Peter STEINER
Technische Universität Wien
Institute for Energy Systems and Thermodynamics
Getreidemarkt 9/E302
A-1060 Vienna, AUSTRIA
peter.p.steiner@tuwien.ac.at

Karl SCHWAIGER
Technische Universität Wien
Institute for Energy Systems and Thermodynamics
Getreidemarkt 9/E302
A-1060 Vienna, AUSTRIA

Markus HAIDER
Technische Universität Wien
Institute for Energy Systems and Thermodynamics
Getreidemarkt 9/E302
A-1060 Vienna, AUSTRIA

Heimo WALTER
Technische Universität Wien
Institute for Energy Systems and Thermodynamics
Getreidemarkt 9/E302
A-1060 Vienna, AUSTRIA

Martin HÄMMERLE
Technische Universität Wien
Institute for Energy Systems and Thermodynamics
Getreidemarkt 9/E302
A-1060 Vienna, AUSTRIA

ABSTRACT

The significant increase of fluctuating renewables leads to great challenges for the power grids and for the power suppliers: the flexibility of their power plants has to rise to be sufficiently competitive. For thermal power plants the integration of thermal energy storages (TES) seems to be a promising approach. Therefore the so called sandTES technology, an active particle based TES system, is introduced. In a second step it is used to demonstrate the flexibility enhancement via TES integration. Thereby a novel concept for integrating this type of TES is presented and afterwards discussed. The results give an overview about the chances and restrictions of this implementation concept.

INTRODUCTION

A major issue in today's electricity markets is the increasing amount of fluctuating renewables, which have a big impact on grid stability. Photovoltaics and wind power provide electricity regardless to the load demand, which can lead to situations of strong over- or under-capacities in the power grid. In regions where these renewables are prioritized, thermal power plants more often need to run in low load conditions or even have to be shut down. Due to the resulting mechanical and economical challenges, the number of decommissioned thermal power plants in Europe is rising. To be sufficiently competitive, the load flexibility and plant dynamics have to be improved.

Therefore the integration of thermal energy storage (TES) systems into thermal power plants seems to be an appropriate solution: during periods of overcapacities in the power grid, thermal energy can be taken out of the power plant process by charging a TES. Since the part load range of thermal power plants is mainly limited by the boiler, this method is a promising way to enhance the low load capacity. Also the speed of load change can be affected in a positive way, because of the simultaneous heat extraction via the TES. Conversely, in times of higher electricity demand, the stored thermal energy can then be returned by discharging the TES; thus feeding back the thermal energy into the power plant process at a suitable spot.

In literature different concepts, regarding to the points of charging and discharging, are discussed. Most common concepts are, running a TES in parallel to the steam generator or to some preheaters. Also the TES integration into the flue gas line is considered [1]. Apart from this, different types of TES are investigated, mostly categorized in sensible, latent or thermochemical storage systems [2]. Especially for high temperature application, the sensible TES are most accurately investigated and even proven. For instance, molten salt has been used in solar thermal power plants for years [3]. An upcoming trend seems to be the usage of particles as storage medium, aiming at the high achievable temperatures.

The focus of the present paper is on a potential concept for the TES integration into a thermal power plant. At first a novel sensible TES technology, called sandTES, is presented. A typical thermal power cycle is introduced to outline the present plant limitations, referring to the flexibility characteristics. Based on this power cycle, a concept for integrating a sensible TES is demonstrated. The sandTES technology is implemented, although other TES systems, e.g. using molten salt, could be applied in a similar way. The implementation concept for increasing load flexibility with a sandTES system is discussed in detail.

SANDTES

The sandTES technology is being developed at the Institute of Energy Systems and Thermodynamics (IET) of the Technische Universität Wien. Its aim is to achieve an active TES, which exceeds the previous temperature limits of common sensible TES systems. These systems often use molten salt or thermal oil, which have a maximum temperature of about 550 °C and 400 °C, respectively [4]. Besides, molten salt solidifies at temperatures below approx. 250 °C, which further reduces the potential temperature range. As the name suggests, the sandTES basically is run with (quartz) sand as storage medium, which enables maximum temperatures up to 1000 °C. Although sand is a cheap storage medium, other materials like corundum are considered due to their higher energy density.

The core of the sandTES technology is a particle/fluid heat exchanger (HEX), in which a dense particle suspension is fluidized e.g. by air. The thereby achieved fluid-like behaviour of the suspension and the horizontal pressure gradient (caused by the height difference of the bed between inlet and outlet) makes it flow through the HEX. The flow directions of both heat transfer medium and working fluid (e.g. water/steam) are reversible, which is necessary if only one HEX should fit for charging as well as discharging mode. To reduce exergetic losses during the heat transfer, the particles flow in countercurrent to the working fluid, which is contained in a tube bundle. The heat contained in the fluidization air can be largely recovered by recuperators. To reduce the losses due to auxiliary equipment, the pressure drop through the bed and the blower mass flow have to be kept low. The vertical pressure drop of the fluidization air through the suspension mostly depends on the height of the fluidized bed, see Eq. (1)

$$\Delta p_{fb} = (1-\psi)\left(\rho_p - \rho_f\right) \cdot g \cdot \Delta H_{fb} \qquad (1)$$

with the vertical pressure drop Δp_{fb}, the gravity g, the density of the particles ρ_p and fluid ρ_f, the corresponding height ΔH_{fb} and the porosity of the bed ψ. The fluidization air mass flow correlates with the fluidization grade μ, see Eq. (2)

$$\mu = \frac{u_{act}}{u_{mf}} \qquad (2)$$

with u_{act} the actual superficial velocity, and u_{mf} the minimum fluidization velocity, below which the fluidized bed collapses. The fluidization grade needs to be higher than 1 at every point of the HEX. This is the reason, why the mean value is stated at about 3 to 4. Since u_{mf} decreases with the particle size, very fine powders (in the magnitude of 60-100 microns) are preferred to further reduce auxiliary power. More specific technical details are presented in [5].

In Fig. 1 a simplified process diagram of a sandTES system is shown to introduce the basic storage concept. To charge the TES, cold sand falls out of the filled silo (e.g. silo 1) and is fed via a screw into the HEX. Because of the horizontal pressure gradient, the storage material within the fluidized bed flows through the device, while getting heated up by the working fluid. At the outlet, the hot sand falls into a bucket conveyor, which transfers the sand upwards into silo 2, in which it is stored. For discharging, the direction can be reversed, so that the hot sand flows back through the HEX from silo 2 to 1 while cooling down. Meanwhile the hot exhaust air cools down in the recuperator by heating up the fresh air stream. After filtering, the exhaust air leaves the system through a chimney.

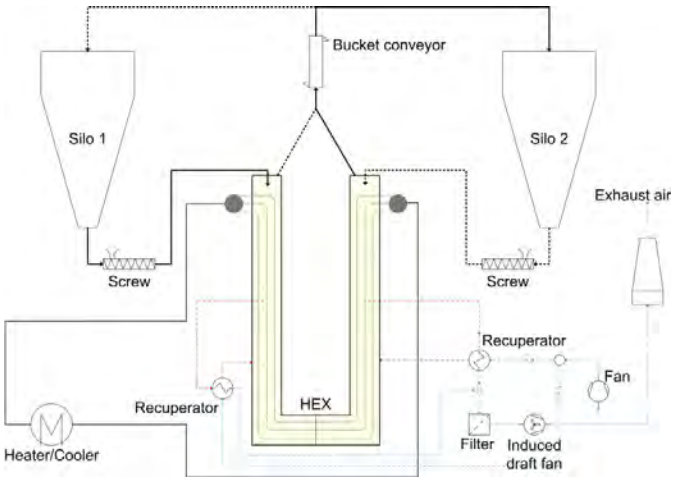

Fig. 1: Process Diagram of a basic sandTES system

For proving the concept, a pilot plant is being put in operation at the IET's laboratory site. Insightful conclusions about the stability and optimization criteria are expected by the measurements [5].

PROCESS INTEGRATION

The simulations performed in this work were carried out with the commercial process simulation tool EBSILON®Professional. With this tool a model of a thermal power plant, based on the reference power plant North Rhine-Westphalia (RPP NRW) was rebuilt. RPP NRW is a state of the art super-critical sliding pressure power plant, developed in Germany. For this work it was decided to create a model with a

reduced nominal power by a factor of 2, due to the current trend to build smaller power plants.

The nominal data of the model are listed in Table 1. Therein the boiler output represents the fuel heat input without boiler losses. The generator output excludes auxiliary power. The cooler pumps aren't considered for this model, wherefore the auxiliary power is slightly lowered. The definitions of the net efficiency η_{Net} and the gross efficiency η_{Gross} are shown in Eq. (3) and Eq. (4) where P means the respective output. The fuel heat input is calculated with the lower heating value (LHV).

$$\eta_{Net} = \frac{P_{Net}}{P_{Fuel,LHV}} \quad (3) \qquad \eta_{Gross} = \frac{P_{Generator}}{P_{Fuel,LHV}} \quad (4)$$

Table 1: Nominal data of the basic cycle model

Description	Value	Unit
Boiler output	600	MW_{th}
Fuel heat input	651	MW_{th}
Net output	294	MW_{el}
Generator output	307	MW_{el}
Live steam pressure	285	bar
Live steam temperature	600	°C
Reheater steam temperature	620	°C
Turbine inlet pressure	285	bar
Condenser pressure	45	mbar
Net efficiency	45.2	%
Gross efficiency	47.1	%

The corresponding process flow sheet is shown in Fig. 2. The model includes the water/steam cycle on the right-hand side and also the combustion streams on the left-hand side. The power plant is built up with 8 feed water preheaters and a turbine set divided in a high (HP), intermediate (IP) and low pressure (LP) turbine. The boiler consists of the combustion chamber and the steam generator, which are modeled separately.

For conventional thermal power plants a boiler load range of 40 % to 100 % with nearly constant steam temperatures is reported [1]. For the turbines a minimum part load in the range of 20 % seems to be realizable [6]. Choosing the more restrictive criterion, the lowest part load for the model was set to 40 %. EBSILON®Professional provides a part load mode, which was used to calculate the chosen minimum load case. The results are shown in Table 2. The relative values always refer to the nominal data.

Table 2: Boiler part load 40 %

Description	Unit	Value	Rel. [%]
Boiler output	MW_{th}	240	40
Fuel heat input	MW_{th}	251	39
Net output	MW_{el}	111	38
Generator output	MW_{el}	114	37
Live steam pressure	bar	160	56
Live steam temperature	°C	~600	100
Reheater steam temperature	°C	~620	100
Turbine inlet pressure	bar	105	37
Condenser pressure	mbar	32	70
Net efficiency	%	44.1	98
Gross efficiency	%	45.6	97

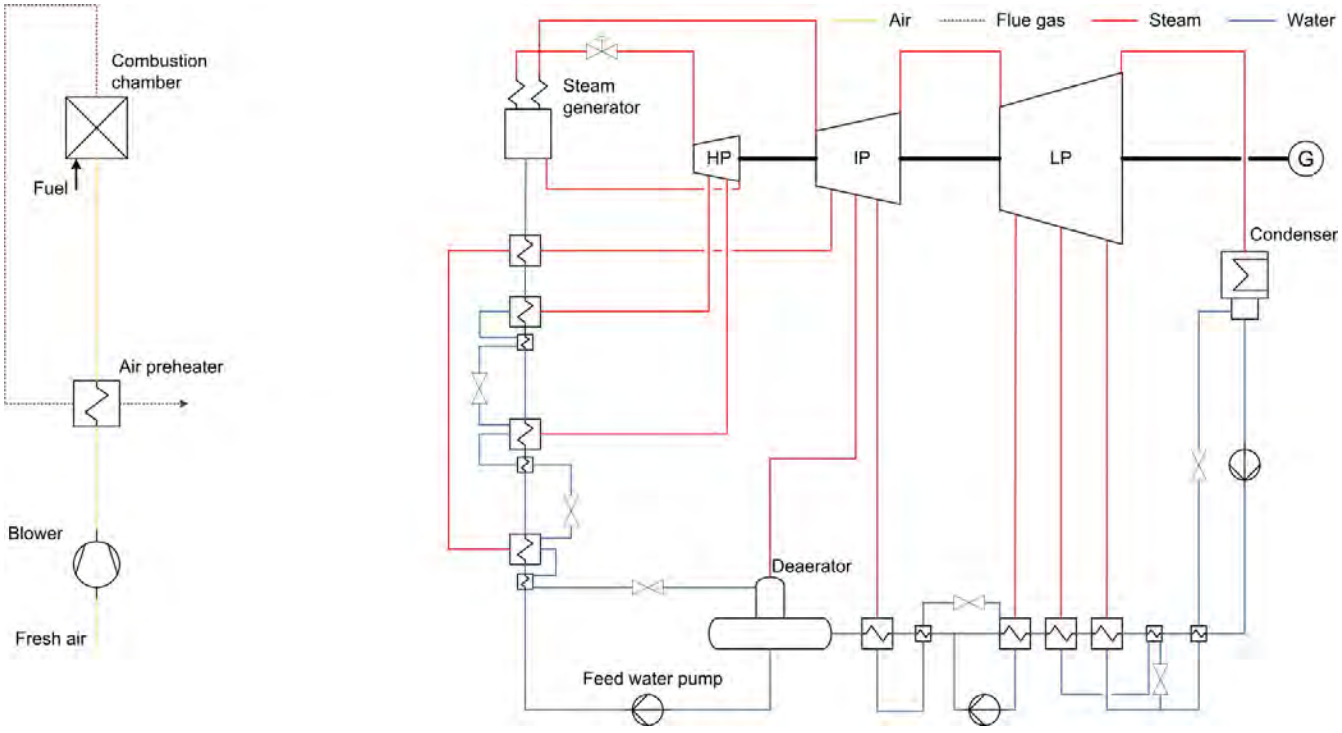

Fig. 2: Process flow sheet of the basic cycle model with combustion streams (left) and water/steam cycle (right)

Due to the restrictions of the boiler minimum load, the boiler has to be decoupled from the turbine, to gain a further reduction of the net output. The decoupling can be achieved via TES integration e.g. by running the appropriate HEX in parallel to the steam generator. As mentioned in the introduction, the following remarks are based on the sandTES technology, although other sensible TES systems could be implemented analogically.

A basic concept for TES integration, with a brief overview following, is shown in Fig. 4. In the case of charging, a live steam mass flow is branched before the high pressure turbine. Further on, this stream is put into the HEX, where it is cooled down and condensed while heating up the storage medium. The heated storage medium, in the first place coming from the cold silo, is then stored in the hot silo. The heat losses via the fluidization air can be largely recovered by a recuperator. The pressure drop through the fluidized bed can be assumed in the range of hundred mbar.

At the end the condensed water out of the HEX is inserted back to the cycle in front of the steam generator. This branched water/steam mass flow didn't pass the turbines, wherefore the turbine mass flow and with it the resulting net output is reduced. Due to Stodola's law, the steam pressure before the turbine decreases with the turbine mass flow, if a nearly constant condenser pressure is assumed. To decouple this turbine inlet pressure from the boiler pressure, a control valve is installed. As a result, the minimum part load of the whole power plant can be further reduced, despite the steam generator being hardly affected.

Obviously, the pressure drop over the control valve should be minimized, to lower the related exergetic losses. Vice versa the exergetic losses caused by the heat transfer in the HEX should be minimized too, wherefore the thermodynamic mean temperature has to be maximized. These two objectives are opposing, which can be seen in Fig. 3.

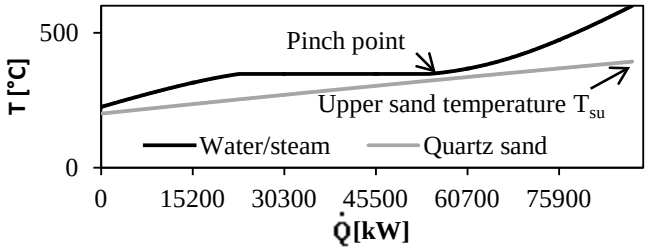

Fig. 3: $\dot{Q}$,T-graph for charging the storage medium

Keeping the in- and outlet temperatures of the water/steam, the lower temperature of the sand and the pinch point constant, the upper temperature of the sand T_{su} increases with the pressure of the water/steam. Due to the turbine inlet pressure determined by Stodola's law, a higher pressure before the valve (in the boiler and the HEX) leads to a higher pressure drop over the valve, accompanied by the exergetic losses. At power plants with multiple turbine sets, it might be an opportunity to switch off a turbine set and therefore keeping the turbine inlet pressure at nominal level. In this work a boiler pressure of 160 bar in part load cases is chosen, being aware of the further

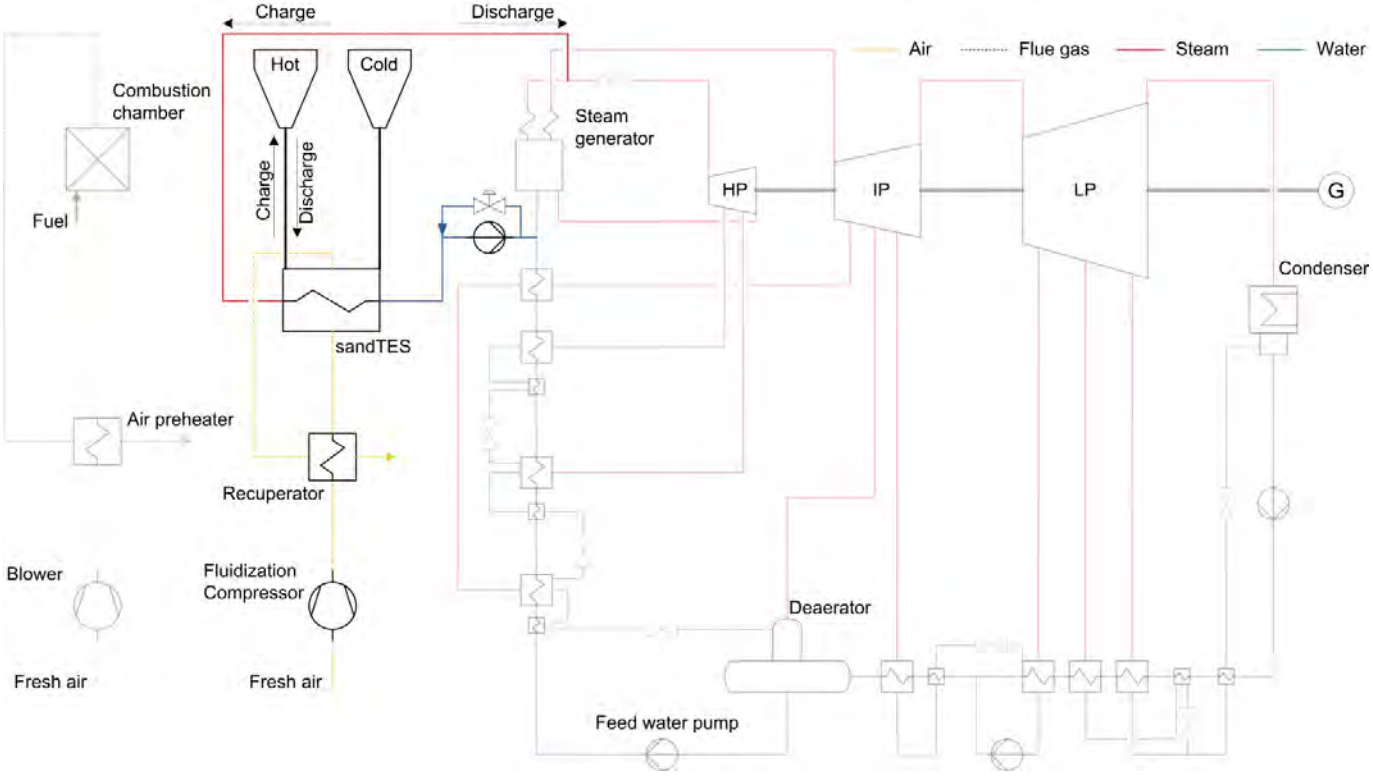

Fig. 4: Process flow sheet for a TES run in parallel to the steam generator for charging and discharging

investigations to be done.

Coming back to the discharging mode in Fig. 4, the water/steam and the sand streams get reversed; thus the water is branched in front of the steam generator and heated up in the sandTES-HEX by the storage medium. In this way the cooled sand is transported back into the cold silo. The produced live steam is then fed back in front of the high pressure turbine.

Because of the terminal temperature difference during the charging as well as the discharging process, the nominal steam parameters cannot be reached. At least the live steam and the reheater steam temperatures are decreasing. This affects the whole basic cycle, regarding the preheaters but also the turbines and hence the net output.

Moreover two separate HEXs have to be built, as the pressure and temperature levels, the mass flows and the heat capacities are strongly diverging for condensing the live steam in charging mode and evaporating the preheated water in discharging mode. The potential especially for retrofit application at a thermal power plant seems doubtful, wherefore this concept is discarded for this work.

In the following sections, two improved solutions are introduced, which will be discussed afterwards.

Variant 1

To avoid the stated issues concerning the discharging mode, a new concept was considered, which is shown in Fig. 5. The charging mode is equal to the one described above regarding Fig. 4. The only difference is that the fluidization air now can be branched from the fresh air line. It is then used for fluidization and afterwards mixed with the fresh air again. As a consequence, the heated fluidization air doesn't need to be recuperated, since the heat can directly be transferred into the combustion chamber. Despite the already low fluidization air mass flow, the heat losses can thereby be further reduced. Also the recuperators are not necessary. Depending on the dimensions of the HEX and with it the vertical pressure drop through the fluidized bed, a separate blower for charging seems suitable to keep the pressure level in the fresh air stream low.

Consequently, for discharging the TES, it seems reasonable, to transfer all of the heat directly via the fluidization air into the combustion chamber; without affecting the water/steam cycle. Thus, the preheated fresh air is redirected through the sandTES, where it is further heated up. If the air preheater doesn't fit for the higher pressure difference, a compressor has to be added in front of the sandTES-HEX.

Afterwards this hot air flows into the combustion chamber, wherefore the fuel mass flow can be lowered. Due to the much higher air mass flow and the not necessarily needed tube bundles in the discharge mode, another separate and specialized HEX, gaining a low minimum temperature difference, should be considered. A lower height of this HEX leads to a smaller pressure drop through the fluidized bed in the range of about 100 mbar. To achieve a compact HEX-design, the fluidization grade has to be increased.

To show the improvement regarding the low load capability achieved by the TES integration, a charging case at 40 % boiler mass flow and the associated full load discharging case were calculated. The data for this concept, with a chosen

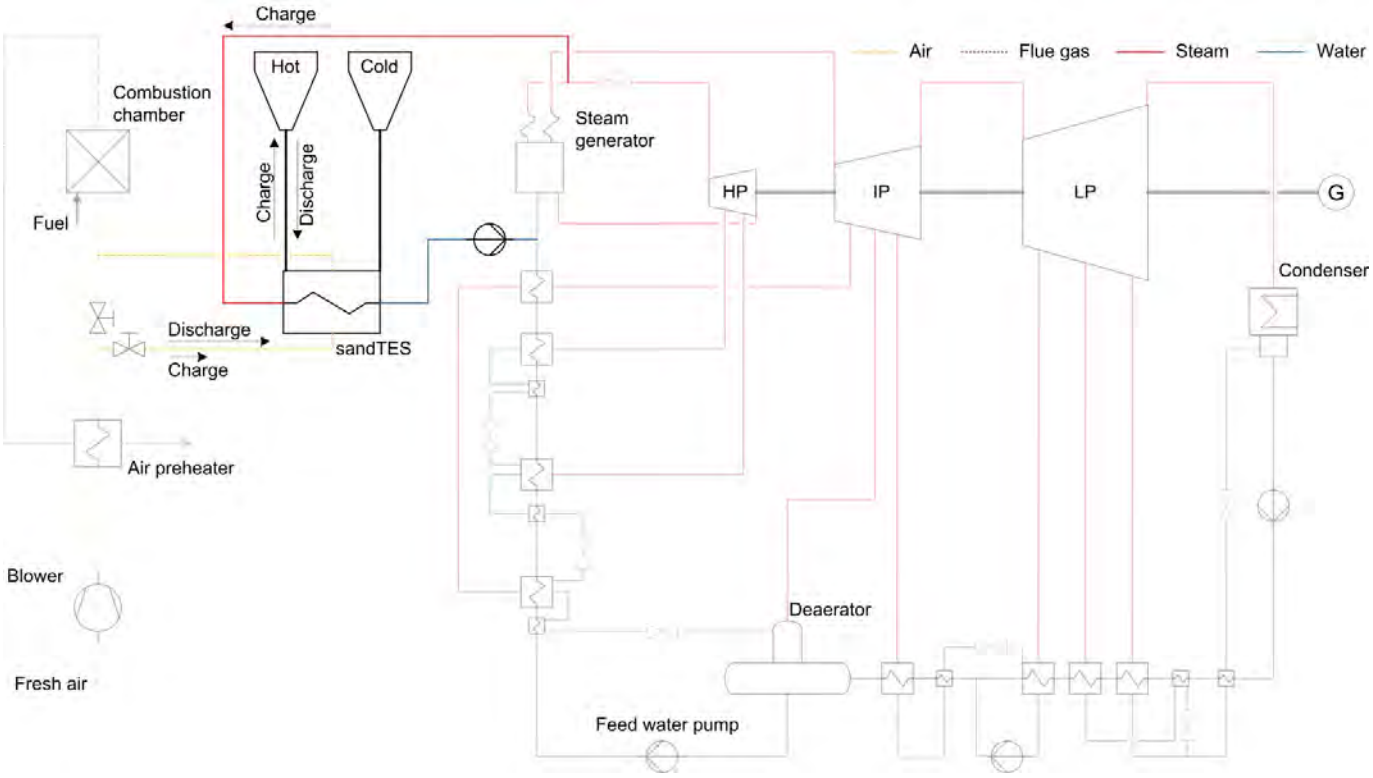

Fig. 5: Process flow sheet for a TES run in parallel to the steam generator for charging; discharging via air preheating

Table 3: Variant 1 in charging and discharging mode

Description	Unit	40 % Charge	Rel. [%]	100 % Discharge	Rel. [%]
Boiler output	MW_{th}	231	39	600	100
Fuel heat input	MW_{th}	239	37	600	92
Net output	MW_{el}	61	21	292	99
Generator output	MW_{el}	65	21	306	100
Live steam pressure	bar	160	56	285	100
Live steam temperature	°C	~600	100	600	100
Reheater steam temperature	°C	~620	100	620	100
Turbine inlet pressure	bar	59	21	285	100
Condenser pressure	mbar	28	63	45	100
Net efficiency	%	25.6	57	48.6	107
Gross efficiency	%	27.1	58	51.1	108
TES output	MW_{th}	86		43	
Estimated TES auxiliary power	MW_{el}	0.18		3.9	
Sand mass flow	kg/s	427		214	
Sand lower temperature	°C	200		200	
Sand upper temperature	°C	393		393	
Minimum temperature difference	°C	25		5	

boiler pressure of 160 bar in the HEX, is shown in Table 3.

The net output is reduced to 21 % of the nominal value, while the boiler remains at 39 % part load. The pressure drop from the boiler outlet to the turbine inlet is about 101 bar, which induces some exergetic losses. While charging, a heat flow of 86 MW can be achieved with an inlet temperature of 200 °C and a sand mass flow of 427 kg/s. It should be noted, that the auxiliary power for fluidization is very low due to the extremely low fluidization velocities.

For discharging, the cycle nearly reaches the nominal cycle values, except for the fuel heat input, which is reduced. Thus, the thermal energy is restored by saving fuel. At discharging the auxiliary power is significantly increased, because of the high fresh air mass flow needed for transporting the heat into the combustion chamber. The heat flow and with it the sand mass flow is about two times smaller than in charging mode, restricted by the fresh air mass flow. Therefore the discharging time is two times longer.

A bottleneck of the system is the lower sand temperature while discharging. Because of the temperature of the fresh air, coming from the air preheater, the lowest sand temperature is determined. For a further reduction of the lower sand temperature, the sand could be cooled down by additional feed water preheaters. A low sand temperature extends the useable temperature range of the material in two ways: obviously decreasing the lower sand temperature, but also, referring to Fig. 3, increasing the achievable upper sand temperature, which is limited due to the pinch point. Fig. 6 shows the upper sand temperature T_{su} for 50 °C, 100 °C, 150 °C and 200 °C lower sand temperatures depending on the boiler pressure.

A higher temperature range lowers the needed sand mass flow, which easily can be seen in Eq. (5).

$$\dot{Q}_{sandTES} = \dot{m}_{Sand} \cdot c_p \cdot \Delta T \tag{5}$$

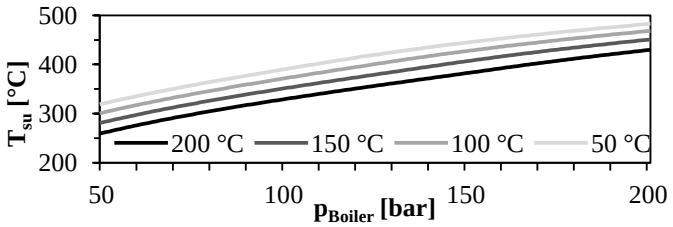

Fig. 6: Achievable upper sand temperatures

The dependency of the mass flow ratio x on the boiler pressure is again shown for four different lower sand temperatures in Fig. 7, where x is defined in Eq. (6).

$$x = \frac{\dot{m}_{Sand}}{\dot{m}_{Water/steam}} \tag{6}$$

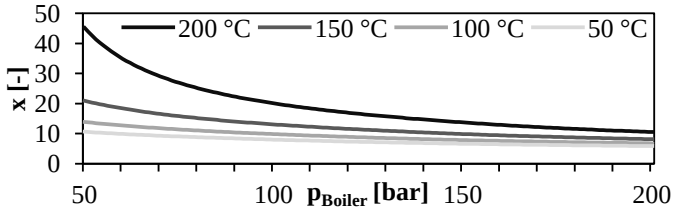

Fig. 7: Capable mass flow ratios

An increasing boiler pressure increases the reachable hot sand temperature and also the associated pressure drop over the valve, whereby the sand mass flow decreases.

Therefore the reduction of exergetic losses due to the pressure drop over the valve is opposed to the minimization of the sand mass flow.

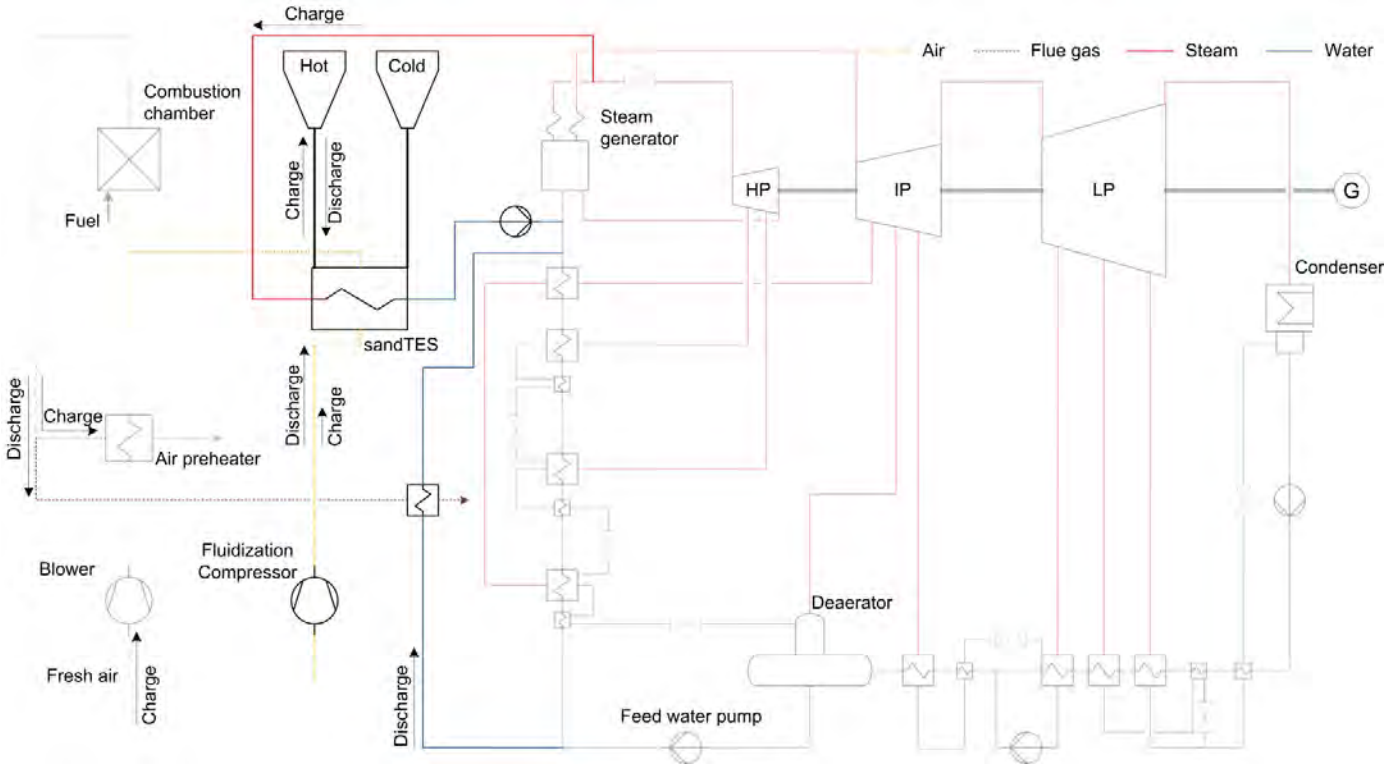

Fig. 8: Process flow sheet for a TES using live steam for charging and air preheating for discharging. The flue gas is cooled by a feed water preheater.

Variant 2

An adjusted concept for gaining a higher temperature range is shown in Fig. 8. In contrast to Variant 1, the flue gas is bypassing the air preheater during discharging, wherefore it is cooled down by a feed water preheater. As a result, the fresh air temperature decreases near to ambient temperature, which subsequently lowers the cold sand temperature. As mentioned above, the sand mass flow is thereby minimized.

The cases for charging and discharging were calculated analogically to variant one, with 40 % and 100 % boiler mass flow, respectively. The corresponding data are summarized in Table 4. The net output again is reduced to 21 % of the nominal value, while the sand is charged with a heat flow of 88 MW. In discharging mode this heat flow rises to 96 MW, since the temperature range is fairly extended.

Table 4: Variant 2 in charging and discharging mode

Description	Unit	40 % Charge	Rel. [%]	100 % Discharge	Rel. [%]
Boiler output	MW_{th}	231	39	599	100
Fuel heat input	MW_{th}	241	37	583	90
Net output	MW_{el}	62	21	301	102
Generator output	MW_{el}	65	21	316	103
Live steam pressure	bar	160	56	285	100
Live steam temperature	°C	~600	100	600	100
Reheater steam temperature	°C	~620	100	620	100
Turbine inlet pressure	bar	59	21	285	100
Condenser pressure	mbar	28	63	46	103
Net efficiency	%	25.5	56	51.6	114
Gross efficiency	%	26.9	57	54.1	115
TES output	MW_{th}	88		96	
Estimated TES auxiliary power	MW_{el}	0.17		3.9	
Sand mass flow	kg/s	218		238	
Sand lower temperature	°C	50		50	
Sand upper temperature	°C	453		453	
Minimum temperature difference	°C	25		5	

RESULTS AND DISCUSSION

As outlined in the introduction, the integration of TES systems into thermal power plants seems to be an appropriate way to soften the existing limitations for power plant operation. In this section the introduced basic cycle is compared with the two variants of the advanced TES implementation concept.

As it is reported in literature, the boiler part load is the limiting factor compared to the turbine. 40 % minimum load for the boiler seems realistic, while the live steam and reheater temperatures do not yet drop off too far from the nominal values. Both the implementation variants achieve an enhancement of the low load capability by a factor of 2, as can be seen in Table 3 and Table 4. Of course, the efficiencies during charging drop for both variants, what is partly recovered during the discharging period.

Comparing Table 3 and Table 4 for the first and second variant with each other leads to similar plant parameters of the plant in charging mode. Only the fuel heat input of variant 1 is slightly lower than for variant 2, which leads to a higher net efficiency. Also in discharging mode the plant parameters vary, which mainly concerns the fuel heat input. At this, variant 2 shows the higher net efficiency.

Overall, the greater differences appear at the sand parameters, which affect the discharging and charging duration. Therefore both variants are compared regarding to a whole circuit of charging and discharging. Such a circuit consists of the charging and an attached discharging period, which is depending on the associated TES output. The corresponding TES parameters are summarized in Table 5.

Table 5: Data for storage and circuit (circuit = charge + discharge)

Description	Unit	Variant 1	Variant 2
Charging time (40 % load)	min	60	60
Discharging time (100% load)	min	120	55
Storage sand mass	to	1537	785
Storage sand volume	m³	1215	621
Storage sand capacity	MWh_{th}	86	88
Circuit net energy	MWh_{el}	644	337
Circuit fuel energy	MWh_{th}	1437	776
Circuit net efficiency	%	44.8	43.5

For the sake of simplicity, the duration of charging is set to 1 hour, wherefore the storage capacity is determined by the corresponding sand mass flow. Further on, the discharging duration is set, referring to the sand mass flows and TES outputs. It can be seen, that the discharging duration of variant 2 is about 2 times shorter than for variant 1. It should be mentioned, that the sand volume and mass in Table 5 is by a factor of 10 to 20 lower than the values realized in state of the art solar thermal installations.

To further outline the differences between the variants, the circuit net efficiency $\eta_{Net,Circuit}$ is defined, see Eq. (7). E_{Net} is the electricity fed into the grid, E_{Fuel} is the lower heat value multiplied with the fuel mass fired in the combustion chamber, during the whole circuit of charging and discharging.

$$\eta_{Net,Circuit} = \frac{E_{Net,Charge} + E_{Net,Discharge}}{E_{Fuel,Charge} + E_{Fuel,Discharge}} \tag{7}$$

As it can be seen, variant 2 reduces the storage size nearly by the factor of 2, whereas the net efficiency over a circuit is slightly decreased. This lower circuit efficiency of variant 2 comes from the short discharging duration of only 55 minutes at the high net output level (100 %). This also seems reasonable because of the thermodynamic mean temperature, which decreases for variant 2 due to the lowered cold sand temperature. Vice versa, the TES system of variant 2 seems more flexible, because of the nearly equal periods. Additionally variant 1 only fits for low fresh air temperatures after the preheater and high upper sand temperatures.

As it can be seen, the circuit efficiencies aren't that much decreasing compared to the basic cycle, because of the not considered storage losses. Comparing the values of Table 1 and Table 5, one can realize that the efficiency of energy storage is rather high.

Especially the second variant, due to the smaller dimensions of the storage silo, seems retrofittable, although issues concerning space at thermal power plants have to be considered more in detail. With a height of 15 m a cylindrical silo with a diameter of 7.3 m (10.2 m) can be filled with sand for variant 2 (variant 1), by running the TES system for one hour. Both variants need a bucket conveyor and screws for the sand transport at high temperature levels, which is the main disadvantage of the technology. At IET also sandTES based technologies without the need for conveying systems are being developed.

As mentioned in the introduction, thermal oil or molten salt are possible heat storage media too, which also fit for these variants of TES integration. For instance, thermal oil could be charged in a water/steam-oil HEX and discharged via finned tube bundles in the fresh air line. Only the temperature ranges are more restricted, since the upper temperatures are determined by about 400 °C for oil and 550 °C for salt. Binary molten salt solidifies below approx. 250 °C, which is a further restriction. In Table 6 the quartz sand used in this work, corundum as another solid material, nitrate salts and thermal oil (Dowtherm A) with the achievable temperature ranges regarding to variant 1 and 2, are listed. Out of their energy

Table 6: Energy densities of sensible storage media [3][7][8]

Description	Unit	Quartz sand		Corundum		Nitrate salts	Dowtherm A
Volumetric heat capacity	MJ/m³K	1.3		2.5		2.9	1.9
Temperature range	°C	50-450	200-400	50-450	200-400	250-450	50-400
Energy density	MJ/m³	510	255	986	515	548	668

densities and capable temperature ranges it can be concluded that quartz sand has chances in the same application field as molten salts or thermal oils. Moreover, sand is a very cheap natural material with high longevity. Corundum, a mass produced article, used e.g. for fracking, surpasses the others due to the high energy density, which makes it very attractive for TES applications.

CONCLUSION

The rapid rise of fluctuating renewables leads to major issues concerning grid stability. Since direct storing of electricity in large quantities isn't achievable at the moment, indirect storage systems and the improvement of the flexibility of existing power plants are obvious options. A novel high temperature TES, called sandTES, was introduced. This potential technique is suited for flexibility enhancement of thermal power plants. A model of a super-critical 300 MW_{el} thermal power plant was set up in a commercial process simulation software. Based on that model, two variants of a novel concept for TES integration were introduced to demonstrate the achievable low load enhancement. The basic idea of this novel concept is the usage of the fresh air for restoring the thermal energy. The results show, that in the chosen case the minimum plant part load can be reduced by a factor of 2. In real world applications the achievable minimum load reduction depends on the minimum part loads of both the boiler and the turbine.

The two introduced integration variants mostly differ in the usable temperature ranges, which correlate with the associated mass flows and efficiencies. It can be seen, that a higher temperature range decreases the sand mass flow, but also the efficiency.

The use of particles as heat storage medium seems to be an attractive opportunity compared to other common materials like molten salt or thermal oil: the energy density of sand is only slightly smaller, whereas corundum even exceeds these ranges.

The objective of the work was to identify possible TES integration concepts and to show their main restrictions. Hence, economical investigations, involving material prices, dimensions of the HEX, detailed impacts on the boiler operation, durability of the material, environmental impacts or risks to health have to be done in future works. Further on, a potential for optimization exists, e.g. for the pressure level of the boiler. Finally exergetic and dynamic investigations have to be done. The shown integration concepts for particle storage systems are only one variant among several others, which will be published in the near future.

NOMENCLATURE

c_p	Spec. isobaric heat capacity [kJ/(kgK)]
E	Energy [J]
g	Gravitational constant [m/s²]
H	Height [m]
HP	High pressure
IP	Intermediate pressure
LP	Low pressure
$\dot{m}$	Mass flow [kg/s]
p	Pressure [Pa]
P	Power [MW]
Q	Heat [kJ]
$\dot{Q}$	Heat flow [MW]
T	Temperature [°C]
u	Velocity [m/s]
x	Mass flow ratio [-]

Greek letters

η	Efficiency [-]
μ	Fluidization grade [-]
ρ	Density [kg/m³]
ψ	Porosity [-]

Subscripts

act	Actual
$Boiler$	Boiler
$Charge$	Charging mode
$Discharge$	Discharging mode
el	electrical
f	Fluid
fb	Fluidized bed
$Fuel,$ LHV	Fuel (Lower heating value)
$Generator$	Generator
$Gross$	Gross
mf	Minimum fluidization
Net	Net
$Net, Circuit$	Net, for a circuit
p	Particle
$Sand$	Sand
$SandTES$	SandTES HEX
sl	Sand lower
su	Sand upper
th	thermal
$water/steam$	Water/steam cycle

ACKNOWLEDGMENTS

The K-Project GSG-GreenStorageGrid (Grand no. 836636) is funded in the framework of COMET - Competence Centers for Excellent Technologies by the Federal Ministry of Transport, Innovation and Technology, the Federal Ministry of Science, Research and Economy, the Vienna Business Agency, the Federal Province of Lower Austria and by the Federal Province of Upper Austria. The program line COMET is administered by the Austrian Research Promotion Agency (FFG). The authors would like to thank also the project partners Valmet GesmbH., EVN AG, ENRAG GmbH. and Primetals Technologies GmbH for the pleasant and constructive working relationship.

Special thanks go to the sandTES research team for the helpful support and the numerous discussions.

REFERENCES

[1] Niels Brinkmeier, 2015,“Flexibility of thermal power plants” PhD, IWBT, TU Braunschweig, Braunschweig (in German).

[2] Pinel P., Cruickshank C. A., Beausoleil-Morrison I., and Wills A., 2011,“A review of available methods for seasonal storage of solar thermal energy in residential applications,” Renewable and Sustainable Energy Reviews, 15(7), pp. 3341–3359.

[3] Tian Y., and Zhao C., 2013,“A review of solar collectors and thermal energy storage in solar thermal applications,” Applied Energy, 104, pp. 538–553.

[4] Liu M., Steven Tay N., Bell S., Belusko M., Jacob R., Will G., Saman W., and Bruno F., 2016,“Review on concentrating solar power plants and new developments in high temperature thermal energy storage technologies,” Renewable and Sustainable Energy Reviews, 53, pp. 1411–1432.

[5] Peter Steiner, Karl Schwaiger, Heimo Walter, Markus Haider, 2016,“Active fluidized bed technology used for thermal energy storage,” in Proceedings of the ASME 2016 Power and Energy Conference, June 26-30, Charlotte, North Carolina, Paper no: PowerEnergy2016-59053

[6] Norbert Latk, Michael Syrbe, Uwe Gampe, 2015,“Erste Untersuchungen zur Niedriglastfahrweise einer Dampfturbine großer Leistung,”

[7] Kuravi S., Trahan J., Goswami D. Y., Rahman M. M., and Stefanakos E. K., 2013,“Thermal energy storage technologies and systems for concentrating solar power plants,” Progress in Energy and Combustion Science, 39(4), pp. 285–319.

[8] NIST,“NIST Chemistry WebBook,” http://webbook.nist.gov/cgi/cbook.cgi?ID=C14808607&Mask=2, Internet-Link Dec. 20, 2015.

Paper 4
(in German)

P. Steiner, M. Haider, K. Schwaiger

Flexibilisierung und Mindestlastabsenkung kalorischer Kraftwerke mittels Einbindung thermischer Hochtemperatur-Energiespeicher

Tagungsband Kraftwerkstechnisches Kolloquium
Dresden, 2016

Flexibilisierung und Mindestlastabsenkung kalorischer Kraftwerke mittels Einbindung thermischer Hochtemperatur-Energiespeicher

Peter Steiner, Markus Haider und Karl Schwaiger

Abkürzungsverzeichnis

H	Heizwert
$\dot{H}$	Enthalpiestrom
P	Leistung
t	Zeit

Griechische Buchstaben

η	Wirkungsgrad

Indizes

Br	Brennstoff
E	Entlade-Betrieb
Generator	Generator
L	Lade-Betrieb
Netto	Netto
Netz	Elektrisches Netz
u	unterer
Zyklus	Gesamter Lade- und Entladezyklus

Im Zuge der Energiewende und dem damit einhergehenden Anstieg des Anteils an erneuerbaren Energien wie Windkraft oder Photovoltaik am Strommarkt wird es für Betreiber konventioneller Kraftwerke zunehmend schwieriger, wirtschaftlich zu arbeiten. Da die Zahl der Volllaststunden bedingt durch den sinkenden Strompreis abnimmt, müssen kalorische Kraftwerke öfter abgeschaltet werden. Gleichzeitig reichen die bisher installierten Speicherkapazitäten im Stromnetz nicht aus, um die wetter- und nachfragebedingten Schwankungen im Stromnetz auszugleichen. Entsprechende Batteriespeicher sind in dieser Größenordnung über Jahre hinaus nicht zu erwarten, was wiederum zur Notwendigkeit eines möglichst flexiblen Kraftwerksparks führt. Um ein Kohlekraftwerk wirtschaftlich betreiben zu können, ist es notwendig, Regelkapazität zur Verfügung zu stellen. Dies führt zu einer erhöhten Anzahl an Teil- und Tieflaststunden und zu schnelleren An- bzw. Abfahrzeiten. Neben technischen Herausforderungen wirkt sich dies negativ auf die Lebensdauer der Kraftwerke aus, die vielfach für den Volllastbetrieb konzipiert wurden.

Trotz der Möglichkeit, durch technische Maßnahmen sowohl in Neubauprojekten als auch bei Nachrüstungen eine Verbesserung der Tieflastfähigkeit und eine Steigerung der Lastgradienten zu erzielen, sind noch weitreichendere Maßnahmen wünschenswert.

Neben schon bekannten Ansätzen, wie beispielsweise die Nutzung des elektrischen Stroms in Zeiten von Überproduktion zur Elektrolyse oder Methanol-Produktion, stellt auch die Integration von thermischen Energiespeichern (TES) in den bestehenden Kraftwerks-Prozess eine attraktive Möglichkeit dar. Bereits umgesetzte Konzepte in Solarkraftwerken nutzen Speichersysteme mit Salzschmelzen als Speichermedium. Die im Bereich von 100-240 °C liegenden Gefrierpunkte dieser Salzmischungen sind für den Einsatzbereich der Flexibilitätssteigerung problematisch.

Mit einer neuartigen, am Institut für Energietechnik und Thermodynamik (IET) der TU Wien entwickelten TES-Technologie, die für höchste Temperaturen konzipiert ist, können bestehende Kraftwerksanlagen besonders vorteilhaft flexibilisiert werden. Einerseits können wegen der hohen Temperaturdifferenzen hohe Energiespeicherdichten erreicht werden, andererseits können die hohen Frischdampftemperaturen moderner Kraftwerke (600 bis 620 °C) bei direkter Rückspeicherung über einen Dampferzeuger erzielt werden.

Inhalt dieses Artikels ist die Einführung und Diskussion verschiedener Konzepte zur effizienten Integration eines TES-Systems in den Prozess eines Kohlekraftwerks. Es wird zuerst die bereits erwähnte SandTES-Technologie vorgestellt und erklärt. Anschließend werden mögliche Lösungskonzepte anhand des Referenzkraftwerks Nordrhein-Westfalen gezeigt. Darunter finden sich Lösungsansätze, die sich hinsichtlich Lade- aber auch Entlademethode unterscheiden. So kann beispielsweise Frischdampf vor der Turbine ausgekoppelt und zur Erwärmung des Speichermaterials genutzt werden. Alternativ kann elektrische Energie des Generators zum Betrieb einer Elektrode verwendet werden, welche wiederum das Speichermaterial erwärmt. Außerdem ist auch eine Kombination dieser Varianten möglich. Die Rückspeicherung der thermischen Energie kann einerseits über den Frischluft-Strang durch Luftvorwärmung, andererseits über direkte Dampfproduktion erfolgen. Abschließend werden die Varianten hinsichtlich Nachrüstbarkeit, Effizienz und Lastdynamik diskutiert.

1. SandTES

Die SandTES-Technologie ist eine aktive Hochtemperatur-Speichertechnologie, deren Ziel es ist, die Maximaltemperaturen bisheriger TES-Systeme zu übertreffen und Erstarrungsprobleme zu eliminieren. Salzschmelzen sind mit Maximaltemperaturen von rund 550 °C begrenzt. Zusätzlich dürfen im Fall des sogenannten *Solar Salt* Minimaltemperaturen von ca. 250 °C nicht unterschritten werden, da die Salzschmelze sonst erstarrt. Die SandTES-Technologie verwendet feinkörnige Partikel als Wärmeträgermedium. Die Partikel können bei Temperaturen von Umgebungstemperatur bis zu 1000 °C und mehr eingesetzt werden. Es werden Partikelschüttungen aus Quarzsand, aber auch aus Korund verwendet. Quarzsand besticht durch die niedrigen Materialkosten, während mit Korund höhere Energiedichten erzielt werden können.

Das Herzstück der SandTES-Technologie stellt ein Wirbelschicht-Gegenstrom-Wärmeübertrager (WÜ) dar, der die Wärme zwischen dem Wärmespeichermedium (Partikel) und dem jeweiligen Arbeitsmedium (z. B. Wasser/Dampf) überträgt. Um diese Wärmeübertragung möglichst effizient zu gestalten, muss ein Gegenstrom realisiert werden. Dazu wird eine im Wärmeübertrager befindliche Partikelschüttung fluidisiert, also mit einem ausreichend großen Luftvolumenstrom vom Boden nach oben hin durchströmt. Ab der sogenannten Lockerungsgeschwindigkeit beginnen die einzelnen Partikel zu schweben, was der Partikelschüttung flüssigkeitsähnliche Eigenschaften verleiht. Dies ermöglicht unter speziellen Randbedingungen einen horizontalen Fluss der Partikel durch den WÜ, wenn am einen Ende ein Sandmassenstrom zu-, am anderen Ende wieder abgeführt wird. Treibende Kraft ist hierbei die entstehende Höhendifferenz zwischen Partikelein- und -austritt.

Das Arbeitsmedium wiederum wird in einem Rohrbündel im Gegenstrom zur außen geführten Partikelsuspension befördert. Je nach Anwendungsfall kann dabei das Wärmespeichermedium Wärme an das Arbeitsmedium abgeben oder von ebendiesem aufnehmen.

Die Wärme, die von der Fluidisierungsluft beim Durchströmen des Bettes aufgenommen wird, kann mittels Rekuperatoren rückgewonnen und zur Fluidisierungs-

luftvorwärmung verwendet werden.

Im Unterschied zu den in der Kraftwerkstechnik üblichen Wirbelschicht-Feuerungen werden nur sehr geringe Luftgeschwindigkeiten im Bereich von rund 20 mm/s und dementsprechend niedrige Luft-Massenströme gefahren. Grundlage für die niedrigen Luftgeschwindigkeiten ist eine feine Partikelkörnung im Bereich von 60 bis 100 µm, woraus eine geringe Lockerungsgeschwindigkeit resultiert.

Neben dem Luftmassenstrom ist der Druckverlust im Wärmeübertrager der zweite wesentliche Einfluss auf die zur Fluidisierung notwendige Gebläseleistung. Dieser bestimmt sich aus dem Druckverlust durch das Bett und den Druckverlusten im Düsenverteilerboden bzw. sonstigen Regulierungsventilen. Je nach Baugröße variiert dieser Druckverlust im Bereich von 100 bis 500 mbar. Weitere Details zum SandTES-Wärmeübertrager sind [1] zu entnehmen.

Anhand Abbildung 1 soll im Folgenden der Prozessablauf eines Ladevorgangs skizziert werden. In der dargestellten Ausführungsvariante ist der Wärmeübertrager Wasser-Dampf-seitig als Zwangdurchlauf-Kondensator mit Enthitzungs- und Unterkühlungsteil ausgeführt.

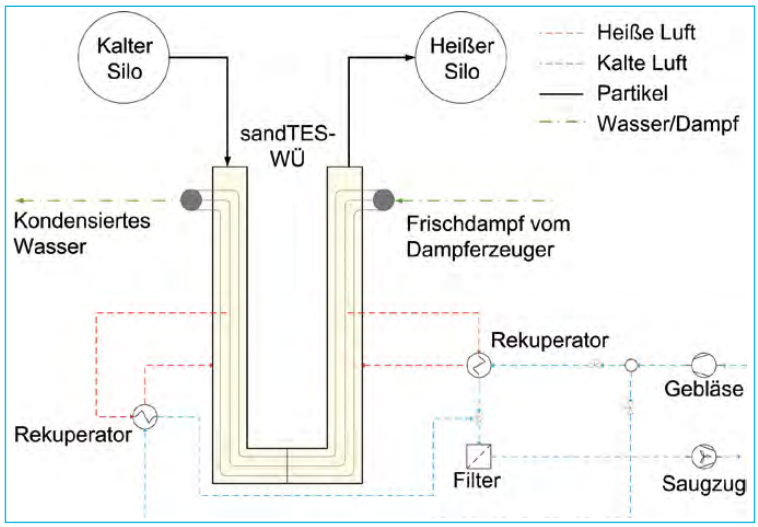

Abb. 1:
Fließschema eines SandTES beim Ladevorgang

In einer Anwendung zur Flexibilisierung eines Kohlekraftwerks kann beispielsweise Frischdampf noch vor der Hochdruckturbine ausgekoppelt werden und in einem SandTES-Wärmeübertrager niedergeschlagen werden. Die dabei abzuführende thermische Energie kann auf die Partikelsuspension übertragen werden. Dazu werden Partikel aus dem kalten Silo in den Wärmeübertrager gefördert, durch welchen sie im Gegenstrom zum Wasserdampf fließen. Am anderen Ende kann der mittlerweile heiße Partikelstrom den Wärmeübertrager verlassen, um im heißen Silo gespeichert zu werden. Zum Entladen der thermischen Energie können die Strömungsrichtungen im Wärmeübertrager umgekehrt werden. Alternativ ist hier ein zweiter separater Wärmeübertrager vorzusehen, der dann auf die entsprechenden Randbedingungen spezialisiert werden kann.

Es sei erwähnt, dass die SandTES-Technologie Fördersysteme zum Transport

der Partikel vom bzw. in den Silo benötigt. Dafür kommen im Wesentlichen Becherwerke und Förderschnecken in Frage.

Am IET wird auch eine auf Partikeln basierende TES-Technologie entwickelt, die gänzlich ohne Fördertechnik auskommt. Zur Validierung des SandTES-Konzepts wird momentan eine 280-kW_{th}-Pilotanlage am Laborstandort des IET in Betrieb genommen. Ein Machbarkeitsnachweis sowie die Optimierung wesentlicher Auslegungsparameter sind Ziel der Versuchsreihen.

2. Integrationsmöglichkeiten

Im folgenden Abschnitt werden verschiedene Varianten zur Integration eines SandTES-Systems in den Prozess eines Kohlekraftwerks vorgestellt.

Als Grundlage dafür dient das Referenzkraftwerk Nordrhein-Westfalen (RKW NRW), welches für die in EBSILON®Professional durchgeführten Prozesssimulationen herangezogen wurde. Das entsprechende Fließschema ist in Abbildung 2 dargestellt, während die Prozessparameter in Tabelle 1 aufgelistet sind. Links in Abbildung 2 ist der Luft-/Rauchgasstrang zu erkennen, rechts davon der Wasserdampfkreislauf. Dieser besteht neben der Hochdruck- (HD), Mitteldruck (MD)- und Niederdruckturbine (ND) im Wesentlichen aus einem Kondensator, der Niederdruck- und Hochdruckvorwärmstrecke und einem Dampferzeuger. Der Kessel wird in zwei Teilen modelliert, einmal als Dampferzeuger für den Wasserdampfkreislauf, einmal als Brennkammer für den Luft-/Rauchgasstrang. Als minimale Teillast mit noch annähernd konstanten Frischdampf-Temperaturen wurde eine Kesselleistung von 40 % angenommen [2].

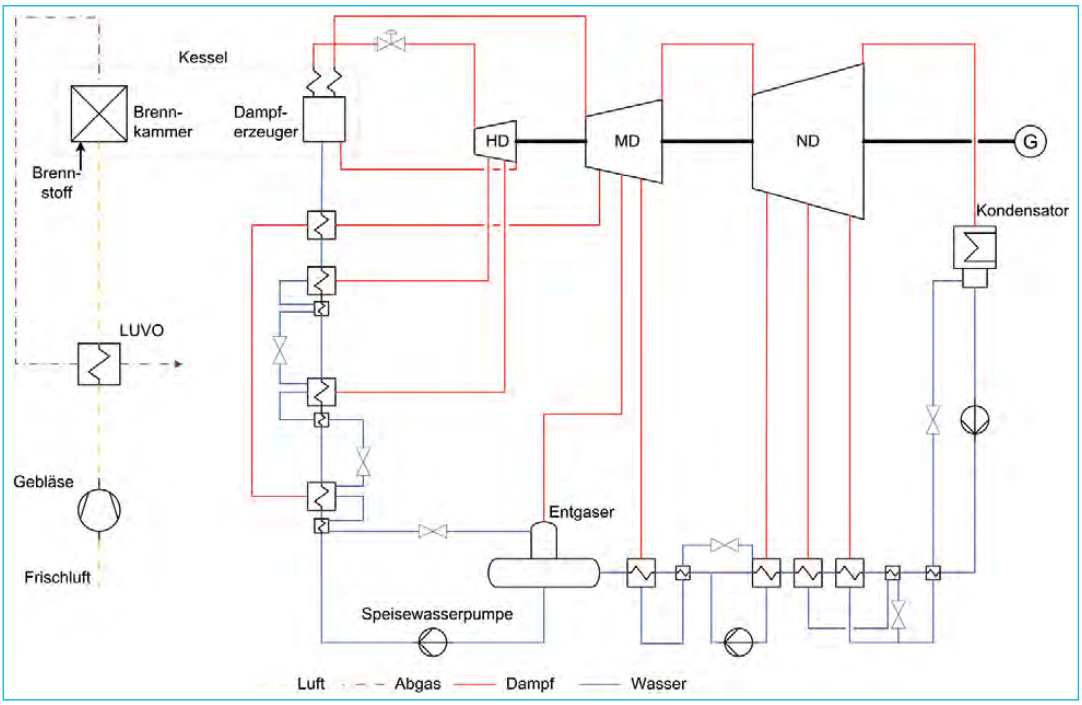

Abb 2: Fließschema Referenzkraftwerk Nordrhein-Westfalen

Bezeichnung	Einheit	Volllast	Teillast 40 %	Rel. [%]
Kesselleistung	MW_{th}	600	240	40
Brennstoffleistung	MW_{th}	652	258	40
Netzleistung	MW_{el}	294	110	37
Generatorleistung	MW_{el}	307	114	37
Frischdampfdruck	bar	285	115	40
Frischdampftemperatur	°C	600	~600	100
Zwischenüberhitzertemperatur	°C	620	~620	100
Turbineneintrittsdruck	bar	285	104	36
Kondensatordruck	mbar	45	32	71
Nettowirkungsgrad	%	45,1	42,3	94
Bruttowirkungsgrad	%	47,0	44,2	94

Tab. 1: Prozessparameter Referenzkraftwerk Nordrhein-Westfalen

Die angeführten Netto- bzw. Brutto-Wirkungsgrade berechnen sich wie in Gleichung (1) bzw. Gleichung (2) angegeben, wobei P_{Netz} für die in das Stromnetz eingespeiste elektrische Leistung und $P_{Generator}$ für die insgesamt vom Generator erzeugte elektrische Leistung stehen. $\dot{H}_{\mathrm{Br}}$ bezeichnet den mit dem Brennstoff zugeführten Enthalpiestrom, welcher sich aus dem unteren Heizwert H_u und dem Massenstrom des Brennstoffs bestimmt.

$$\eta_{Netto} = \frac{P_{Netz}}{\dot{H}_{Br}} \qquad (1)$$

$$\eta_{Brutto} = \frac{P_{Generator}}{\dot{H}_{Br}} \qquad (2)$$

Die Kühlwasserpumpen sowie verschiedene Anlagenteile zur Abgasreinigung sind nicht im Modell abgebildet.

Vorweg sei erwähnt, dass alle im Folgenden behandelten Varianten mit dem SandTES-System als Hochtemperatur-Speicher und mit Korund (Al_2O_3) [3] als Wärmespeichermedium berechnet wurden. Diese Varianten können – gegebenenfalls mit eingeschränkten Temperaturbereichen – analog auf andere Speichersysteme mit anderen Speichermedien übertragen werden. Der maximale Temperaturbereich des Feststoffspeichers wurde mit 50-800 °C festgelegt. Die maximale Speichertemperatur hat natürlich Konsequenzen auf die zur Anwendung kommenden Materialien und Ausführungsvarianten von Silos und Fördertechnik sowie deren spezifische Investitionskosten. Der Temperaturbereich des Speichers ist demnach im Sinne einer wirtschaftlichen Optimierung festzulegen.

2.1. Laden

In Abbildung 3 ist das bereits eingeführte RKW NRW dargestellt. Die Abbildung wurde auf der linken Seite um ein SandTES-System im Ladebetrieb erweitert. Wie schon eingangs erwähnt, besteht ein solches TES-System aus zwei getrennten Silos und aus zwei spezialisierten Wärmeübertragern. Zwecks Übersichtlichkeit ist nur der Lade-Wärmeübertrager dargestellt. Der zum Entladen des Speichers zusätzlich notwendige Entlade-Wärmeübertrager ist in dieser Grafik nicht berücksichtigt.

Im Ladebetrieb muss das Speichermedium erwärmt werden, was im Folgenden einerseits mit abgezweigtem Frischdampf, andererseits mit direkt vom Genera-

tor abgezweigtem Strom bewerkstelligt werden kann. Als dritte Variante ist eine Kombination der ersten beiden Varianten vorgesehen.

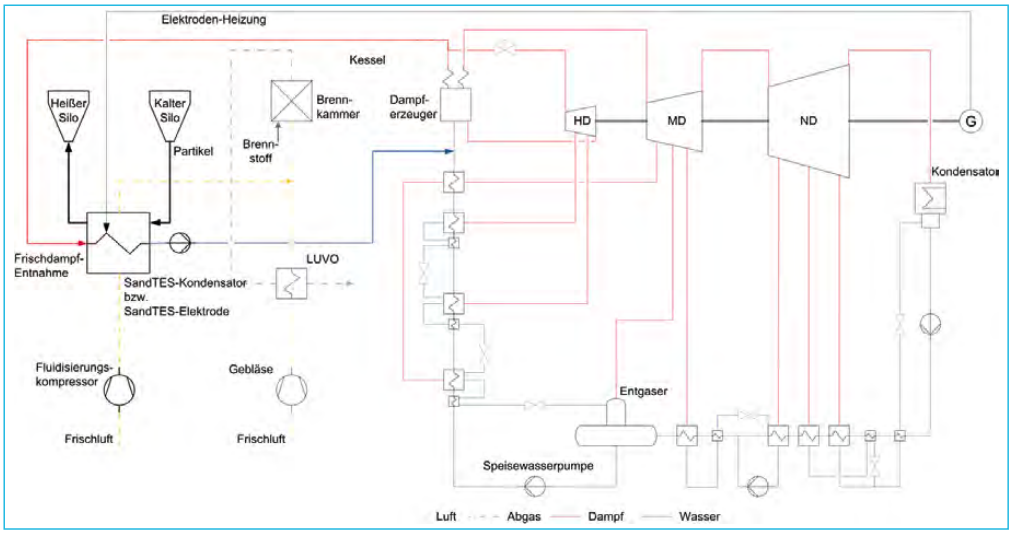

Abb. 3: Fließschema der Ladevarianten

2.1.1. Frischdampf-Entnahme

Ziel dieser Variante ist es, die bereits über die Feuerung eingespeiste Energie wieder aus dem Dampfkraftprozess zu entnehmen und in einem SandTES-System zwischen zu speichern. Der eingezeichnete SandTES-Wärmeübertrager steht somit für einen Wärmeübertrager mit eingebautem Rohrbündel, in welchem der abgezweigte Frischdampf niedergeschlagen wird, um die Wärme dabei auf den Partikelstrom zu übertragen. Die eingezeichnete Elektroleitung vom Generator zum Wärmeübertrager ist in diesem Fall inaktiv.

Zu beachten ist, dass bedingt durch die einzuhaltende Pinchpunkt-Temperatur, bei festgelegten Wasserdampfparametern und festgelegter Partikel-Eintrittstemperatur, auch die Partikel-Austrittstemperatur festgelegt ist. Diese ist somit vom Druck im Rohrbündel abhängig und steigt wegen der größer werdenden Sattdampftemperatur mit diesem an [4].

Vorteil dieser Variante ist, dass nur Verluste zufolge der Wärmeübertragung und Hilfsenergie auftreten.

2.1.2. Elektroden-Heizung

Bei dieser Variante ist die eingezeichnete Entnahme-Dampfleitung inaktiv. Der SandTES-Wärmeübertrager ist mit Hochtemperatur-Elektroden ausgestattet und wird über den Generator des Kraftwerks mit elektrischer Energie versorgt. Vorteile dieser Variante sind einerseits die weitaus höheren erreichbaren Partikeltemperaturen, da die Pinchpunkt-Problematik nicht zum Tragen kommt. Dies führt zu niedrigen Massenströmen und kleineren Silos. Andererseits die verbesserte Dynamik, da hier auf keine Wärmespannungen in dickwandigen Bauteilen zufolge hoher Temperaturgradienten Rücksicht genommen werden muss. Der

Wasserdampfkreislauf bleibt unberührt, was sich wegen der konstanten Fahrweise positiv auf die Lebensdauer des Kraftwerks auswirkt. Diese Vorteile werden allerdings mit dem geringeren Wirkungsgrad erkauft, da der gespeicherte Strom selbst auch schon mit Verlusten (thermischer Wirkungsgrad des Kraftwerks) erzeugt wurde. Dieses Konzept kann mit dem Schlagwort *Power to Heat to Power* bezeichnet werden.

2.1.3. Kombination Frischdampf-Entnahme und Elektroden Heizung

Abschließend wird noch die Kombination der beiden Varianten vorgestellt. Bei dieser Methode ist der eingezeichnete SandTES-Wärmeübertrager sowohl mit einem Rohrbündel als auch mit den in Serie angeschlossenen Hochtemperatur-Elektroden ausgestattet. Im ersten Teil des Wärmeübertragers wird der Partikelstrom mit Wasserdampf auf eine möglichst hohe Temperatur vorgewärmt und anschließend mit den Elektroden auf ein höheres Temperaturniveau gebracht. Somit lassen sich die Vorteile beider Varianten nutzen, nämlich die thermische Energie möglichst effizient zu speichern, aber trotzdem hohe Speichertemperaturen und hohe Lastwechselgeschwindigkeiten zu erzielen.

2.2. Entladen

Um den Speicherzyklus abzuschließen, muss klarerweise die eingespeicherte thermische Energie wieder in den Kraftwerksprozess rückgespeist werden. Die Partikel müssen also vom heißen Silo über einen entsprechenden Wärmeübertrager in den kalten Silo befördert und dabei abgekühlt werden. Hierfür sollen im Folgenden zwei Varianten vorgestellt werden. In Abb. 4 ist erneut ein Fließschema des RKW NRW dargestellt, ergänzt um ein SandTES-System auf der linken Seite der Darstellung. Beim Entladen symbolisiert der SandTES-Wärmeübertrager entweder einen Luftvorwärmer (SLUVO) oder einen SandTES-Dampferzeuger. Der zuvor diskutierte, zum Laden zusätzlich notwendige SandTES-Wärmeübertrager ist zwecks Übersichtlichkeit wieder nicht dargestellt.

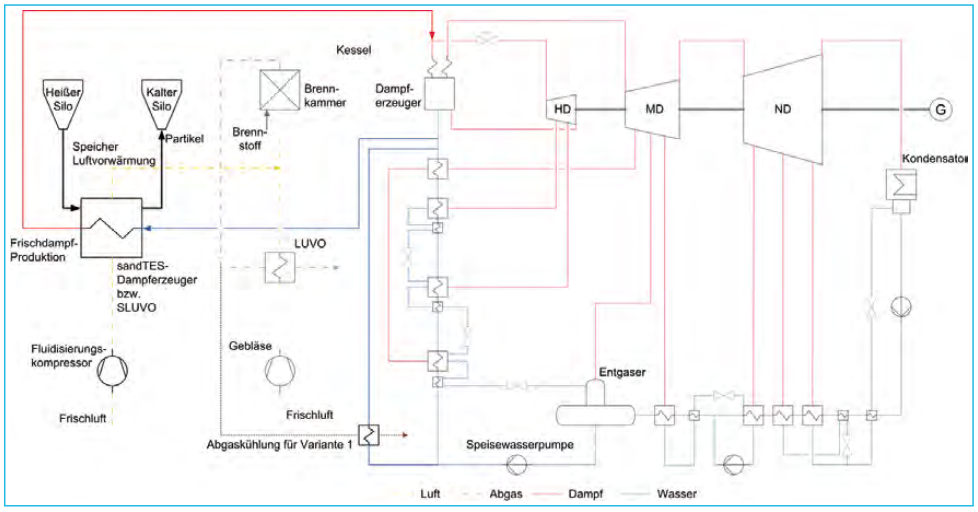

Abb. 4: Fließschema der Entladevarianten

2.2.1. SLUVO

Beim SLUVO handelt es sich, wie der Name schon vermuten lässt, um einen Luftvorwärmer. Dieser soll die in den Partikeln gespeicherte thermische Energie zumindest teilweise an die Frischluft der Feuerung übertragen. Dieser SLUVO kann wahlweise als Kolonnen-Wirbelschicht-Wärmeübertrager, Kolonnen-Fallstrom-Wärmeübertrager oder als Kolonnen-Zyklon-Wärmeübertrager ausgeführt sein. Durch die erhöhte Enthalpie des Frischluftstroms kann in weiterer Folge der Brennstoffmassenstrom reduziert werden.

Um die Partikel möglichst weit abzukühlen, ist es von Vorteil, die rauchgasseitige Luftvorwärmung zu reduzieren. Durch die Minimierung des Entnahmedampfes für die HD-Vorwärmer sinkt die Speisewasser-Eintrittstemperatur in den Dampferzeuger. Die Wärmeübertragung im Economizer steigt zufolge der entstehenden höheren Temperaturdifferenzen. In Dampferzeugern mit DENO$_x$-Katalysator muss abhängig vom gewählten Temperaturhub im Wärmeübertrager unter Umständen rauchgasseitig nach dem Katalysator ein zusätzlicher Economizer eingebaut werden.

2.2.2. SandTES-Dampferzeuger

Bei der zweiten, auf den ersten Blick naheliegenderen Entlade-Variante symbolisiert der Wärmeübertrager aus Abb. 4 einen SandTES-Dampferzeuger. Dieser kann parallel zum bestehenden Kraftwerksdampferzeuger betrieben werden. Nachteilig, zumindest in Kombination mit dem Dampf-Ladevorgang, sind die Frischdampfparameter, die wegen der Grädigkeiten beim Laden und auch Entladen nicht gehalten werden können. Dieses Problem besteht nicht bei einer Elektroden-Heizung, da der Sand auf die Frischdampf- bzw. Zwischenüberhitzer-Temperaturen aufgeheizt werden kann.

3. Ergebnisse

Im Folgenden werden die Simulationsergebnisse der verschiedenen Varianten vorgestellt. Um eine möglichst gute Vergleichbarkeit zu erreichen, wird für alle Berechnungen von einer Kessellast von 40 % ausgegangen, um dann mittels TES-Integration die elektrische Netzlast auf 20 % der Nennlast zu reduzieren. Die Frischdampfdrücke bei 40 % Teillast, welche auch im Kondensator-SandTES herrschen (TES-Dampfdruck), wurden mit 115 bar festgelegt. Ausgenommen davon ist Variante 1b, die das Potenzial höherer Kesseldrücke bei Anwendung des Kondensator-SandTES veranschaulichen soll. In den Entladezyklen wird der Speicher jeweils bei Turbinen-Volllast entladen.

In Tab. 2 ist eine Übersicht verschiedener Kombinationen der zuvor genannten Lade- bzw. Entlademethoden angeführt. Im oberen Bereich der Tabelle finden sich die wesentlichen Parameter für den Ladezyklus, gefolgt von denen des Entladezyklus. Im untersten Bereich sind die Parameter für einen gesamten Speicherzyklus, bestehend aus dem Ladezyklus und dem darauffolgenden vollständigen Entladezyklus, angeführt.

	Parameter	Einheit	Variante 1a	Variante 1b	Variante 2a	Variante 2b	Variante 3	Variante 4
Laden	Lademethode	-	Dampf	Dampf	Strom	Strom	Dampf & Strom	Strom
	Ladezeit	s	3.600	3.600	3.600	3.600	3.600	3.600
	TES-Leistung	MW	79	65	52	52	63	52
	TES-Dampfdruck	bar	115	200	-	-	115	-
	Partikelmassenstrom	kg/s	188	123	62	91	74	91
	TES-Hilfsleistung	kW	254	166	83	123	101	123
Entladen	Entlademethode	-	Luft	Luft	Luft	Luft	Luft	Dampf
	Entladezeit	s	3.054	2.077	1.154	1.145	1.394	1.145
	TES-Leistung	MW	94	113	162	162	162	162
	Partikelmassenstrom	kg/s	221	213	192	286	192	286
	TES-Hilfsleistung	kW	5.365	5.121	4.521	4.566	4.521	385
Gesamtzyklus	Max. Partikeltemperatur	°C	452	545	800	800	800	800
	Min. Partikeltemperatur	°C	50	50	50	321	50	321
	Silovolumen heiß	m³	342	224	112	166	136	166
	Energiedichte	MJ/m³	837	1.052	1.667	1.122	1.667	1.122
	Zykluswirkungsgrad	%	43	43	37	37	39	37

Tab. 2: Simulationsergebnisse verschiedener Lade- und Entladevarianten

Zwecks Vergleichbarkeit wurde exemplarisch für alle Varianten dieselbe Ladezeit von einer Stunde angenommen. Die angeführten TES-Leistungen beziehen sich auf den zwischen Arbeitsmedium und Partikelstrom übertragenen Wärmestrom. Die Hilfsleistung beinhaltet die notwendige elektrische Leistung für das Gebläse und für ein Becherwerk mit einer großzügig abgeschätzten Höhe von 50 m. Das Silovolumen berechnet sich aus der Ladezeit, dem entsprechenden Partikelmassenstrom und einer Schüttdichte von 1975 kg/m³ für Korund. Die Energiedichte berücksichtigt die für den angegebenen Partikel-Temperaturbereich gespeicherte thermische Energie, bezogen auf das Silovolumen. Abschließend wird, zwecks Bewertung, der thermische Netto-Zykluswirkungsgrad des Kraftwerks $\eta_{\text{Netto,Zyklus}}$ angeführt, der sich, wie in Gleichung (3) angegeben, aus den in das elektrische Netz eingespeisten Leistungen $P_{Netz,E/L}$ und die durch den Brennstoff zugeführten Enthalpieströme $\dot{H}_{Br,E/L}$) jeweils bei der Ladezeit t_L und Entladezeit t_E bestimmt. Für alle TES-Wärmeübertrager wurde eine minimale Temperaturdifferenz von 25 °C zwischen dem Partikelstrom und dem jeweiligen Prozessstrom gewählt. Aufgrund der variablen Entladezeiten liefert der Netto-Zykluswirkungsgrad eine zwar einfache, aber nur qualitative Vergleichsmöglichkeit der vorgestellten Varianten hinsichtlich der Effizienz. Bei perfekter Stromspeicherung würde der Zykluswirkungsgrad zwischen den Werten bei Volllast und Teillast (ca. 43,7 %) liegen. Bei völligem Verlust der Energie des eingespeicherten Stromes würde der Zyklus-Wirkungsgrad in etwa 10 Prozentpunkte unter dem Mittelwert liegen (ca. 33,1 %).

$$\eta_{Netto,Zyklus} = \frac{t_L \cdot P_{Netz,L} + t_E \cdot P_{Netz,E}}{t_L \cdot \dot{H}_{Br,L} + t_E \cdot \dot{H}_{Br,E}} \qquad (3)$$

4. Diskussion

Abschließend werden die in Tabelle 2 angeführten Varianten miteinander verglichen. Vorweg sei erwähnt, dass klarerweise nach hohen Wirkungsgraden bei möglichst geringen Massenströmen und Volumina getrachtet wird. Außerdem ist die jeweils angeführte TES-Leistung im Entladefall immer als Maximum anzusehen. Diese kann bei Bedarf durch Reduktion des Partikelmassenstroms oder durch nur teilweises Aufheizen des Luftmassenstroms gesenkt werden, was die Entladezeiten verlängert.

Beginnend bei Variante 1, also dem Laden mit Frischdampf in einem SandTES-Kondensator und dem Entladen über den Luftstrang, wird sofort ersichtlich, dass hier ein Parameter, nämlich der Dampfdruck, großen Einfluss auf die relevanten Kenndaten hat. Um die festgelegten Tieflastkriterien (40 % Kesselleistung, 20 % Netzleistung) zu erreichen, muss bei niedrigen Drücken weitaus mehr thermische Energie entnommen werden, was in Kombination mit den niedrigeren erreichbaren maximalen Partikeltemperaturen zufolge der Pinchpunkt-Problematik zu höheren Massenströmen beim Laden und auch beim Entladen führt. Entsprechend dem resultierenden größeren Silovolumen sinkt somit bei niedrigen TES-Drücken die Energiedichte. Die Zykluswirkungsgrade unterscheiden sich hingegen nur unwesentlich.

Variante 2 wiederum nutzt zum Laden anstelle des Frischdampfes direkt den vom Generator produzierten elektrischen Strom zum Betrieb von Hochtemperatur-Heizstäben, während der Entladevorgang wieder über den Luftstrang läuft. Es fällt auf, dass die benötigte TES-Leistung beim Laden und somit die zu speichernde thermische Energie im Vergleich zu den Varianten 1 weiter gesunken ist. Im Gegenzug steht aber auch weniger Energie zum darauffolgenden Entladen bereit, was sich in der geringen Entladezeit und dem deutlich niedrigeren Wirkungsgrad wiederspiegelt. Die niedrige notwendige TES-Leistung im Ladebetrieb in Kombination mit der hohen Temperaturdifferenz des Partikelstroms führt allerdings zu einem niedrigen Silovolumen und einer hohen Energiedichte.

Variante 3 vereint die Lademethoden der beiden ersten Varianten: Zuerst wird der Partikelstrom mit Dampf erwärmt und anschließend mit einer Elektrode auf die Endtemperatur gebracht. Das Entladen erfolgt wieder über den Luftstrang. Die Energiedichte ist zufolge der gleichen Temperaturdifferenz wie bei Variante 2 ident. Das Silovolumen hingegen ist, wegen der höheren Ladeleistung und der daraus folgenden größeren gespeicherten Energiemenge, leicht erhöht. Die Werte für Massenströme, Wirkungsgrad und Entladezeit liegen jeweils zwischen den Werten von Variante 1 und 2.

Die Variante 4 setzt zum Entladen auf direkte Dampfproduktion. Wegen der erhöhten minimalen Partikeltemperatur, die wegen der Pinchpunkt-Problematik zu niedrigen maximalen Partikeltemperaturen führt, kann zum Laden sinnvollerweise nur die Elektrode alleine eingesetzt werden. Die Ladeleistung ist dieselbe wie die der Variante 2, allerdings ist der zugehörige Partikelmassenstrom wegen der niedrigeren Temperaturdifferenz erhöht. Zum Entladen wird ein SandTES-Dampferzeuger parallel zum bestehenden Dampferzeuger geschaltet.

In der Wahl der Entladeleistung ist man nicht eingeschränkt. Für den Vergleich wurde dieselbe Entladeleistung wie für Variante 2 gewählt. Bedingt durch die niedrigere Temperaturdifferenz zwischen Partikelein- und -austritt steigt der Partikelmassestrom deutlich an. Silovolumen, Wirkungsgrad und Energiedichte liegen wiederum zwischen den jeweiligen Werten für Variante 1 und Variante 2. Die Hilfsleistungen der verschiedenen Varianten, jeweils für Laden bzw. Entladen, liegen in einer ähnlichen Größenordnung und sind verglichen mit der TES-Leistung gering. Die Hilfsleistungen beim Entladen über Luft sind zufolge der hohen Volumenströme, trotz des niedriger angenommenen Druckverlusts von 200 mbar, deutlich größer. Die geringere Hilfsleistung von Variante 4 beruht auf den niedrigen Fluidisierungsluft-Volumenströmen analog zu den Wärmeübertragern im Ladebetrieb.

Die Energiedichten aller Varianten liegen auf einem hohen Niveau, auch im Vergleich zu Salzschmelzen mit Energiedichten von rund 800 MJ/m³ (im Temperaturbereich zwischen 250 und 550 °C).

Die berechneten Zykluswirkungsgrade liefern – wie schon oben erklärt – ein nur qualitativ belastbares Bild. Durch die unterschiedlich langen Entladezeiten sinkt dieser Zykluswirkungsgrad je kürzer der Entladezyklus (also der Zyklus bei hohem thermischem Wirkungsgrad des Kraftwerks) ist. Die Tendenz der unterschiedlich verlustreichen Speicherung kann damit trotzdem veranschaulicht werden.

Trotz des niedrigen Wirkungsgrades von Variante 2 kann diese gerade mit dem Elektroden-Laden durch Vorteile bei der Nachrüstbarkeit punkten. Niedrige Massenströme, kleine Wärmeübertrager und Silos sowie ein flexibles Design sprechen für diese Variante. Der TES kann für beliebige Kessel- oder Turbinenlasten ausgelegt werden, da der Wasserdampfkreislauf auch beim Laden nicht beeinflusst wird. Dies verspricht auch hohe Lastwechseldynamiken, weil beispielsweise nicht auf Temperaturgradienten in dickwandigen Bauteilen geachtet werden muss.

Nachteilig sind gegebenenfalls die hohen Temperaturen an der Elektrode, den Wärmeübertragern und den Silos.

Insbesondere bei der Entlademethode über Luft ist die konstruktive Ausführung stark vom jeweiligen Kraftwerkstyp abhängig. Bei der Luftzuführung z. B. bei Staubfeuerungen, ist auf konstruktive und verfahrenstechnische Randbedingungen bei den Brennern zu achten. Somit kann es notwendig sein, nur einen Teil des Frischluftmassenstroms im TES vorzuwärmen, wenn Probleme hinsichtlich Maximaltemperaturen oder Stabilität der Brenner zu befürchten sind. Des Weiteren muss die Auslegung Rücksicht auf die verschiedenen Druckniveaus im Luft-/Rauchgasstrang nehmen.

5. Zusammenfassung

Die in Europa bestehenden Kohlekraftwerke wurden in der Vergangenheit hauptsächlich für den Grundlast-Betrieb konzipiert. Durch die volatilen Strommärkte besteht vermehrt der Bedarf, die Lastschwankungen im Netz auszugleichen. Da

entsprechende Speicherkapazitäten nicht verfügbar sind, ist es notwendig, die bestehenden Kraftwerke nachzurüsten, um deren Flexibilität hinsichtlich Tieflast und Lastwechseldynamik zu verbessern.

Eine Möglichkeit besteht darin, thermische Energiespeicher (TES) in den Kraftwerksprozess zu integrieren. An der TU Wien wurde ein Hochtemperatur-Wärmespeicher entwickelt, der als Speichermedium Partikel wie Quarzsand oder Korund verwendet.

In dieser Arbeit wurden verschiedene Konzepte zur Integration vorgestellt und ausführlich diskutiert. Darunter finden sich einerseits Möglichkeiten zum Laden über Dampfauskoppelung oder Heizstäbe, andererseits Möglichkeiten zum Entladen über Luftvorwärmung oder Dampfproduktion.

Der Vergleich zeigt die Vor- und Nachteile der verschiedenen Konzepte auf. Hinsichtlich der Nachrüstbarkeit weisen die Konzepte Strom-Laden kombiniert mit Luft- oder Dampf-Entladen wesentliche Vorteile auf, wie beispielsweise niedrige Massenströme und Silovolumina sowie hohe Flexibilität bei der Auslegung. Mit den beiden Konzepten sind auch Auslegungen denkbar worin die Netto-Blocklast über mehrere Stunden auf null gesenkt werden kann. Diese Vorteile werden allerdings durch eine niedrigere Effizienz erkauft.

Zur weiteren Analyse dieser Integrationskonzepte sind Untersuchungen mit Schwerpunkt auf die erzielbare Dynamik sowohl bei Lastsenkung/Laden als auch bei Laststeigerung/Entladen, auf Kosten, auf konstruktive Details wie beispielsweise die Brenner oder eine genaue Betrachtung der Verbrennungsvorgänge in der Brennkammer notwendig.

6. Quellen

[1] Steiner, Peter; Schwaiger, Karl; Walter, Heimo and Haider, Markus: *Active fluidized bed technology used for thermal energy storage*, Proceedings of the ASME 2016 Power and Energy Conference (PowerEnergy 2016-59053).

[2] Brinkmeier, Niels: *Flexibility of thermal power plants*. PhD Thesis, IWBT, TU Braunschweig, 2015.

[3] NIST (National Institute of Standards and Technology), *NIST Chemistry WebBook*, URL: http://webbook.nist.gov/cgi/cbook.cgi?ID=C14808607&Mask=2 (letzter Aufruf: 24.07.2016).

[4] Steiner, Peter; Schwaiger, Karl; Haider, Markus; Walter, Heimo and Hämmerle,Martin: *Increasing Load Flexibility and Plant Dynamics of Thermal Power Plants via the Implementation of Thermal Energy Storages*. Proceedings of the ASME 2016 Power and Energy Conference, 2016 (PowerEnergy 2016-59181).

Paper 5

P. Steiner, K. Schwaiger, M. Haider, H. Walter

System Analysis of Central Receiver Concepts with High Temperature Thermal Energy Storages: Receiver Technologies and Storage Cycles

AIP Proceedings of the
SolarPaces 2016 Conference
October 11-14, 2016
Abu Dhabi, UAE

System Analysis of Central Receiver Concepts with High Temperature Thermal Energy Storages: Receiver Technologies and Storage Cycles

Peter Steiner[1, a)] Karl Schwaiger[1], Markus Haider[1], Walter Heimo[1]

[1]*Institute for Energy Systems and Thermodynamics, Technische Universität Wien, Getreidemarkt 9/E302, A-1060 Vienna, Austria*

[a)]Corresponding author: peter.p.steiner@tuwien.ac.at

Abstract. Reducing the levelized cost of electricity for solar thermal electricity (STE) plants is the most important challenge of this technology. A bottleneck at state of the art STE plants is the heat storage medium (HSM) with its temperature limits. To replace the commonly used molten salt, particles like quartz sand or corundum, enabling temperatures up to 1000 °C, are proposed as new HSM. The temperature raise leads to economical challenges, which have to be analyzed more in detail. In this work two STE plant concepts based on particles as HSM are introduced and discussed to outline advantages and issues concerning this technology.

INTRODUCTION

One major advantage of solar thermal electricity (STE) plants compared to photovoltaics (PV) is the dispatchability, which leads to a decoupling of the electricity generation and demand. The levelized cost of electricity (LCOE) has to be minimized, which can be achieved by increasing the efficiency of such STE plants.

State of the art central receiver STE plants like SolarReserve's Crescent Dunes (CD) use nitrate based molten salt as a sensible heat storage medium (HSM) in a two tank system. The maximum temperature of this molten salt is at about 560 °C, while a minimum temperature of approximately 250 °C has to be exceeded to prevent freezing. The thereby limited steam temperatures of the appropriate Rankine power cycle lead to reduced thermal efficiencies. Also the energy density of the HSM is strongly affected. Molten salt is an expensive HSM, which has a significant impact on the overall investment costs. A cheap high temperature HSM could lead to a lowered LCOE.

Much research in recent years has focused on particles like quartz sand or corundum to become this new HSM. Temperatures beyond 1000 °C are feasible, where there is no relevant lower temperature limit. The slightly lower specific isobaric heat capacity is overcompensated by the extremely high temperature range. Moreover, these materials are by orders of magnitude cheaper, compared to molten salt.

Various concepts applying particles as HSM have been examined, which can be roughly divided into direct and indirect storage cycles. At direct storage cycles the particles get straight heated up in a particle receiver to afterwards be stored in a silo. On demand the hot particles feed the particle-based steam generator of an appropriate power cycle. These direct storage cycles using particles suffer from poor heat transmission especially at the particle receiver, leading to lower peak fluxes and thus to huge absorbers and higher thermal losses. Also an elaborate conveying technology is necessary for transporting the particles from the ground up to the receiver on the top of the about 150 to 250 m high tower.

For indirect storage cycles a heat transfer medium (HTM) is heated up in a receiver to transfer the thermal energy to the particles via an additional heat exchanger (HEX) on the ground. Again, the heated particles can be stored in a silo to power a particle-based steam generator on demand. As HTM liquid sodium or fluoride-salt are envisaged, to achieve higher temperatures and hence higher receiver efficiencies. Especially the high conductivity of sodium allows high peak fluxes and as a consequence small receivers with efficiencies above 90 % [1]. Liquid

sodium has already been used in nuclear power plants for decades and various projects in solar power research seized this technology in recent years. Attention has to be paid to safety issues, as liquid sodium reacts with water and air.

For the main components of the two cycle types, the receiver and the particle HEX, different technologies are proposed in the scientific community. Direct and indirect receivers have been conceived, as well as fluidized or moving bed particle HEX [2].

In this work a thermal energy storage (TES) technology called sandTES is presented, which is based on a fluidized bed HEX. In addition two STE plant concepts, implementing this sandTES technology and using corundum particles as HSM are considered and compared.

The first concept implements a direct storage cycle with an indirect particle receiver. It requires large bucket conveyors. The second concept applies an indirect storage cycle with a tubular liquid receiver. To avoid the large bucket conveyors, liquid sodium is used in the receiver for the heat transfer to the HSM corundum [3], which is stored in a silo on the ground. As mentioned before, an additional particle-sodium HEX is needed, but instead, the bucket conveyors can be saved. Both concepts use a water/steam power cycle similar to the one of CD.

At the end of the paper, calculations carried out in Matlab as well as process simulations performed in Ebsilon®Professional, are presented and discussed.

SANDTES

The sandTES technology is being developed at the Institute of Energy Systems and Thermodynamics (IET) of the TU Wien. Its aim is to achieve an active TES, which exceeds the previous temperature limits of common sensible TES systems. As the name suggests, the sandTES-technology basically is run with (quartz) sand as storage medium, which enables maximum temperatures beyond 1000 °C. Although sand is a cheap storage medium, other materials like corundum are also considered due to their higher energy density.

The core of the sandTES technology is a counter-current particle/fluid HEX, in which a dense particle suspension is fluidized by auxiliary air. The distinctive feature compared to standard (stirred tank) fluidized bed technology is that the particles follow a plug flow characteristic along the HEX. Thanks to several patented features the bed height is kept nearly constant, and a near-perfect counter-current behavior is enabled. There is almost no parasitic bed inventory and the flow direction through the fluidized bed can be inversed in a very short time (minutes). The heat contained in the fluidization air can be largely recovered by air/air-recuperators. To reduce the losses due to auxiliary equipment, the pressure drop through the bed and the blower mass flow have to be kept low. The vertical pressure drop of the fluidization air through the suspension mostly depends on the height of the fluidized bed, see Eq. (1)

$$\Delta p_{fb} = (1-\psi)(\rho_p-\rho_f)\cdot g\cdot \Delta H_{fb} \tag{1}$$

with the vertical pressure drop Δp_{fb}, the gravity g, the density of the particles ρ_p and the fluid ρ_f, the corresponding height ΔH_{fb} and the porosity of the bed ψ. The fluidization air mass flow correlates with the fluidization grade μ, see Eq. (2)

$$\mu = \frac{u_{act}}{u_{mf}} \tag{2}$$

with u_{act} the actual superficial velocity, and u_{mf} the minimum fluidization velocity, below which the fluidized bed collapses. The fluidization grade needs to be higher than 1 at every point of the HEX. This is the reason, why the mean value is stated at about 3 to 4. Since u_{mf} decreases with the particle size, very fine powders (in the magnitude of 60-100 microns) are preferred to further reduce auxiliary power. More specific technical details are presented in [2,4,4,4–7].

In Figure 1 a simplified process diagram of a sandTES system is shown to introduce the basic storage concept. To charge the TES, cold sand falls out of the filled silo (e.g. silo 1) and is fed via a screw into the HEX. Because of the horizontal pressure gradient, the storage material within the fluidized bed flows through the device, while getting heated up by the working fluid. At the outlet, the hot sand falls into a bucket conveyor, which transfers the sand upwards into silo 2, in which it is stored. For discharging, the direction can be reversed, so that the hot sand flows

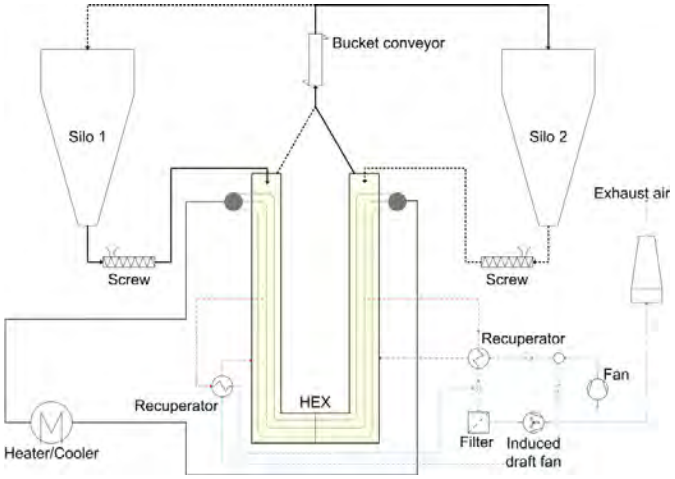

FIGURE 1. Process flow sheet of the sandTES pilot plant [5]

back through the HEX from silo 2 to 1 while cooling down. Meanwhile the hot exhaust air cools down in the recuperator by heating up the fresh air stream. After filtering, the exhaust air leaves the system through a chimney. For proving the concept, a 280 kW_{th} pilot plant is put in operation at the IET's laboratory site. Insightful conclusions about the stability and optimization criteria are expected by the measurements [5].

PLANT CONCEPTS

In this section the two STE plant concepts are introduced: an indirect particle receiver with a direct storage cycle (IPDSC) using corundum as HSM and a sodium receiver with an indirect storage cycle (SRISC) using corundum as HSM and liquid sodium as HTM.

As already indicated in the introduction, the comparison aims to outline contrasts and issues at using corundum as the more advantageous HSM.

A main problem concerns the conveying technology, since the particles have to be transported up the tower to the receiver. As pneumatic transportation is not applicable due to the high heat and auxiliary losses, bucket conveyors or pan conveyors seem to be the only option. Bucket conveyors available on the market are limited at a maximum temperature of about 300 °C, where the pan conveyors run tilted with an angle up to 60 ° to the horizontal, leading to an complex plant layout [8]. As the bucket conveyor seems to be the superior solution, an economizer in the water/steam cycle is needed to cool down the particles below 300 °C. This is slightly harming the thermal efficiency, but seems nevertheless to be the better choice.

Problems concerning conveying technology can be largely avoided by applying an intermediate sodium cycle. At least one accident has been reported in test installations based on liquid sodium. But since the reaction of sodium with water is much more hazardous compared to the reaction with air, it seems acceptable to use small amounts just for the heat transfer cycle and not for storage silos, if separated from any water appearance [9].

For a more specific analysis, process simulations based on a STE plant similar to CD were carried out. Thus, a central receiver plant powering a subcritical water/steam cycle is examined. The appropriate receiver data are listed in Table 1. The corresponding data for the power cycle are summarized in Table 2. Details and results of the simulations are discussed in the following sections.

Receiver & Storage Cycle

As input boundary for the STE plant the same heliostats field was assumed for both storage cycles, consequently leading to an equal input heat flow $\dot{Q}_{In}$. A simplified 1D receiver model was used for a rough calculation of the heat flows and temperatures at the receiver. The calculations rely on the equations (3) and (4) with σ_{SB} the Stefan Boltzmann constant, $\alpha_{Convection}$ the heat transfer coefficient due to convection losses, T_{env} the temperature of the

TABLE 1. Nominal receiver data

Parameter	Unit	IPDSC		SRISC	
$T_{HTM,min}$	°C	285	*285*	370	*370*
$T_{HTM,max}$	°C	800	*800*	700	*750*
$\dot{q}_{In}$	kW_{th}/m^2	303	*386*	2010	*2500*
h_{abs}	kW/m^2K	0.9	*1.2*	10	*10*
$\dot{Q}_{In}$	MW_{th}	720	*720*	720	*720*
$\dot{Q}_{Net}$	MW_{th}	601	*619*	673	*674*
$\dot{Q}_{Reradiation}$	MW_{th}	23	*18*	2	*2*
$\dot{Q}_{Convection}$	MW_{th}	59	*46*	8	*7*
$\dot{m}_{HTM}$	kg/s	989	*1021*	1616	*1409*
d_{abs}	m	30	*24*	8	*6*
H_{abs}	m	16	*16*	9	*9*
A_{abs}	m^2	2372	*1863*	357	*287*

TABLE 2. Nominal power cycle data

Parameter	Unit	CD	IPDSC	SRISC
$\dot{Q}_{Boiler}$	MW_{th}	269	250	280
P_{Net}	MW_{el}	110	110	123
$\dot{m}_{Livesteam}$	kg/s	98	82	92
$T_{Livesteam}$	°C	540	600	600
$T_{Reheater}$	°C	540	620	620
p_{High}	bar	116	190	190
$p_{Intermediate}$	bar	40	40	40
p_{Low}	bar	3	3	3
$p_{Condenser}$	bar	0.1	0.1	0.1
$\dot{m}_{HSM}$	kg/s	640	411	724
η_{Net}	%	40.8	44.0	44.0
η_{Gross}	%	43.4	46.8	46.8

environment, a chosen absorptivity α_{opt} of 0.95 (assuming a selective coating) and an emittance of 0.1. For the absorber, thus the outer receiver surface, the incoming solar irradiation $\dot{Q}_{In}$ must be equal to the sum of re-radiation and convection losses ($\dot{Q}_{Reradiation}$ and $\dot{Q}_{Convection}$) plus to the heat flow to the HTM $\dot{Q}_{Net}$. The local temperatures of the HTM T_{HTM} are defined via the caloric equation of state, where h_{abs} is the heat transmission coefficient (conduction + convection) at the absorber, c_{pm} the mean isobaric heat capacity and $\dot{m}_{HTM}$ the mass flow of the HTM [2,6].

$$\dot{q}_{In}A_{abs} = \frac{1}{\alpha_{opt}}[\sigma_{SB}\varepsilon(T_{abs}^4)+\alpha_{Convection}(T_{abs}-T_{env})+h_{abs}(T_{abs}-T_{HTM})]A_{abs} \quad (3)$$

$$h_{abs}A_{abs}(T_{abs}-T_{HTM,mean}) = \dot{m}_{HTM}c_{pm}(T_{HTM,max}-T_{HTM,min}) \quad (4)$$

At the chosen process parameters and based on a tube conductivity of 25 W/mK, the material temperatures at the absorber surface T_{abs} reach about 1074 °C for the IPDSC receiver and 888 °C for the SRISC receiver, wherefore material issues become important. The receiver tube surface temperatures in this paper are definitely ambitious, and

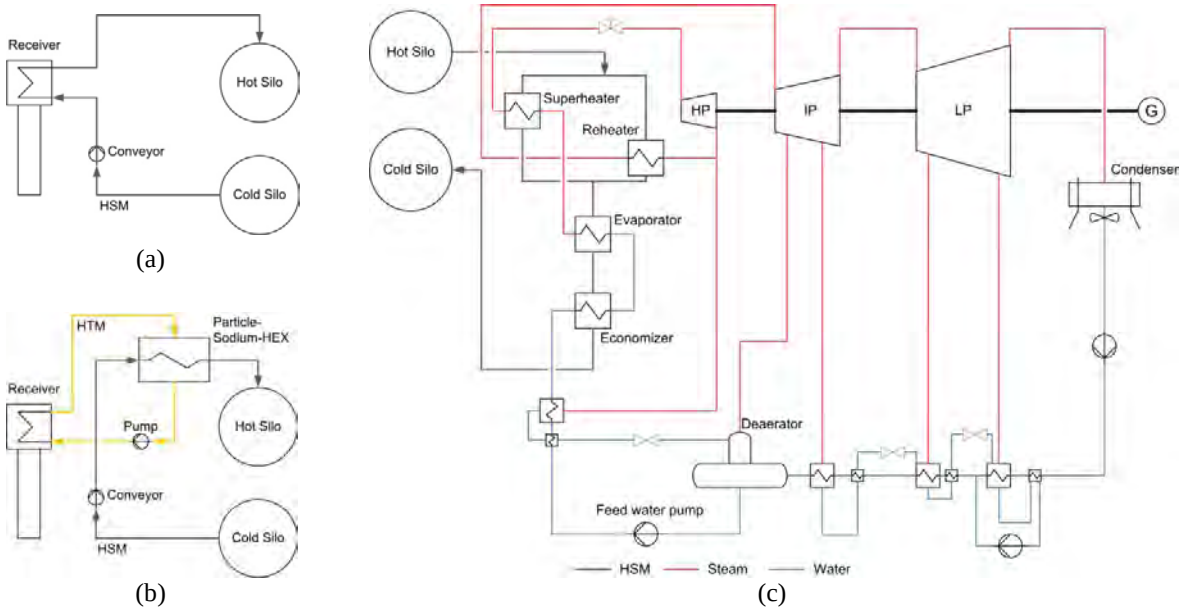

FIGURE 2. Process flow sheet of the STE plants with the IPDSC in (a), the SRISC in (b) and the water/steam cycle in (c).

they are at the frontier of what can be achieved by super alloys or by ceramic materials such as SiSiC. In the case of the indirect particle receivers, the challenges are limited to the field of thermo-mechanics. In the case of sodium there are also potential corrosion issues which would have to be investigated before an implementation to pilot plants or full scale plants. A clear advantage of both receiver types is that the medium in the receiver tubes is only marginally above the ambient pressure, thus minimizing the stress components resulting from internal pressure. The occurring receiver losses, mainly the reradiation and convection losses, directly affect the net heat flow available for the storage system. Because of an assumed equal solar multiple of 2.4, which is the ratio of the receiver net heat flow $\dot{Q}_{Net}$ to the steam generator heat flow $\dot{Q}_{Boiler}$, the steam generator and hence the electric net output P_{Net} are defined. In this way, the enhancement of the receiver and the storage cycle can be clearly quantified by the additional electric net output.

Figure 2 shows a simplified flow sheet of the STE plant. In (a) the direct storage cycle is shown. A bucket conveyer unit transports the corundum particles 200 m upwards to an indirect fluidized bed receiver [6], where they get heated up. As the maximum temperature of the bucket conveyor is limited, only the cold particles can be transported. Therefore a cascaded design, using gravity for the particle transport from the receiver to the hot silo and further on to the steam generator seems preferable.

Due to the lower heat transfer coefficient of fluidized beds, the achievable heat fluxes $\dot{q}_{In}$ on the particle receiver surface A_{abs} remain in the range of 300 kW_{th}/m^2. This overall result in a huge diameter d_{abs} and height H_{abs} of the absorber, see Table 1. The maximum temperature of the HTM, in this case also the HSM, seems ambitious, but enables the high energy densities, which can be seen at the mass flow of the HTM and later in the results section at the volumetric capacity of the silos.

The listed heat flows in Table 1 lead to a receiver efficiency $\eta_{Receiver}$ of approximately 83 %, which is calculated relying on equation (5).

$$\eta_{Receiver} = \frac{\dot{Q}_{Net}}{\dot{Q}_{In}} \tag{5}$$

The italic numbers for the IPDSC in Table 1 show an alternative case with enhanced heat transfer coefficients due to finned receiver tubes. The receiver efficiency thereby could be increased up to 86 %.

In Figure 2 (b) the indirect storage concept is depicted. The HTM is heated up in a tubular sodium receiver, wherefore an additional sodium-particle HEX on the ground is necessary to transfer the heat to the HSM. Nevertheless the bucket conveyors can be saved. The design data of this sodium-particle sandTES-HEX are summarized in Table 3 with the temperatures T_{HSM} and the mass flow $\dot{m}_{HSM}$ of the HSM and the auxiliary power P_{Aux} needed for the blowers. The size of the HEX is characterized by the product $(hA)_{HEX}$, the area A_{HEX} and the height H_{HEX} of the HEX.

TABLE 3. Design parameter of the sodium-particle HEX

Parameter	$\dot{Q}_{Net}$	$T_{HSM,min}$	$T_{HSM,max}$	$\dot{m}_{HSM}$	P_{Blower}	$(hA)_{HEX}$	$A_{Bed,HEX}$	A_{HEX}	H_{HEX}
Unit	MW_{th}	°C	°C	kg/s	kW_{el}	MW_{th}/K	m^2	m^2	m
Value	673	330	660	1744	156	15	668	30472	2.2

In this concept, the maximum temperature of the liquid sodium is the limiting factor. The authors did not find enough extensive research which would allow to say that the way for applications beyond 600 °C is free [10]. Nevertheless, the theoretical maximum sodium temperature is 873 °C. So there is a justified hope that after additional research work the application range of liquid sodium in solar thermal receivers can be extended up to 750 °C or even beyond. In order to avoid too much optimism, the maximum sodium temperature in our study was limited to 700 °C.

As mentioned before, the safety concerns are the main disadvantage of liquid sodium, which is believed to be acceptable, if only few amounts of sodium are used and the contact with water is barred.

The peak fluxes on the receiver surface were chosen in the range of 2000 kW/m², although even higher fluxes up to 2500 kw_{th}/m^2 are reported in literature [10]. These high heat fluxes lead to a minimized receiver design and the according low losses. The receiver efficiency is at approximately 93 %, referring to equation (5). The italic letters in Table 1 for the SRISC show an additional case with both increased maximum temperature of the sodium and an enhanced peak flux, resulting in a slightly higher receiver efficiency of 94 %.

TABLE 4. Parameters of the steam generator's components (left: IPDSC, right: SRISC)

Parameter	Unit	Reheater		Superheater		Evaporator		Economizer	
$\dot{Q}_{HEX}$	MW_{th}	51	58	100	115	69	82	60	67
$\dot{m}_{HSM}$	kg/s	155	281	305	555	460	836	460	836
P_{Blower}	kW_{el}	4	29	10	45	57	83	182	111
$(hA)_{HEX}$	kW/K	289	782	542	1305	772	1098	1420	1059
A_{HEX}	W_{th}/m^2K	509	1359	731	1438	1277	1906	2547	1467
$A_{Bed,HEX}$	m^2	42	108	69	197	74	111	329	231
H_{HEX}	m	1.4	2.1	1.9	2.1	1.8	1.9	2.3	2.7

Power Cycle

The calculations done in this work are based on a subcritical water/steam cycle similar to CD. The steam parameters - for both concepts and a similar power plant to CD summarized in Table 1 - are slightly enhanced, to outline the potential of the temperature raise compared to molten salt STE plants. The net efficiency η_{Net} of CD was calculated with about 41 %, where modern supercritical power plants with steam temperatures beyond 600 °C already reach more than 45 %.

Figure 2 (c) shows the applied power cycle, with the high pressure (HP), intermediate pressure (IP) and low pressure (LP) turbines, the air cooled condenser, various pre-heaters and the steam generator. The heated particles stored in the hot silo are used for feeding the steam generator, which consists of an economizer, the evaporator, the super- and the reheater. The last two are fed in parallel to reduce the particle mass flows.

As it can be seen from Table 2, the two concepts using particles as HSM mostly differ in the net heat flow, hence the boiler heat flow and the electric net output. As mentioned before, the lower heat losses of the sodium receiver directly result in a higher electric output of the power cycle at similar steam conditions.

However, a closer look at Table 2 reveals the other disadvantage of the SRISC. The limited maximum temperature results in comparatively high mass flows of the HSM, due to the lowered temperature difference between water/steam and the particles. This also can be seen in Table 4, where the design parameters of the steam generators, each consisting of four sandTES-HEXs, are summarized. The calculations were carried out with an advanced Matlab tool, which was developed at the IET. The heat transfer coefficient was assumed as 500 W/m^2K, where the maximum mass flux of the HSM was set to 75 kg/m^2s.

The heat flows $\dot{Q}_{HEX}$ of the SRISC HEXs are each slightly higher than the IPDSC's. Furthermore, as a consequence of the lower temperature difference, the HSM mass flows of SRISC are nearly twice as high. This can also be seen at the product $(hA)_{HEX}$, which is an indicator for the HEX size. The auxiliary power - in these considerations including the blowers needed for fluidization - correlates with the HEX dimensions $A_{Bed,HEX}$ and H_{HEX}. Additionally the power for the conveying system and the pumps have to be considered, but do not affect the conclusion.

The deviation at the economizers is a result of the fixed HSM mass flow of the super- and reheater. The economizer cannot cool down the HTM too far, leading to a higher temperature difference.

RESULTS & DISCUSSION

In this section the presented concepts and the according data are summarized and discussed. In Table 5 the most significant parameters regarding the overall design of the STE plant are listed for both particle concepts to be discussed further on.

TABLE 5. STE Plant design parameters

Parameter	$\eta_{Receiver}$	η_{Net}	E	V_{Silo}	A_{abs}	$A_{HEX,total}$
Unit	%	%	MJ/m^3	$10^3\ m^3$	m^2	m^2
IPDSC	83	44,0	913	10	2372	5064
SRISC	93	44,0	581	17	357	36642
CD	90	40,8	712	14	n. A.	n. A.

As mentioned in the introduction, the main goal of developing new STE plant concepts is to reduce the LCOE for being competitive on the electricity market. A higher total plant efficiency leads to an increased power output at similar boundary conditions. Thus, the much greater receiver efficiency of the SRISC can lead to a decreasing LCOE.

Nevertheless, an economic optimum has to be found. A raise of the temperatures not only leads to higher efficiencies, but also to significantly higher material and manufacturing costs for all thereby concerned STE plant components. Nickel-based alloys or even ceramics have to be considered, whereas especially at ceramics joining technology seems critical, referring to safety issues with liquid sodium.

The most affected component regarding high temperature persistence is the receiver, meaning the particle receiver as well as the tubular receiver. Because of the much higher material need and manufacturing effort for the particle receiver, as a result of the huge dimensions, the particle receiver is not only less efficient, but also more expensive.

Also the conveying technology seems problematic regarding the plant layout, erection costs and maintenance effort. Furthermore the auxiliary power for e.g. a bucket conveyor exceeds the electricity consumption of the compared liquid sodium pumps, as it is difficult to recover the potential energy of the particles.

The HSM has a key role in STE plants. At the moment the state of the art HSM molten salt is the bottleneck for achieving higher efficiencies, because of the highly limited temperature range for plant operation. The energy density E influences the size of the HEX surfaces A_{HEX} and the volume of the storage silos V_{Silo}. Furthermore, the HSM itself has a great impact on the investment costs. In this work a nominal load storage capacity of 10 hours was specified, similar to CD. It is clear, that compared to the IPDSC the almost twice as high needed storage volume of the SRISC leads to higher costs for the silo, the accompanying insulation and the material itself. The storage volume as well as the energy density of CD is in the middle of the two proposed concepts.

As power cycles various concepts are in discussion, like modern supercritical water/steam Rankine cycles with enhanced steam parameters, similar to the parameters examined in this work. As another often proposed cycle the supercritical carbon dioxide (sCO2) cycles are in discussion. The net efficiency can be further increased and the power island has a very compact layout. However, supercritical water/steam cycles are only getting economically beneficial at electric power plant outputs in the range of 600 MW_{el} and beyond. The sCO2 cycles are just in development and no utility-scale plants are built up to now.

Finally, the various HEXs have to be mentioned. The SRISC not only needs an additional sandTES-HEX, also the other HEXs of the power cycle are clearly larger, again leading to higher investment costs for material and insulation.

For the considerations in this work, the heliostats field with far the largest stake of the costs was kept constant at about 1.200.000 m² heliostats surface.

Summing up, the SRISC promises higher efficiencies, a less expensive receiver and does not need particle conveyor technology. On the other hand, an additional sodium-particle HEX is needed and all the HEXs on the ground are bigger. A raise of the maximum acceptable sodium temperature could compensate for this disadvantage, but this clearly requires more research effort.

CONCLUSIONS

The dispatchability seems to be the main advantage of STE plants compared to photovoltaics. Even though, the LCOE has to be decreased for being sufficiently competitive on the electricity market as power supplier. This can be achieved by increasing efficiencies of the STE plants. State of the art STE plants using molten salt suffer from their limited maximum temperatures, lowering both the power cycle efficiency and the energy density. The storage medium molten salt is costly.

In this paper particles are proposed as heat storage medium, which can be applied either in a direct storage cycle with a particle receiver or an indirect storage cycle with e.g. liquid sodium as heat transfer medium.

However, various issues are raised using particles as heat storage medium. The direct cycle has to deal with an oversized receiver and with bucket conveyors. On the other hand, the indirect particle cycle needs much larger silos and particle-HEXs, due to the smaller temperature differences. Also the challenges of handling liquid sodium have to be considered.

In future work a detailed cost analysis has to be done to figure out, which concept finally leads to the most economically beneficial plant and hence the lowest LCOE.

ACKNOWLEDGMENTS

The K-Project GSG-GreenStorageGrid (Grand no. 836636) is funded in the framework of COMET - Competence Centers for Excellent Technologies by the Federal Ministry of Transport, Innovation and Technology, the Federal Ministry of Science, Research and Economy, the Vienna Business Agency, the Federal Province of Lower Austria and by the Federal Province of Upper Austria. The program line COMET is administered by the Austrian Research Promotion Agency (FFG). The authors would like to thank also the project partners Valmet GesmbH., EVN AG, ENRAG GmbH. and Primetals Technologies GmbH for the pleasant and constructive working relationship.

Special thanks go to the sandTES research team for the helpful support and the numerous discussions.

REFERENCES

[1] Ho C. K., and Iverson B. D., 2014,“Review of high-temperature central receiver designs for concentrating solar power,” Renewable and Sustainable Energy Reviews, 29, pp. 835–846.

[2] Schwaiger K., 2016,“Development of a novel Particle Reactor/Heat-Exchanger Technology for Thermal Energy Storages,” Disseratation, Institut für Energietechnik und Thermodynamik, TU Wien, Wien.

[3] NIST, 2015,“NIST Chemistry WebBook,” http://webbook.nist.gov/cgi/cbook.cgi?ID=C14808607&Mask=2.

[4] P. Steiner, K. Schwaiger, H. Walter, and M. Haider, 2016,“Active fluidized bed technology used for thermal energy storage,” Proceedings of the ASME 2016 Power and Energy Conference(PowerEnergy2016-59053).

[5] P. Steiner, K. Schwaiger, M. Haider, H. Walter, and M. Hämmerle, 2016,“Increasing Load Flexibility and Plant Dynamics of Thermal Power Plants via the Implementation of Thermal Energy Storages,” Proceedings of the ASME 2016 Power and Energy Conference, 2016(PowerEnergy2016-59181).

[6] Schwaiger K., Haider M., Haemmerle M., Steiner P., and Obermaier M.-D., Concept of a utility scale dispatch able solar thermal electricity plant with an indirect particle receiver in a single tower layout, p. 60004.

[7] P. Steiner, K. Schwaiger, H. Walter, M. Haider, and M. Hämmerle, 2016,“Fluidized Bed Particle Heat Exchanger for Supercritical Carbon Dioxide Power Cycles,” ASME IMECE 2016.

[8] Schwaiger K., and Haider Markus, 2015,“Desing of a utility scale solar thermal tower system based on particle receivers and fluidized bed technology: Proceedings of the SASEC2015,”

[9] Nicholas Bartos, James Fisher, and Andrew Want,“Vast Solar,”

[10] Boerema N., Morrison G., Taylor R., and Rosengarten G., 2012,“Liquid sodium versus Hitec as a heat transfer fluid in solar thermal central receiver systems,” Solar Energy, 86(9), pp. 2293–2305.

Paper 6

P. Steiner, K. Schwaiger, H. Walter, M. Haider, M. Hämmerle

Fluidized Bed Particle Heat Exchanger for Supercritical Carbon Dioxide Power Cycles

Proceedings of the ASME 2016 International Mechanical Engineering Congress and Exposition IMECE2016
November 11-17, 2016, Phoenix, Arizona, USA

Proceedings of the ASME 2016 International Mechanical Engineering Congress and Exposition
IMECE2016
November 11-17, 2016, Phoenix, Arizona, USA

IMECE2016-67104

FLUIDIZED BED PARTICLE HEAT EXCHANGER FOR SUPERCRITICAL CARBON DIOXIDE POWER CYCLES

Peter STEINER
Technische Universität Wien
Institute for Energy Systems and Thermodynamics
Getreidemarkt 9/E302
A-1060 Vienna, AUSTRIA
peter.p.steiner@tuwien.ac.at

Karl SCHWAIGER
Technische Universität Wien
Institute for Energy Systems and Thermodynamics
Getreidemarkt 9/E302
A-1060 Vienna, AUSTRIA

Heimo WALTER
Technische Universität Wien
Institute for Energy Systems and Thermodynamics
Getreidemarkt 9/E302
A-1060 Vienna, AUSTRIA

Markus HAIDER
Technische Universität Wien
Institute for Energy Systems and Thermodynamics
Getreidemarkt 9/E302
A-1060 Vienna, AUSTRIA

Martin HÄMMERLE
Technische Universität Wien
Institute for Energy Systems and Thermodynamics
Getreidemarkt 9/E302
A-1060 Vienna, AUSTRIA

ABSTRACT

Numerous studies in the field of power generation deal with efficiency and flexibility enhancement of power plants. Supercritical carbon dioxide (sCO_2) power cycles promise significantly higher efficiencies and very compact constructions compared to conventional Rankine cycles. An opportunity to increase the flexibility of such power cycles, is the integration of Thermal Energy Storage (TES) systems into the process. In this work the sandTES technology, a particle based TES system is introduced, which can be used to improve the load change characteristics of power plants even at highest temperatures. After introducing the main concept and the key technologies of the sandTES technology, a utility scale heat exchanger for implementation in a high temperature sCO_2 power cycle is presented and discussed. Finally crucial design parameters of the presented heat exchanger (HEX) are outlined as well as their influences on the HEX dimensions are discussed.

INTRODUCTION

In times of rising energy demand combined with highly volatile electricity markets, efficiency and flexibility of power plants are becoming more and more important for being competitive as energy supplier. At thermal power plants the obvious choice for enhancing the thermal efficiency is to increase the thermodynamic mean temperature of a cycle, which is mostly achieved by raising the upper cycle temperature. Due to material strength this maximum cycle temperatures are limited: common Brayton cycles reach temperatures above 1200 °C, while today's Rankine cycles remain slightly above 600 °C. Ambitious projects already achieve temperatures up to 700 °C. Despite the still lower temperatures of these Rankine cycles, the variety of possible energy sources heating the cycle is a great advantage, making it a widespread technology. The field of application reaches from conventional fuel fired over nuclear power plants to renewables like biomass or solar thermal electricity (STE) power plants.

A promising approach for a further enhancement of power plant efficiencies is the utilization of Brayton cycles using supercritical carbon dioxide (sCO_2) as working fluid. Thermal efficiencies of sCO_2 cycles are about 4 % points higher than of water/steam cycles at similar boundary conditions [1].

As mentioned above, flexibility in electricity generation is a main requirement for future power plants. Generally the implementation of thermal energy storage (TES) systems into thermal power plants increases load flexibility [2, 3]. For example, the water/steam cycle of a STE plant can be heated by molten salt, which itself is heated up from a solar field. This molten salt can be simply stored in tanks, leading to dispatchability of the STE plant, which is a major advantage compared to photovoltaics. The application of solar salt, the state of the art heat storage medium (HSM) in these STE plants, is limited at a maximum temperature of approximately 550 °C. This restriction of course influences the upper temperature of the power cycle, resulting in lower thermal efficiencies. Besides, solar salt solidifies at temperatures below approx. 250 °C, which further reduces the potential temperature range.

The usage of particles as HSM is a promising alternative. The slightly more elaborate handling of these particles is compensated by the high achievable temperatures of up to 1000 °C.

At the Institute for Energy Systems and Thermodynamics (IET) of the TU Wien a novel fluidized bed technology, called sandTES, is developed for realizing an efficient particle-fluid HEX, which can be applied in thermal power plants e.g. for TES systems. This technology is currently under validation via a 280 kW_{th} pilot plant.

In this work the focus is on the above mentioned sandTES technology. Since this technology uniquely provides operation at highest temperatures, an application in combination with a high temperature sCO_2 power cycle seems convenient for realizing a supremely flexible and efficient power cycle.

First a brief introduction about sCO_2 cycles is given, to point out the challenges at TES implementation. Subsequently the principles and features of the sandTES technology are introduced as well as the governing design criteria are discussed. Furthermore a design case based on a utility-scale STE plant, applying a sCO_2 cycle and a sandTES system is presented. The appropriate particle-sCO_2 HEX is examined in detail regarding dimensions, efficiency and needed auxiliary power.

SUPERCRITICAL CO_2 POWER CYCLES

Tendencies in power plant design are going towards higher temperatures to enhance efficiencies in electricity generation. As modern Rankine cycles with pressures of about 290 bar and temperatures at approx. 600 °C at the turbine inlet are limited by material strength, alternate cycles concepts, referring to the sCO_2 cycles, are discussed. Due to the high energy density of sCO_2 compared to water/steam a very compact design of turbo machinery and heat exchangers [4] is enabled. This overall results in a raise of the highest possible cycle temperature up to 800 °C leading to accordingly higher Carnot factors [1].

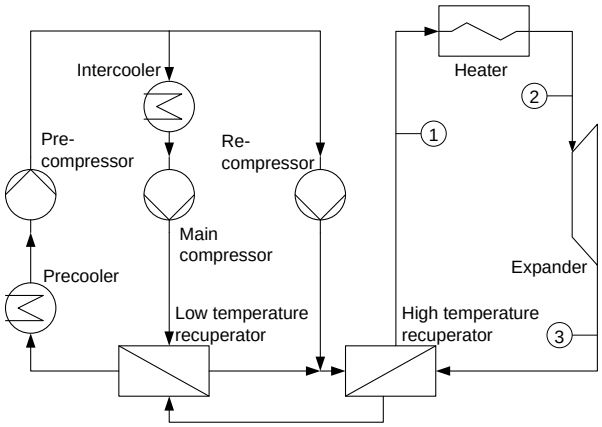

FIGURE 1. PARTIAL COOLING CYCLE

Compared to conventional Brayton cycles, the carbon dioxide benefits from low compressibility factors Z near the critical point. Thus, the isobar curves in a T-S-graph are rather close to each other. Looking at Eq.(1) it gets clear that falling compressibility factors lead to rising densities ρ at constant values for the pressure p, the gas constant R and the temperature T.

$$Z = \frac{p}{\rho \cdot R \cdot T} \tag{1}$$

These high densities, especially near the critical point, lead to low technical work and thus to low compression power needed, which results in high thermal efficiencies in the range of 50 % [5]. It has to be mentioned, that previous studies mostly neglect pressure drop in the HEXs, which potentially leads to lower efficiencies in real life application.

Figure 1 shows a process flow sheet of a 55 MW_{el} STE plant, applying a sCO_2 power cycle. Three relevant spots are marked to outline the main challenges at TES implementation. In table 1 the process parameters for these three marked spots are listed. The temperature and the pressure in point 2 are predefined pa-

TABLE 1. PROCESS DATA

Name	1	2	3	Unit
T	485	750	531	°C
p	253	250	72	bar

rameters, resulting in a stated temperature behind the expander at a chosen pressure ratio. To achieve the claimed high thermal efficiencies, the heat after the expander in point 3 has to be recuperated in large amounts. Thus, the heat has to be transferred to the feeding stream in front of the heater (point 1). At a high expander outlet temperature, the temperature in point 1 has to get high, to decrease losses. Thus, the heat flows exchanged in the cooler as well as in the heater are thereby reduced. In this case, the heater would be replaced by a sandTES HEX, a particle-fluid HEX, which is explained in detail in the following section.

As the temperature difference at the heater (between point 1 and 2) is rather low, sensible TES systems are struggling: Due to the first law of thermodynamics the HSM mass flow has to be increased, resulting in higher amounts of the HSM to be stored. To increase this temperature difference, the partial cooling cycle was chosen. Although the recompression cycle is generally accepted as most efficient layout, the partial cooling cycle is suggested for applications in combination with sensible TES systems, because of the higher temperature difference at the heater and the accompanying mass flow reduction of the HSM [1, 6]. Additionally to the higher temperature difference at the heater, the partial cooling cycle is more flexible when running at various operation conditions, which is bought by a slightly lower thermal efficiency. The recompression cycle layout is very similar to the partial cooling cycle; only the precompressor and precooler are left.

To sum up, high efficiencies can be achieved at sCO_2 power cycles, due to the ability of a further temperature rise. Therefore a high temperature TES system is necessary to additionally gain a highly flexible cycle. As the energy density of sensible HSM can be significantly increased by using a preferably high temperature difference, a special cycle layout is recommended.

SANDTES

As mentioned in the introduction, the development of TES systems for the application in electricity generation cycles goes towards high temperatures. Therefore the aim of the sandTES technology is to achieve an active TES, which exceeds the previous temperature limits of common sensible TES systems. In this section the principles and key developments are explained [3, 7].

As the name suggests, the sandTES relies on (quartz) sand as storage medium, which enables highest temperatures. Sand is a low cost storage medium, but also other materials like corundum (Al_2O_3) are considered due to their higher energy density.

The core of the sandTES technology is a particle/fluid HEX, in which a dense particle suspension is fluidized e.g. by air. The thereby achieved fluid-like behaviour of the suspension and the horizontal pressure gradient (caused by the height difference of the bed between inlet and outlet) makes it flow through the HEX. The flow directions of both, heat transfer medium and working fluid (e.g. sCO_2), are reversible, which can be advantageous if only one HEX should fit for charging as well as discharging mode. In the present study, the reversible flow option of the sandTES technology is not necessary, because the heat source for the sCO2 cycle is like an external heat source e.g. a discontinuous batch process from a blast furnace process. To reduce exergetic losses during the heat transfer, the particles flow in countercurrent to the working fluid, which is contained in a tube bundle.

The heat carried by in the fluidization air can be largely recovered by recuperators. To reduce losses due to auxiliary equipment, the pressure drop through the bed and the blower mass flow have to be kept low. The vertical pressure drop of the fluidization air through the suspension mostly depends on the height of the fluidized bed, see Eq. (2)

$$\Delta p_{fb} = (1-\Psi)(\rho_p - \rho_f) \cdot g \cdot \Delta H_{fb} \tag{2}$$

with the vertical pressure drop Δp_{fb}, the gravity g, the density of the particles ρ_p and fluid ρ_f, the corresponding height H_{fb} and the porosity of the bed Ψ. The fluidization air mass flow correlates with the fluidization grade μ, see Eq. (3)

$$\mu = \frac{u_{act}}{u_{mf}} \tag{3}$$

with u_{act} the actual superficial velocity, and u_{mf} the minimum fluidization velocity, below which the fluidized bed collapses.

The fluidization grade needs to be higher than 1 at every point of the HEX. This is the reason, why the mean value is stated at about 3 to 4. Since u_{mf} decreases with the particle size, fine powders (in the magnitude of 60-100 microns) are preferred to further reduce auxiliary power. Because of the low fluidization velocities, no erosion problems occur, despite the high temperatures.

In Fig. 2 a simplified process diagram of the sandTES system is shown to introduce the basic storage concept. To charge the TES, cold particles fall out of the filled cold silo and are fed by some conveying system (e.g. via a screw) into the HEX of some heat source. For example, a direct particle receiver could heat up the particles in the tower of a STE plant. Further on, the meanwhile hot particles are transported to the hot silo, to be stored. From there on the particles can be put into the sandTES HEX (e.g. a particle-sCO_2 HEX) whenever it is desired. Because of the horizontal pressure gradient in the HEX, the storage material within the fluidized bed flows through the device, while heating up the working fluid. At the outlet of the sandTES HEX, the cold particles fall e.g. into a bucket conveyor, which transfers the particles back into the cold silo, to close the loop. Meanwhile the hot exhaust air cools down in the recuperator by heating up the fresh air stream. After filtering, the exhaust air leaves the system.

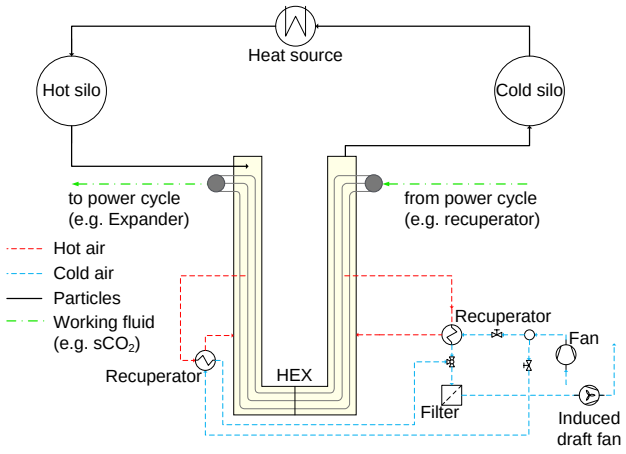

FIGURE 2. BASIC SANDTES PROCESS FLOW SHEET

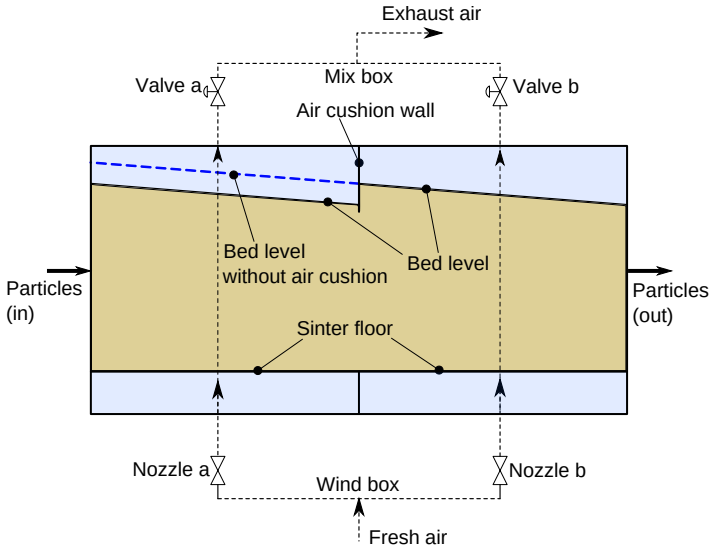

FIGURE 3. SEGMENT OF A SANDTES HEX

Key Technologies

As it is a challenging task to implement a horizontal plug flow for particle suspensions, two key technologies were developed at the IET: the *nozzle distributor floor technology* for controlling the fluidization air distribution and the *air cushion technology* for controlling the height of the bed. These two technologies allow a stable, efficient and flexible fluidized bed HEX, enabling a countercurrent flow of the particle suspension and the working fluid.

Both mentioned technologies rely on Eq. (4), which says, that the vertical pressure drop through the HEX Δp_{HEX} is aggregated of the individual pressure losses of the nozzle Δp_{Nozzle}, the fluidized bed Δp_{fb} and the valve Δp_{Valve}. The compound pressure drop Δp_{HEX} has to be equal at every cross section along the particle's flow direction (axis).

$$\Delta p_{HEX} = \Delta p_{Nozzle} + \Delta p_{fb} + \Delta p_{Valve} = const. \tag{4}$$

Figure 3 shows a simplified segment of a sandTES HEX without the horizontal tube bundle, but with the according air piping. The particles (beige) are flowing from the left to the right side. Obviously the fluidization air is coming from the bottom and is collected at the top. The distributor tube at the bottom, the so called wind box, is fed by one blower. The air coming from this blower, gets split after the wind box, passes the fluidized bed in vertical direction and leaves the HEX at the top collector tube, which is called mix box.

For a first viewing, the nozzles and valves in Fig. 3 shall be ignored ($\Delta p_{Nozzle} = \Delta p_{Valve} = 0$). The level of the fluidized bed on the left side runs along the dotted line. By inserting a mass flow on the one side of the HEX and removing it on the other side, a height difference between in- and outlet appears. Thus, a sloped bed surface results, which is depending on a virtual viscosity of the fluidized bed; similar to liquids.

As it can be seen from Eq. (2), the vertical pressure drop in a fluidized bed Δp_{fb} increases with the bed height, but is independent from the superficial velocity u_{act}. Therefore the vertical pressure drop through the fluidized bed is different in every cross section of the HEX along the flow direction of the particles. The air mass flow tends to move the path of least resistance, resulting in a highly unequal distribution of the fluidization air and hence the fluidization grade along the HEX axis.

To overcome this problem, the nozzles a and b after the wind box are inserted ($\Delta p_{Nozzle} > 0$; $\Delta p_{Valve} = 0$). Because of the quadratic dependency of the pressure drop through a nozzle Δp_{Nozzle} by the corresponding fluid velocity u_{Nozzle}, an increasing mass flow results in an increasing pressure drop, which can be seen in Eq. (5):

$$\Delta p_{Nozzle} = \zeta \cdot \frac{\rho_f \cdot u_{Nozzle}^2}{2} \tag{5}$$

Depending on the pressure loss coefficient ζ, these nozzles soften the aforementioned uneven air distribution, by compensating for the different pressure drops through the bed. Thus, Eq. (4) can be fulfilled due to an additional pressure loss term, evening the overall pressure loss through the HEX. However, a high pressure loss coefficient increases not only the stability of the air distribution, but also the pressure drop, leading to higher auxiliary power needed.

Within one nozzle box, the problematic remains the same, which suggests a high resolution, thus a high number of noz-

zles. For that reason the sinter floor, which consists of numerous porous sinter plates, is additionally inserted. These sinter plates, with a porosity of about 10 to 30 microns, induce a continuous vertical pressure drop along the particle's flow direction. Due to the big area of the sinter floor, the superficial air velocities are very low, leading to a laminar flow and thus to a moderate stabilizing effect. Furthermore the particles can be retained from the nozzles, preventing plugging the air piping. The aggregate of the nozzles, the sinter floor and the chamber in between make each up a so called nozzle box, which is a constructive entity.

As it can be imagined, the slope of such a fluidized bed level leads to serious bed heights for a long HEX channel, resulting in great masses, which are not participating at the heat exchange, because of the distance to the horizontal tube bundle below. Therefore it is advisable to set down the bed surface as far as possible.

As it can be seen in Fig. 3, the top of the HEX is divided into two chambers by the gas tight air cushion walls. The air cushion technology, consisting of these chambers and the valves, again leads back to Eq. (4), postulating an identical overall pressure loss in every cross section of the HEX. If the pressure loss of the valve Δp_{Valve} (similar to Eq. (5), but with variable ζ) in the left chamber is slowly rising, at least one other term of Eq. (4) has to decrease, since the equation still has to be satisfied. This is the reason, why the pressure drop through the fluidized bed has to sink. Referring to Eq. (2), any of the parameters Ψ, ρ_f or ΔH_{fb} needs to fall, which mainly concerns the bed height. Thus, the pressure drop through the fluidized bed is shifted to the valve, which leads to a lower bed height.

It has to be mentioned, that Fig. 3 shows just two nozzles and two air cushions for the sake of simplicity, which also can be seen in the next section. Various combinations are part of the design optimization of such HEX.

For proving the concept, a pilot plant is being put in operation at the IET's laboratory site. Insightful conclusions about the stability and optimization criteria are expected by the measurements [3].

Particle-sCO_2 Heat Exchanger

In this section, to consider the utility scale dimensions, a design case of a 121 MW_{th} particle-sCO_2 HEX, which could be used in a 55 MW_{el} STE plant, is presented. The calculations were carried out with a MATLAB based design tool, which is coded at the IET. The boundary conditions for the HEX, namely the design process parameter, are listed in Table 2.

Due to material issues the sCO_2 cycle parameters are still restricted, although enhancing these parameters seems likely in the near future when e.g. ceramics can be applied less expensively. At this fluidized bed HEX an air mass flow is needed for fluidization, which is heated up while passing the bed. The according heat loss is rather low ($\dot{Q}_{Air} = 55\,\mathrm{kW}$) and can be largely recuperated.

TABLE 2. HEX DESIGN PARAMETER

Name	Al_2O_3	CO_2	Unit
T_{in}	800	485	°C
T_{out}	529	705	°C
$\dot{m}$	369	436	$\frac{kg}{s}$
p_{in}	1.9	250	bar
Δp	0.3	2.5	bar

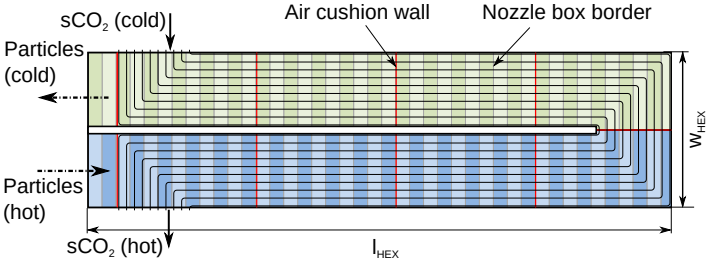

FIGURE 4. HEX TOP VIEW

As particle medium corundum (Al_2O_3) [8] with an average particle diameter of 50 microns is used. The higher density and with it the higher energy density compared to quartz sand allows a more compact HEX and storage design.

Figure 4 shows the layout of the HEX, which is further on roughly summarized and explained. As it can be seen, the particles are inserted at the hot side and are flowing in countercurrent to the sCO_2 in a meander shaped channel to the cold side, while heating up the sCO_2. The flow directions of both media can be reversed, although it isn't necessary at a STE plant.

The red lines represent the air cushion walls, thus the borders between the different air cushion chambers. The number of air cushions is largely independent of the nozzle distributor floor. Therefore a number of 4 air cushions per turn is chosen to limit the maximum bed height. The area on the left side of both turns, above each two outer nozzle boxes, are reserved for feeding the HEX with the particles. In these segments the tube bundle is missing, with the intent to relieve a uniform temperature distribution in the vertical at this entry sections. Above these segments, there are no air cushions placed because of difficulties at transporting particles into a pressurized chamber.

The height level of the bed is shown in Fig. 5. The dotted line represents the bed height without air cushions, where the solid line clearly outlines the advantage of the air cushion technology. Only the actual bed height of the entry and exit segments

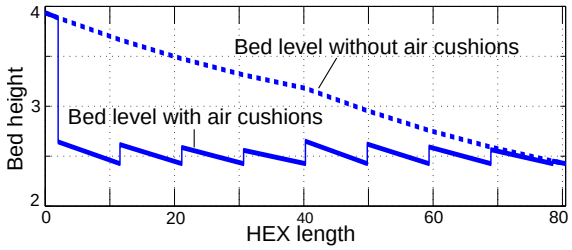

FIGURE 5. BED LEVEL ALONG HEX AXIS

(without air cushions) are at the original level. If the pressure loss of the air cushion valve increases, the pressure drop through the fluidized bed and with it the according bed height has to fall, to satisfy Eq. (4). Thus, the total vertical pressure drop of the HEX has to stay constant. It can be concluded, that the bed height is thereby reduced from approx. 4 m to about 2.5 m (excluding the edge regions), leading to a much more compact HEX design.

Coming back to Fig. 4 it can be seen, that the HEX is also divided in 2 wind boxes, which are highlighted in blue and green. Thus, every turn is fed by one blower. The light and dark coloured fields in each of these turns always represent one nozzle box, overall resulting in 42 nozzle boxes per turn.

As it has been mentioned before, the nozzle distributor floor tends to counterbalance the unequal fluidization grade distribution. Of course, the deviations just can be limited, not eliminated. The additional pressure drop of a nozzle is a consequence of the higher air mass flow passing it, see Eq. (5).

In Fig. 6 the fluidization grade μ is shown along the axial length of the HEX. The dotted line represents a fluidization grade of 1, below which the fluidized bed collapses. Looking at the first of the two segments in this graph, the expected curve shape is illustrated. On the left side, where the bed is at its highest level, only a low pressure drop over the nozzle is needed. This can be seen at the low fluidization grade, which requires a corresponding low air mass flow. Going to the right side, the bed height decreases, leading to a higher pressure drop over the nozzle with the associated higher fluidization grade. Changes at the air pressure and temperature at various points lead to an expansion and

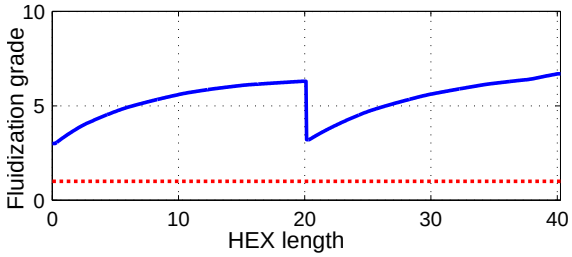

FIGURE 6. FLUIDIZATION GRADE ALONG HEX AXIS

TABLE 3. HEX LAYOUT PARAMETER

Name	$w_{channel}$	l_{axial}	w_{HEX}	l_{HEX}	h_{bed}
Value	2.5	40	5.3	20	2.4
Unit	m	m	m	m	m

so on to the resulting shape of the curve.

Now it is getting clearer, why the splitting in different wind boxes is that much important. If there was only one wind box along the whole axial length of the HEX, the needed pressure drop for stabilizing and the accompanying higher air mass flows and fluidization grades would increase, leading to a highly uneven air distribution. Feeding every windbox with its own blower allows a cut in the curve, to set it back down to the design point fluidization grade. As a result, the range of fluidization grades is fairly constrained in the range of 3 to 6.5. The required pressure loss of the nozzle distributor floor remains in the range of 32 mbar to 190 mbar.

Once again, it shall be outlined, that the pressure above the nozzle distributor floor of the HEX is mainly independent of how it is originated. Thus, it does not matter, if the pressure above the nozzle distributor floor relies on a higher bed or a higher pressure drop over the valve.

Finally the dimensions of this HEX design are summarized in Table 3, where $w_{channel}$ represents the width of the flow channel and l_{axial} the rolled out length of this channel. The overall dimensions of the HEX with the width w_{HEX}, the length l_{HEX} and the height h_{bed} illustrate the compact design. The ground of about 106 m^2 combined with a procedurally needed height below 2.5 m seems rather low for this 121 MW_{th} scale. It has to be mentioned, that it might be useful to choose a higher width of the HEX w_{HEX}, to ensure maintenance capability.

The cross section of the HEX channel is shown in Fig. 7. Beyond and below the tube bundle, obstructions are installed with the purpose to force a contact of the outer layers of the particle suspension with the tube bundle. These obstructions are the air cushion walls and the ground baffles above the nozzle distributor floor. Still, these layers are very small to minimize the blind zones of the bed.

Also the tube bundle can be seen with the according parameters in Table 4. As a nickel based material alloy 617 was assumed for the strength calculation. n_h is the number of tubes in the horizontal and n_v in the vertical, resulting in a tube bundle of overall 986 tubes. The dimensionless distances between the tube centers, thus the pitch ratios t_h in the horizontal and t_v in the vertical are listed in Table 4, but have to be multiplied with the outer diameter of the tubes d_o. This outer diameter combined with the wall thickness s and the rolled out length l_{axial} of the tubes leads

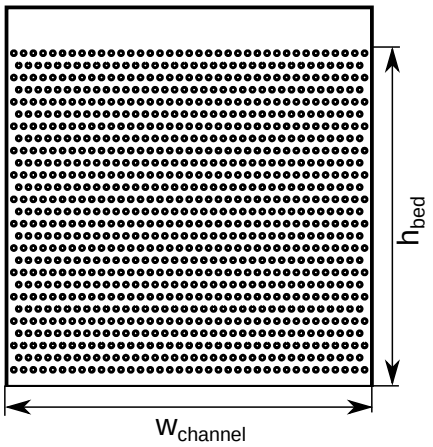

FIGURE 7. CROSS SECTION OF THE HEX CHANNEL

TABLE 4. TUBE BUNDLE PARAMETER

Name	d_o	s	n_h	n_v	t_h	t_v
Value	33.7	7.1	37	27	2	2.5
Unit	mm	mm	-	-	-	-

to the total HEX surface A_{HEX}, see Table 5.

For various HEX applications different mass flux combinations of the particle suspension and the heat transfer medium occur. Therefore, regarding the tube bundle design, the pitches are the main design parameters. At this sCO_2 HEX the mass fluxes of both the particle suspension G_{fb} and the carbon dioxide G_{CO_2} are strongly diverging. Nevertheless, the tubes are set close to each other; thus low pitches were chosen. For example, the pitches of a sandTES HEX at a compressed air energy storage (CAES) plant is in the range of 2, while the ECO of a steam generator shows pitches in the range of 5. A low pitch leads to much more barriers for the fluidization air, which makes a stable fluidization more defying.

The mean heat transfer coefficient h_{mean} in this HEX design is calculated by a correlation from Gnielinski [9] for the tube flow and Gelperin [10] for the fluidized bed. Due to the dependence of the heat transfer coefficient on the fluidization grade, the shape of the curve along the axis is qualitatively similar to Fig. 6. As mentioned before, the auxiliary power P_{Aux} is very low compared to the heat flow in the HEX.

TABLE 5. HEX DATA

Name	A_{HEX}	h_{mean}	G_{fb}	G_{CO_2}	P_{Aux}
Value	3729	341	78	1482	18
Unit	m^2	$\frac{W}{m^2 \cdot K}$	$\frac{kg}{m^2 \cdot s}$	$\frac{kg}{m^2 \cdot s}$	kW

DISCUSSION

As outlined in the introduction the research objective in the field of TES is to enhance the previous temperature limits. A high temperature power cycle coupled with an appropriate TES system leads to both enhanced efficiencies and flexibility. Therefore the combination of the sandTES technology, a particle based TES system, and a sCO_2 power cycle seems to be a promising option.

Particles like quartz sand or corundum are low cost, high temperature materials with high longevity and low risks to health. Although for handling these particles in a HEX, reaching an exergetic efficient countercurrent plug flow, sophisticated technologies are indispensable: The nozzle distributor floor technology to ensure a stable fluidization by evening the air distribution as well as the air cushion technology to limit the blind zone masses above the tube bundle and to gain a more flexible load change characteristic. An obvious disadvantage at using solids in a HEX is the conveyor technology: Pneumatic conveying systems for example are problematic due to the high auxiliary power needed. That is why screws and bucket conveyors seem preferable for transporting the particles between HEX and storage. Both potentially increase maintenance requirements and limit the achievable temperature range. At the IET also sandTES based technologies without the need for conveying systems are being developed.

In the following the main design parameters are roughly discussed. Looking back to Fig. 4 the layout of the particle-sCO_2 HEX impresses with the compact design. Of course, the according main dimensions in Table 3 represent a design relying on mass and energy balances. Due to maintenance capability and constructive reasons, these dimensions have to be adapted for real life application.

Also the intended process parameters for the sCO_2 as well as for the particles have a big impact on the HEX dimensions. It is clear, that higher temperature differences of the media themselves, and also with each other, lead to a more compact HEX design. The high temperatures and pressures of the sCO_2 require high temperature materials and still thick walled tubes. This overall results in a lowered heat transfer coefficient and hence an enlarged HEX design.

For designing the HEX, a tube geometry, regarding the diameter and the wall thickness have to be chosen. The number of tubes is determined by the mass flow and the velocity of the sCO_2. On the other side, the pitches allow to set the needed cross sectional area for the particles, depending on the particle mass flux. Although higher mass fluxes lead to higher pressure losses, with a great impact especially on the sCO_2 cycle's effi-

ciency, the HEX dimensions again can be significantly reduced. With this preset tube bundle geometry, the overall HEX surface can only be adjusted with the axial length of the HEX. As it can be seen in Fig. 7, the tubes are closely positioned to each other. This leads to a higher vertical pressure drop and so on to higher auxiliary power demanded, which still is rather low compared to the nominal heat flow.

As mentioned before, a 280 kw_{th} pilot plant is being put in operation, with the purpose to validate the key parameters for an optimized design:

The slope of the fluidized bed surface in the calculations done for this work, is based on correlations, simulations and previous test rigs. As it is strongly depending on the tube bundle geometry, the fluidization grade and the particle material, insightful conclusion are expected by the measurements. The maximum bed height, a reasonable number of air cushions and the design of the nozzle distributor floor are derived from the slope.

Of course this pilot plant also provides information about the heat transfer characteristics; another major design parameter for this novel HEX technology. The HEX area listed in Table 5 relies on a conservative calculation. Much higher heat transfer coefficients are expected by the measurements, directly resulting in an even more compact HEX layout.

Finally the stability limits and optimization criteria have to be found. The stability of the fluidized bed is ensured by the nozzle distributor floor. Looking back to Eq. 5 it becomes clear, that a minimum pressure drop is required to limit the fluidization grade distribution. To find this minimum pressure drop, stability boundaries have to be investigated, for overall minimizing the needed auxiliary power. Therefore the pressure loss coefficient of the nozzles as well as the number of nozzle boxes and windboxes have to be examined.

Summing up, the sandTES technology promises an efficient way to store thermal energy at highest temperatures. A full proof of concept and the optimization criteria are expected by the pilot plant measurements in the near future.

CONCLUSION

Prior work has documented the need for highly efficient and flexible power plants. State of the art power plants often have difficulties at reaching sufficient operating hours, leading to economical and technical challenges. In this work a combination of a high temperature power cycle using sCO_2 as working fluid and a novel high temperature TES system, based on a fluidized bed HEX, is suggested to enhance both the flexibility and the efficiency. The concept of the TES system and the key technologies were explained in detail to outline the challenging handling of a particle suspension in a countercurrent HEX. Furthermore a utility scale TES HEX, which can be applied in a sCO_2 Brayton cycle is presented. The main dimensions and key parameters of the HEX are shown as well as the potential for optimization is demonstrated.

This HEX design comprises a very compact layout and high efficiencies referring to the needed auxiliary power, the heat loss due to the exhaust air and the exergetic losses during the heat exchange. The integration of such a TES system into a power cycle leads to economic benefits and the accompanying increased competitiveness. Of course, compared to fluids the handling of solids is more expensive, referring to the needed conveyors. Although, there is a HEX in development, comprising a sandTES based technology without the need for conveying systems.

As it applies to all power plant concepts, progress in materials and joining technology will lead to a further improvement of the performance data.

In future work the pilot plant at the IET's laboratory site will bring insightful conclusions about important HEX parameters, leading to an optimized HEX design.

NOMENCLATURE

A	Area [m^2]
d	Diameter [mm]
g	Gravitational constant [m/s^2]
G	Mass flux [kg/m^2s]
h	Heat transfer coefficient [W/m^2K]
H	Height [m]
HEX	Heat exchanger
HSM	Heat storage medium
l	Length [m]
$\dot{m}$	Mass flow [kg/s]
n	Tube number [-]
p	Pressure [Pa]
P	Power [MW]
$\dot{Q}$	Heat flow [MW]
R	Gas constant [J/kgK]
s	Thickness [mm]
sCO_2	Supercritical carbon dioxide
STE	Solar thermal electricity
t	Pitch ratio [-]
T	Temperature [°C]
TES	Thermal energy storage
u	Velocity [m/s]
v	Specific volume [m^3/kg]
w	Width [m]
Z	Compressibility factor [-]

Greeksymbols

Δ	Difference
μ	Fluidization grade [-]
Ψ	Porosity [-]
ρ	Density [kg/m^3]
ζ	Pressure loss coefficient [-]

Subscripts	
act	Actual superficial
Aux	Auxiliary
axial	Axial
bed	Bed
channel	Channel
el	Electric
f	Fluid
fb	Fluidized bed
h	Horizontal
HEX	Heat exchanger
in	Inlet
mean	Mean
mf	Minimum fluidization
Nozzle	Nozzle
o	Outer
out	Outlet
p	Particles
th	Thermal
v	Vertical
Valve	Valve

ACKNOWLEDGMENT

The K-Project GSG-GreenStorageGrid (Grand no. 836636) is funded in the framework of COMET - Competence Centers for Excellent Technologies by the Federal Ministry of Transport, Innovation and Technology, the Federal Ministry of Science, Research and Economy, the Vienna Business Agency, the Federal Province of Lower Austria and by the Federal Province of Upper Austria. The program line COMET is administered by the Austrian Research Promotion Agency (FFG). The authors would like to thank also the project partners Valmet GesmbH., EVN AG, ENRAG GmbH. and Primetals Technologies GmbH. for the pleasant and constructive working relationship.

Special thanks go to the sandTES research team for the helpful support and the numerous discussions.

REFERENCES

[1] Zhiwen Ma, Craig S. Tuchi, Ty Neises, Michael Wagner, 2012. "Thermodynamic study of advanced supercritical carbon dioxide power cycles for high performance concentrating solar power systems". *Proceedings of the ASME 2012 6th International Conference on Energy Sustainability,* ***2012***.

[2] Niels Brinkmeier, 2015. "Flexibility of thermal power plants". PhD thesis, TU Braunschweig, Braunschweig.

[3] P. Steiner, K. Schwaiger, M. Haider, H. Walter, and M. Hämmerle, 2016. "Increasing load flexibility and plant dynamics of thermal power plants via the implementation of thermal energy storages". *Proceedings of the ASME 2016 Power and Energy Conference,* ***2016***(Paper number: PowerEnergy2016-59181).

[4] Ahn, Y., Bae, S. J., Kim, M., Cho, S. K., Baik, S., Lee, J. I., and Cha, J. E., 2015. "Review of supercritical co2 power cycle technology and current status of research and development". *Nuclear Engineering and Technology,* ***47***(6), pp. 647–661.

[5] Iverson, B. D., Conboy, T. M., Pasch, J. J., and Kruizenga, A. M., 2013. "Supercritical co2 brayton cycles for solar-thermal energy". *Applied Energy,* ***111***, pp. 957–970.

[6] Kulhanek, M., and Dostal, V., 2011. "Supercritical carbon dioxide cycles thermodynamic analysis and comparison". *Supercritical CO2 Power Cycle Symposium,* ***2011***.

[7] P. Steiner, K. Schwaiger, H. Walter, and M. Haider, 2016. "Active fluidized bed technology used for thermal energy storage". *Proceedings of the ASME 2016 Power and Energy Conference*(Paper number: PowerEnergy2016-59053).

[8] NIST, Dec. 20, 2015. Nist chemistry webbook.

[9] Gnielinski, V., ed., 2010. *G1 Heat Transfer in Pipe Flow: VDI Heat Atlas*, Vol. 2010. Springer Berlin Heidelberg.

[10] Ainshtei, V. G., and N. I Gelperin, 1966. "Heat transfer between a fluidized bed and a surface". *International Chemical Engineering,* ***1966***.

CURRICULUM VITAE

Persönliche Daten

Vor- und Zuname	Dipl.-Ing. Peter Philipp STEINER, BSc.
Adresse	Buchenstraße 1 8243 Pinggau
Telefon	+43 677 614 650 64
E-Mail	pps@gmx.at
Geburtsdatum	19. August 1989
Staatsangehörigkeit	Österreich

Ausbildung

April 2014 – dato	TU Wien, Doktoratsstudium der technischen Wissenschaften Maschinenbau Forschungsgebiet: Thermische Energiespeicher
April 2012 – April 2014	TU Wien, Master Maschinenbau, Schwerpunkt Energietechnik Leistungsstipendium 2012/13 Mit Auszeichnung bestanden
März 2008 – April 2012	TU Wien, Bachelor Maschinenbau
Juli 2007 – Jänner 2008	Präsenzdienst
September 2003 – Juni 2007	BORG Hartberg Informatikzweig mit naturwissenschaftlichem Schwerpunkt
September 1999 – Juli 2003	Hauptschule Pinggau
September 1995 – Juli 1999	Volksschule Pinggau

Berufserfahrung

April 2014 – dato	TU Wien, Institut für Energietechnik und Thermodynamik Projektleitung SandTES-Pilotanlage
Juli/August 2011	Audi Ingolstadt Ferialpraktikum
Juli/August 2010	MagnaSteyr Graz Ferialpraktikum
Oktober 2009 – Februar 2011	TU Wien Racing Team
Juli/August 2006	Lactoprot Hartberg Ferialpraktikum

Qualifikationen

Sprachen	Deutsch (Muttersprache), Englisch (fließend)
Programme	CFD: Ansys (Fluent, CFX, ICEM), OpenFOAM, LIGGGHTS/CFDEM, Barracuda Prozesssimulation: Ebsilon, IPSEpro, KED, NOWA Programmiersprachen: Java, C++, C#, Matlab, PHP FEM: Ansys Mechanical Leittechnik: B&R Automation Studio, Aprol; LabView Sonstiges: Office, Latex
Hobbys	Segelfliegen, Schach, Laufen, Golf

Wissenschaftliche Arbeiten

Diplomarbeit	Numerische Strömungssimulation einer Pumpturbinenspirale
Projektarbeit	Auslegung eines Peltonturbinenprüfstandes
Bachelorarbeit	Strömungsverhältnisse in einer Kunstvitrine (Strömungsmessung mit LDA und PIV)